FINITE ELEMENT MODELING AND DYNAMIC IMPACT RESPONSE EVALUATION FOR BALLISTIC APPLICATIONS

By

ADVAIT R. BHAT

Bachelor of Science in Mechanical Engineering

Mumbai University

Mumbai, Maharashtra, India

2007

Submitted to the Faculty of the
Graduate College of the
Oklahoma State University
in partial fulfillment of
the requirements for
the Degree of
MASTER OF SCIENCE
December, 2009

FINITE ELEMENT MODELING AND DYNAMIC

IMPACT RESPONSE EVALUATION FOR BALLISTIC

APPLICATIONS

Thesis Approved:

Dr. Jay C. Hanan
Thesis Advisor

Dr. Jim Smay

Dr. Sandip Harimkar

Dr. A. Gordon Emslie
Dean of the Graduate College

ACKNOWLEDGMENTS

I would like to thank Dr. Jay Hanan for his guidance and supervision he has given me during the entire span of this research work and my thesis. I feel extremely privileged to be a part of his research team and would like to extend my deepest gratitude for bringing out the best in me and helping me channelize my efforts in the right directions. He always motivated me to achieve my goals with steadfast dedication and continually encouraged to move forward in spite of witnessing early failures. His scientific attitude and passion for intellectual pursuit has been very inspirational and encouraging during my first steps of being a part of global scientific community.

I would like to thank Dr. Donna Branson and OSU-IPART program for initiating the body armor project and giving my team an opportunity to strive for protecting human lives. This research would not have been possible without the funding and government support under ONR Grant No. N00173-071-G001 awarded by the Naval Research Lab through OSU's Institute for Protective Apparel Research. Major share of the success is owing to the Officers and Personnel from DSM Shooting range North Carolina, US Shooting Academy Tulsa, Tulsa Fire Arms, Tulsa and Stillwater Shooting range, for helping us conduct the ballistic tests. I would like to extend my appreciation to the radiologists at St. Anthony's Hospital in Oklahoma City and Doug Carlson from Servant Medical Imaging in Stillwater for their time and help with CT imaging. I extend my heartfelt thanks to Boshen Fu for bearing with my relentless questions and doubts on the

FEA modeling in ABAQUS. I gratefully thank Dr. Jim Smay and Dr. Sandip Harimkar for being on my thesis committee.

I owe individual and collective acknowledgements to all the colleagues in my research group. First and foremost, I wish to thank Balaji Jayakumar, my only team member on this project, for his lion's share in manufacturing of all the armor plates. It would not have been possible to pull off this research work that demanded endless hours at the lab and regular over night work schedules without your help. Many thanks go to Hrishikesh Bale, who will always be the most respected and senior member of the research team. His creative ideas through all the brain storming sessions have always helped me solve some of the most intriguing problems faced in this research. He will always be admired for his leadership skills and the tough standards that he set for being a good graduate student.

I am thankful to Sarah Staggs, Vijay Krishnan, Sudheer Bandla, Ranjan Mahadevan, Praful Bari , Mujeer Ahmed and Masoud Allahkarami for their help on site of all the ballistic tests and also in the labs. I would also like to extend my sincere regards to Dhivakar, Sarvanan, Giridhar and Swaroop for their help in manufacturing the armor plates. The success of this project is a result of collective effort and support from you all and I am deeply thankful to each one of you.

Last but not the least; I owe utmost gratitude and regards to my parents and my family for their continuous blessings, support and motivation when I needed it the most. Words cannot express my gratitude for my beloved fiancé Lopeeta for bearing with my work schedules and helping me survive so far away from home.

TABLE OF CONTENTS

LIST OF TABLES

Table Page

LIST OF FIGURES

Figure Page

CHAPTER I

1. INTRODUCTION TO ENERGY ABSORPTIVE APPLICATIONS

Energy absorptive applications pertain to the use of physical structures and related modifications to inhibit the transmission of directed kinetic energy during impact. The prime objective in all energy absorptive applications is to ensure the safety and integrity of high priority systems by protecting them from damage inflicted through directed kinetic energy. Energy absorptive applications have been an integral part of many modern industrial sectors like the packaging industry, transport, defense, construction and power generation [1-4]. The nature of these applications varies with the entity having higher safety priority (a finished product for packaging industry and a human user in the case of transport and defense). Variations are also based on the means used for energy dissipation. As defined by Alghamdi [5], "an energy absorber is a system that can totally or partially convert the directed kinetic energy in any other form. Energy converted is either reversible, like pressure energy in compressible fluids and elastic strain energy in solids, or irreversible, like plastic deformation energy". The majority of current energy absorptive systems utilize both reversible and irreversible modes of energy conversion to maximize dissipation. Weight sensitive applications like those in the packaging industry and defense involve constraints that necessitate the absorbers to be less bulky,

rigid, offering better stability with strength and ease of handling per unit mass. In such cases, an irreversible mode of conversion is utilized more predominantly as it positively ensures that damages sustained through intense impact loads are minimal. As a result, absorbers use elastic strain and plastic deformation energy as absorption modes with plastic deformation energy being the majority of the total energy absorbed.

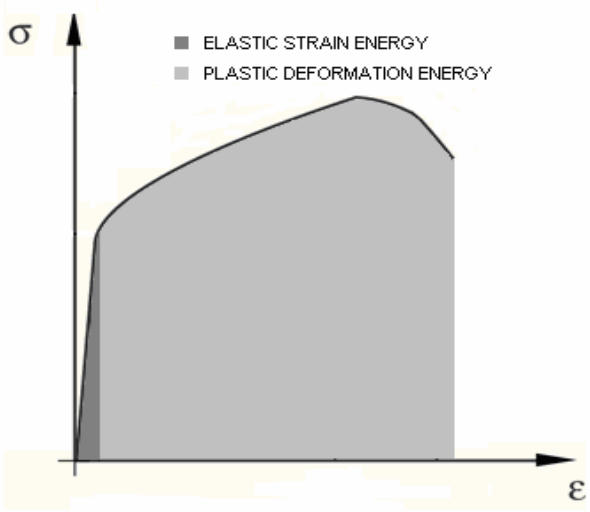

Figure 1 Schematic showing the elastic and plastic energy regions on a Stress – Strain diagram.

As described by Johnson et al. [6], the prime factors that govern the energy conversion through plastic deformation are:

- Deformation and displacement patterns
- Properties of materials involved and their transmission rates
- Load description and application patterns

The design and material selection for absorber systems have evolved over time with continual modifications specifically aimed at further improving their efficiency with each prime factor in consideration. Deformation and displacement patterns are influenced by the design geometry and structural constitution of each component that form the absorber unit. Evolution of load distribution at micro and macro levels is influenced by the

structural geometry as well as by the nature of materials involved. Material properties play the most vital role in governing the energy absorption capacities since they are directly relative. Material properties have been observed to change with the load description and the application rates. These variations significantly affect the end nature of the absorber. It is thus vital to find ways to quantify and compare each of these aspects while designing any energy absorber that suits a particular application. In-depth understanding of the requirements followed by detailed analysis and mechanical tests are essential to evaluate its performance.

The current research work presented here aims to explore the methodology of designing a personal ballistic impact absorber unit. Background literature and research that prompted the design selection of this Hybrid-Composite-Armor plate insert, its material constituents and methods of evaluating its performance are discussed in the upcoming sections. The study illustrates the use of experimental testing and FEA analysis in conjunction as a design procedure for evaluation of dynamic impact behavior of structures. Ballistic resistance evaluation of this Dyneema – Metallic Glass honeycomb lattice sandwich plate concept according to NIJ standards and FEA analysis using ABAQUS 6.8.2 is the final aim.

1.1. Design and Material Developments in Energy Absorptive Applications

Each application demands specific design and material selection which best suits the needs. It also demands a design selection that enables energy dissipation at a predetermined rate and controlled manner. As described by Lu et al. [7], the most fundamental principles that act as guidelines for designing any energy absorber can be briefly outlined as:

- The energy conversion by the structure should be irreversible by plastic deformation and other dissipation processes, rather than storing it elastically.
- The peak reaction force should be kept below a threshold and an ideally constant reaction force should be maintained throughout the deformation process.
- The displacement by deformation or the stroke in the structure should be sufficiently long to absorb the large amount of input energy.
- The deformation mode and energy absorption capacity of the designed structure should be stable and repeatable to ensure reliability during service.
- The structure should be as light as possible with high specific energy absorption capacity.
- Manufacturing, installation and maintenance should be easy and cost effective.

An ideal absorber design adheres to these principles but specific needs as mentioned earlier may necessitate some level of compromise in any of the principles. Success of the design is ultimately judged when it is put in the field of use. Over the years, different designs have been experimentally tested and implemented. The overview by Alghamdi [5] lists out the collapsible structures that have caught research attention. The prominent being drums [8], tubes [9-11], frusta [12], struts [13], and honeycombs [14]. Materials used to make these collapsible structures include metals like steels and aluminum alloys, paper and similar recyclable materials and polymers. Significant work has also been done to verify the effectiveness of these structures when filled with materials like foams, wood fillings and sand [15-17]. Collapsible structures have maximum stroke. When filled with above mentioned materials, variations in the reactive force can be minimized but with a detrimental increase in weight. The strength-to-weight ratio is also found to show

improvements due to controlled collapse. Fiber reinforced composites and Fabric based composite laminate systems have also been used in absorptive applications [18-20]. Advantages of fiber reinforced composites are multifold with regards to fracture toughness, stiffness and specific strength. These structures also improve the design flexibility (control over mechanical properties by governing fiber orientation), durability and ease of handling with a moderate compromise on manufacturing cost. Fabric based composite laminates systems have added improvements over unidirectional counterparts in terms of contourability over 3D structures, inter laminar strength and better damage tolerance [21]. As described by Karger-Kocsis et al. [22], the fracture toughness of knitted composites is better because a more homogeneous distribution of reinforcing fiber bundles can be attained. As illustrated by Khondker et al. [18], knitted fabric composites have enhanced inter-laminar fracture toughness due to strong intermingling and fiber bridging between adjacent layers when compared to regular textile composites [23-24]. In ballistic applications, fabric composite systems fare better than fiber composite systems as described by Grujicic et al. [25].

Monolithic solids like metals and their alloys are the simplest designs for providing impact resistance. Their first use dates even before the initiation of Industrial age. With development in manufacturing technology, steels and their processed variants have been regularly used in energy absorptive applications [26-27]. Other metals like aluminum alloys have also been used for energy absorption as mentioned earlier. More resistant materials to compressive stresses like ceramics have seen increased use as monolithic structures. They have been increasingly used in ballistic armor applications due to their relatively high compressive hardness with low bulk density as compared to the standard

materials used earlier like steels, titanium, aluminum alloys [28]. However their use is limited to only this specific application due to their brittle behavior. Amorphous metal alloys have seen significant improvement in terms of manufacturing technology and processing since their first induction in the 1970s. Research has enabled significant reduction in the required cooling rates by exploiting element combinations and quantities to achieve the "confusion effect" phenomenon [29]. Inherent high strength and elastic modulus makes them better than crystalline metals and the comparative low brittleness makes them a viable option to ceramics with reference to energy absorptive applications. Achievable low density through cellular structures makes Amorphous metals an excellent material choice for energy absorption applications. Compressive mechanical properties of amorphous metal cellular solids have been reported [30-32]. Recent publication by Yang et al. [33] has shown the comparison of strengths exhibited by various bulk metallic glasses as a function of their glass transition temperatures.

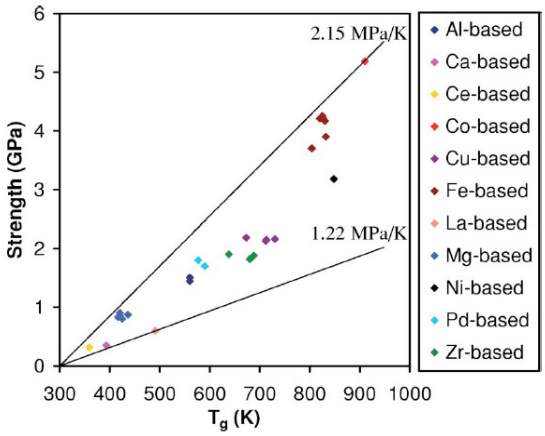

Figure 2 Strengths of amorphous bulk metallic glasses plotted with their glass transition temperatures, Yang et al. [33].

Dynamic compressive properties for Pd based amorphous metal foam have been reported which suggest better energy absorptive capacity than Aluminum foam counter parts of

the same relative density [34]. Results presented indicate that amorphous materials can prove an excellent choice for energy absorptive applications in the near future.

1.2. Ballistics Impact Inhibition: Armor Design & Materials

The post WW2 period opened several avenues for exploring new methods of ballistic impact inhibition. Safety of the human user in the combat zone gained more impetus. With the development of new weapon systems, it was imperative that obsolete armor technology had to be renovated to improve personnel and vehicle protection as a counter measure. The very first armor systems saw the use of monolithic hardened steel plates in flak jackets [35] and tank armor [36] which performed with a inconsistent success rate. The advancement in processing techniques led to the invention of Dual Hardness Armor (DHA) with thicker and better quality plates. Further innovations that followed include Rolled Homogenous Armor (RHA), Cast Homogenous Armor (CHA), High Hardness steel Armor (HHA) and hardened Aluminum alloy armor (MIL - DTL series). To enhance the performance, study of penetration mechanisms gained attention. The science of terminal ballistics was developed to gauge the characteristics and effects of projectile impact like fragmentation and adiabatic heating. With the environment conducive for further development, newer technologies like ceramic and reactive armor systems, ballistic testing standards and methods, analytical and computational simulation codes, fabric based armor, transparent armor etc emerged. Introduction of composite armor technology meant lightweight structures that performed even better than their heavier predecessors. Some significant developments in the armor structures have been listed in Figure 3.

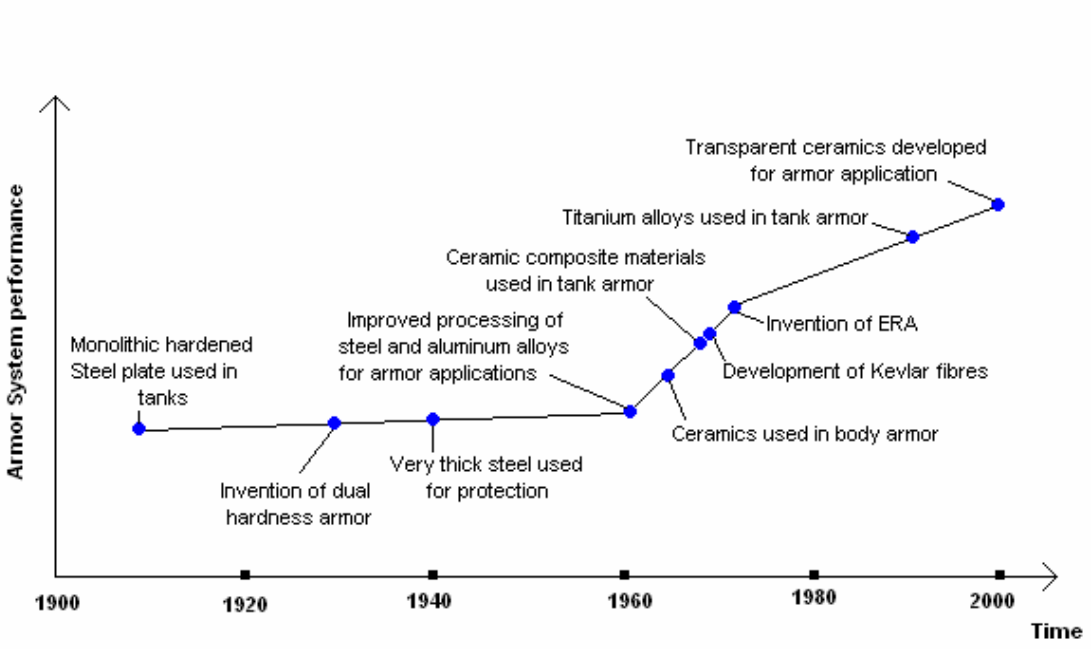

Figure 3 Armor development timeline as illustrated by Hazell [37].

As described by Hazell [37], basic armor designs can be classified as passive or reactive. Reactive armors employ the use of kinetic force to counter the ballistic threat. On the other hand, passive armors utilize the material properties of the constituents to dissipate the impact kinetic energy. Passive armors are most suitable for personnel applications like ballistic vests due to the close proximity. These can be further categorized as disruptors or absorbers. This classification is based on the material property that is specifically utilized to deal with the projectile kinetic energy. Disruptors function as the first impact layers of armor systems that erode the projectile in to fragments and thus disperse the energy away from the user. In order to successfully erode the projectile, disruptors are made from materials that have high strength and high hardness compared to the threat (e.g. ceramics, high strength steels). In contrast, absorbers work by absorbing the kinetic energy through plastic deformation modes. These systems also serve as spall liners to prevent unwanted projectile fragments from penetrating and inflicting damage

post impact (for example: steels, fiber reinforced composites, fabric laminate systems). Most current commercially used armor systems are multilayered composite structures to combine the advantages of both passive systems. Extensive failure in disruptors due to brittle cracking can be reduced when combined with fabric absorber systems, giving a multi-hit capability to the unit. Also fabric based armor systems by themselves are not efficient in defeating armor piercing threats and need disruptors to delocalize the concentrated forces. The ultimate classification of multilayer armor systems is based on the threat specifications they are designed to defeat. The most prevalent standards are the US National Institute of Justice (NIJ) and the European standards (DIN, CEN, and STANAG).

As mentioned earlier, the material properties that make ceramics and high strength steels an excellent choice as disruptors are their high stiffness and hardness. Ceramics have the highest stiffness after diamond and hence have the ability to reasonably defeat armor piercing threats. Properties of some ceramics are listed in Table 1. Successful use of ceramics in body armor have been reported [38-39]. However achieving these favorable properties implies extremely rigid structures that restrict mobility. Conformation to highly curved surfaces is also a difficult task to achieve with the processes currently used for manufacturing ceramics. Hybrid metal-ceramic and metal-ceramic-composite armor has also been used [40]. These armor designs have ceramic layer backed by metals and composites. The most conceivable option to introduce flexibility in armor designs was the use of ballistic fabrics.

Table 1 Material properties of some ceramic materials, Hazell [37].

	Alumina (high purity)	**Silicon Carbide**	**Titanium di-boride**	**Boron carbide**
Bulk density (kg/m^3)	3810 – 3920	3090 – 3220	4450 – 4520	2500 - 2520
Young's Modulus (GPa)	350 – 390	380 – 430	520 – 550	420 - 460
Poisson's Ratio	0.22 – 0.26	0.14 – 0.18	0.05 – 0.15	0.14 – 0.19
Hardness (HV)	1500 - 1900	1800 – 2800	2100 – 2600	2800 - 3400
Fracture Toughness ($MPa.m^{1/2}$)	3 – 5	3 – 5	5 – 7	2 – 3

The first fabrics introduced in armor applications were Nylon based which were used in Flak vests designed to protect against shrapnel [35]. The invention of Kevlar in 1969, by DuPont, lead to the first patented use of fabrics in body armor as a protection against bullet threats (K - 15 vests) [41]. Since then several other fabrics have been introduced for commercial use in armors similar to Kevlar in woven and non woven form. Namely: Aramids like Twaron, Gold Flex and Zylon, Ultra High Molecular Weight Poly Ethylenes like Spectra and Dyneema. Other similar fibers as listed by Machalaba et al. [42] are Terlon, SVM, Armos and Technora. The high fiber tenacity exhibited by these materials was used to improve in-plane properties of woven and non woven composite laminates or fabric bundles.

Table 2 Comparison of material properties for ballistic fibers, Machalaba et al. [42].

Fibers (yarns)	Fiber density, g/cm^3	Deformation modulus, Gpa		Tenacity, GPa*	Elongation at break, %	Moisture content, %**
		Dynamic	Static			
Armos	1.45–1.46	140–160	100–120	4.5–5.5	3.5–4	3–3.5
SVM	1.45–1.46	130–160	95–115	4–4.5	3–3.5	3.5–4.5
PPTA (Terlon, Twaron, Kevlar)	1.45–1.47	140–160	95–120	2.7–3.5	2.5–3	2–3

Table 3 Comparison of material properties of ballistic fibers, Cunniff et al. [43].

Fiber	Strength (σ) (GPa)	Failure Strain (ε) (%)	Modulus (E) (GPa)	$(U)^{\frac{1}{3}}$ (m/s)
PBO	5.20	3.10	169	813
Spectra 1000	2.57	3.50	120	801
600 den. Kevlar KM2	3.40	3.55	82.6	682
850 den. Kevlar KM2	3.34	3.80	73.7	681
840 den. Kevlar 129	3.24	3.25	99.1	672
1500 den. Kevlar 29	2.90	3.38	74.4	625
200 den. Kevlar 29	2.97	2.95	91.1	624
1000 den. Kevlar 29	2.87	3.25	78.8	621
1140 den. Kevlar 49	3.04	1.20	120	612
carbon fiber	3.80	1.76	227	593
E-Glass	3500	4.7	74	559
nylon	0.91	N/A	9.57	482

Fabric based body armors function well against deformable threats by distributing the kinetic energy through the high strength fibers with dissipation modes including fiber shear or fracture, fiber tensile failure or straining and associated delamination or pullout [44]. Other factors that affect their ballistic performance have also been discussed in the overview presented by Cheeseman et al. [45]. To provide isotropic properties when laminated, 0/45° and 0/90° crossply arrangements are used. As stated, the performance of ballistic fabrics against non deformable material projectiles (armor piercing) is limited since the concentration of force over a very small area causes penetration.

Table 4 Comparison of material properties of ballistic fibers, Grujicic et al. [46].

Fiber type	Failure strength, GPa	Failure strain	Axial modulus, GPa	Density, kg/m^3
Aramid	2.8-3.2	0.015-0.045	60-115	1390-1440
HMWPE	2.8-4.0	0.029-0.038	90-140	970-980
LCP	2.7-2.9	0.033-0.035	64-66	1400-1420
PBO	5.4-5.6	0.024-0.026	270-290	1540-1560
PIPD	3.9-4.1	0.011-0.013	320-340	1690-1710
Nylon	0.06-0.08	1.5-2.5	1.0-1.5	1070-1170
S-glass	4.64-4.66	0.053-0.055	82-92	2470-2490

Comparison of some fabric material properties available in literature are as given in Table 2, Table 3 and Table 4. Attempts to retain the flexibility and strength of these fabric systems along with high deformation capability of disruptors have seen a lot of motivation. Inter-laminar strength of fabric laminates have been improved by using 3D weave patterns instead of conventional 2D weaves reflecting in better ballistic performance [47]. Impregnation of woven Kevlar fabrics with colloidal shear thickening fluid have also been used as a method of improving strength of ballistic fabrics without affecting their flexibility [48].

1.3. Development of New Test Methods and Material Modeling

The phenomenon of impact is a dynamic interaction process wherein the media in contact undergo severe changes in terms of deformations in shape, material property evolution and similar physiological changes in a relatively short time duration. As expressed by Ramesh [49], impact has three major consequences namely: stress or shock wave propagation, structural dynamics and vibration issues and as stated before large inelastic deformations at typically high rates. With reference to the extent of energy absorption, dependency on these inelastic deformations (characterized by strains) is the highest, followed by wave propagation characteristics. Vibration issues do not directly affect the total energy absorbed. The evaluation of inelastic properties at different strain rates and wave propagation behavior is an experimental priority for closely estimating the energy

absorption efficiency of structures. Literature discussed earlier in this chapter emphasizes why understanding material properties and dissipation behavior at different rates is of high significance since they vary considerably as the loading rate is increased. Experimental methods developed for this purpose of property and behavior evaluation, as Ramesh [49] states, are colloquially defined as impact experiments. Impact experiments are classified based on their objectives. The classifications are:

- High-strain-rate experiments: Designed to measure the high-strain-rate material properties of a material and to identify rate dependent variations from low-strain-rate or quasi-static values.
- Dynamic failure experiments: Designed to understand the process of dynamic failure process within a material or structure.
- Direct impact experiments: Designed to understand or discover broad impact phenomena (e.g. vehicle crash experiments, ballistic testing)
- Wave propagation experiments: Designed to understand the characteristics of wave propagation within a material or structure.

Amongst the high-strain-rate experiments, the primary techniques used to evaluate rate dependent properties in materials are as listed in Figure 4 [49-50]. Quasi-static domain (10^{-6}-10^{0} s^{-1}) material properties can be studied with servohydraulic machines that can operate in both compression and tension setups according to ASTM standards. The intermediate strain rate domain (10^{0}-10^{2} s^{-1}) is a relatively difficult zone to study and requires unconventional or specialized machines like drop-weight towers for material property evaluation. ASTM standards are also available for these setups.

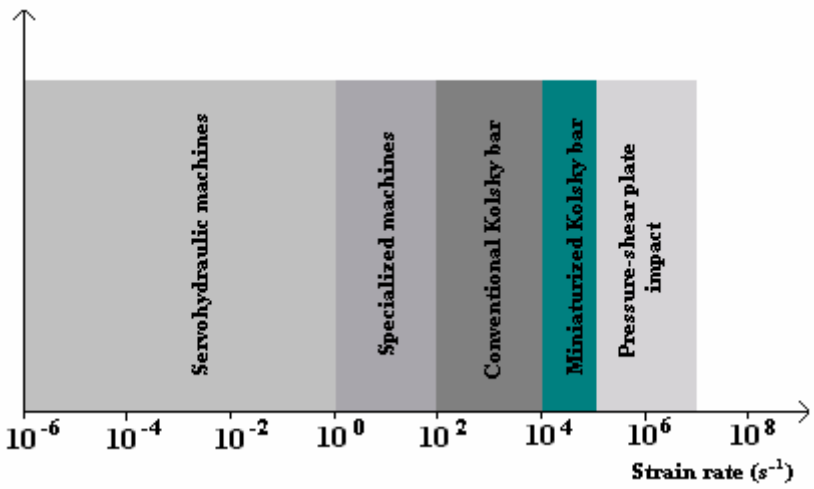

Figure 4 Experimental techniques used for rate dependent material property evaluation [49].

The high strain rate domain (>10^2 s^{-1}) is the zone where most impact related problems can be classified. The most ideal equipment for material property evaluation in this domain is the Kolsky Bar / Split Hopkinson Pressure Bar (SHPB) setup and their modifications. For very high strain rates (> 10^4 s^{-1}), plate impact experimental setups are used.

A traditional Kolsky bar / SHPB relies on using two long bars (input / incident bar and output / transmission bar) to act as impact pulse transducers between which the test sample is sandwiched. A third long bar (striker bar) is used to generate the pulse by high speed impact. The specimen size that can be tested in these setups varies with the dimensions of the bars used as well as the pulse lengths. Outputs are recorded using strain gauges which can generate a stress-strain response by calibration. A schematic representing a Kolsky bar setup is as shown in Figure 5.

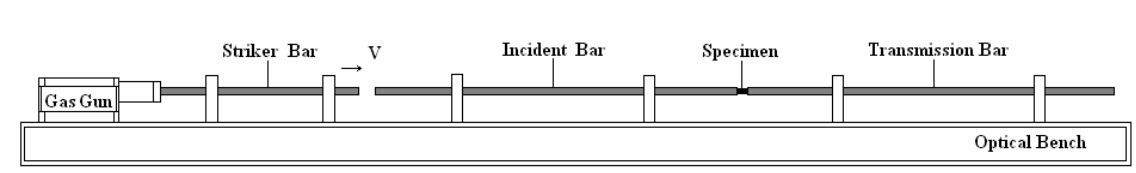

Figure 5 Schematic of a compression Kolsky bar setup mounted on an optical bench.

A variety of materials significant to energy absorptive applications have been tested using Kolsky bar setups. Strain rate dependence in Kevlar fiber bundles have been experimentally evaluated by Wang et al. [51-52]. Similar methods have been used to evaluate dynamic properties of Aramids [53] and polyethylene reinforced composites [54], UHMWPE fibers [55] and Spectra fabric laminates [56]. Modified Kolsky bar setups have been used to test ceramics like silicon carbide and aluminum nitride [57-60]. Dynamic properties of cellular solids and similar collapsible structures have also been tested by Kolsky bars. Dynamic properties of aluminum based foams have been reported [61-65]. The results represented in this literature vary with some aluminum foams showing strain rate sensitivity while others do not. Properties of honeycombs have been investigated at high strain rates by Baker et al. [66] and Wu et al. [67]. The extent of the use of Kolsky bars have seen a steady increase over the years and for numerous other materials form the wide engineering spectrum. This has been clearly reflected through the overview presented by Field et al. [50].

Direct impact experiments are primarily designed to understand the macro level modifications that occur during impact. A small scale experimental setup to carry out direct impact tests is the Taylor impact setup. The experiment involves impacting a material-of-interest rod on to a rigid target plate at high velocities. By the use of high speed photography, deformations and structural modifications are observed. The Final deformation state provides additional information on damage distribution and

identification of weaker zones in the tested structure. Modifications in direct impact setups include rod on rod collinear impact experiments and rigid rod on target experiments similar to ballistics. The nature of direct impact ballistic testing differs from the traditional assumptions of direct impact experiments since both the impacting and the impacted object are susceptible to damage. Identification of failure modes in both these objects form a matter of interest unlike traditional direct impact experiments primarily focusing on one object the other being considered rigid.

Direct impact experiments have been carried out on different materials and structures. Ballistic limits of cellular honeycombs have been evaluated by impacting with rigid rods [68-71]. Analytical models that can numerically predict the failure phenomena in these structures have been presented, and continually modified over time [72-74]. Monolithic metal alloy plates have also been tested for ballistic limits by impacting with accelerated projectiles. Effects of projectile shapes, mass, hardness and composition on the ballistic limit of varying thickness metal plates have been investigated [75-78]. Results have shown significant variations with projectile shapes. This led to development of Numerical investigation of ballistic performance of these plates for comparison with experimental results [79-84]. Ballistic fabrics and related composites have also been subjected to direct impact tests to evaluate their ballistic limits [85]. Their performance has also been verified analytically and numerically through FEA [86].

To assess performance of these materials for armor applications, actual ballistic tests with rifle rounds have also been conducted. Results from these tests have been verified analytically [87-88] and numerically by using FEA [20, 46, 89-99]. Overall, through the published literature and papers it is quite evident that research groups are more inclined

in investigating these materials numerically in conjunction with conducting impact tests. FEA and numerical methods have proved to be advantageous since variations in structures and test conditions are easy to incorporate and fast. A similar approach with actual testing becomes a time consuming process. It is also not cost effective as actual experimental testing involves consecutive material usage.

Accuracy of results from FEA is variable since there are no standards to the procedure to be followed which still necessitates verification with an experimental test. However, FEA simulations have provided valuable understanding of the intrinsic behavior of materials in process of modeling their failure. Evolution in simulation codes and material failure models has improved the efficiency of FEA. Development in simulation codes has been a steady process and has resulted in different software options to carry out the numerical investigations (LS DYNA, AUTODYN, ABAQUS 6 series). With development of new materials, material models have progressed accordingly.

In the past, simple material models have been used to model the material properties of objects undergoing impact in analytical methods. Energy conservation equations and dimensional analysis were the primary modes. Shear and tensile limits were considered as damage criteria. However, material in its entire sense was not covered as strain rate dependence and adiabatic effects were largely excluded. To incorporate strain rate effects and adiabatic heating, a material model by Johnson and Cook was proposed in 1983 [100]. The model was an extension of the Von Mises criteria where in the flow stress was defined by:

$$\sigma_{\text{eq}} = \left[A + Bp^{n}\right]\left[1 + C\ln \dot{p}^{*}\right]\left[1 - T^{*m}\right] \tag{1}$$

where $A,B,C,$ n and m are material constants, $T^{*m} = (T - T_0)/(T_m - T_0)$ is the homologous temperature, where T_0 is the room temperature and T_m is the melting temperature, $\dot{p}^* = \dot{p}/\dot{p}_0$ is a dimensionless strain-rate, and $\dot{p}_0$ is a user-defined reference strain-rate. Camacho et al. [79] then modified the strain-rate sensitivity term in the above equation to avoid unwanted effects if $\dot{p}^* < 1$. The modified version of the Johnson–Cook model can be written as:

$$\sigma_{eq} = [A + Bp^n][1 + \dot{p}^*]^C[1 - T^{*m}] \tag{2}$$

In 1985, a fracture model was proposed by Johnson and Cook which estimated the failure strain for materials under different stress states, strain rate and temperature. The model equation was a five parameter based expression given by:

$$p_f = [D_1 + D_2 \exp(D_3\sigma^*)][1 + \dot{p}^*]^{D_4}[1 + D_5T^*] \tag{3}$$

where, the stress triaxiality ratio is defined as $\sigma^* = \sigma_H/\sigma_{eq}$, where σ_H is the hydrostatic stress, and D_1 to D_5 are material constants. Combination of these two equations can predict the onset and evolution of plasticity in materials and has been used in various research works focused on impact of projectiles on hard metal plates [79-81, 96]. Methods to evaluate these material parameters were described by Johnson-Cook in their publications and have been continually used till date.

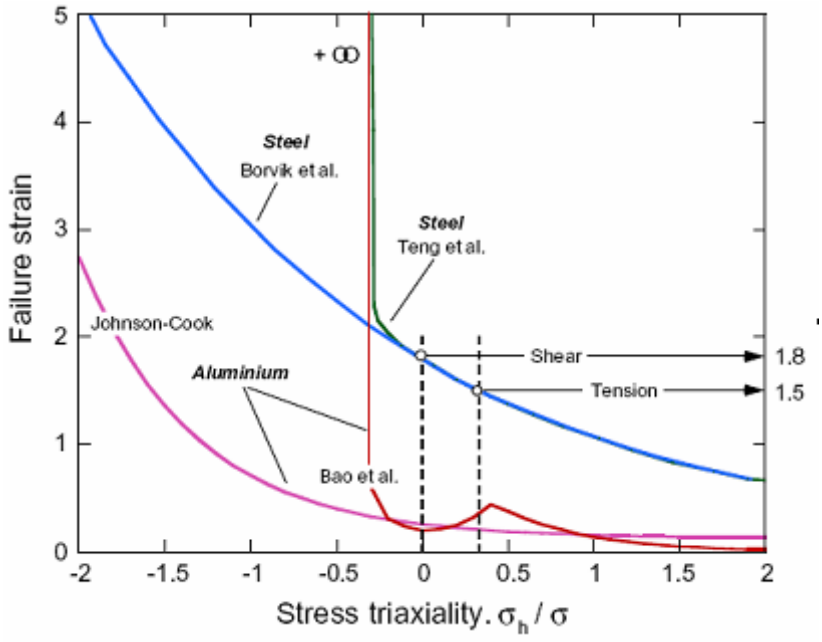

Figure 6 Sample Failure Stress vs Stress triaxiality cures used for evaluating Johnson - Cook damage parameters [84].

In case of other materials like fiber reinforced composites or fabric based composites, plasticity and damage have been modeled by using anisotropy plasticity potential function by Hill [101] and damage initiation criteria by Hashin [102]. Other models have been outlined with the latest material model for composites by Grujicic [25]. Recent damage based models include one involving extended version of material tensile failure and shear behavior by Hooputra [103]. According to this model, damage initiation in metals can be predicted by estimating the strains for ductile failure and shear failure. For ductile damage, the expression for strain is given by:

$$\varepsilon_{\mathrm{eq}}^{**} = d_0 \exp(-c\eta) + d_1 \exp(c\eta) \tag{4}$$

where, η is the stress triaxiality ratio similar to the Johnson-Cook model, and d_0, d_1, and c are material parameters. Similarly for shear damage, the dependent parameter is shear stress ratio (θ) instead of stress triaxiality. Shear stress ratio can be found by:

$$\theta = \frac{1 - k_s \eta}{\phi} \tag{5}$$

where, $\Phi = \tau_{max} / \sigma_{eq}$, τ_{max} is the maximum shear stress and k_s is another material parameter. Technically, the Johnson-Cook model can be considered as a special case of this model. The Mie-Gruneisen equation of state model that defines the pressure volume relationship depending on whether the material is compressed or expanded has also been used in conjunction with the Johnson-Cook model [104]. The Cockcroft-Latham fracture model has also been recently used for projectile impact on high strength steels by Borvik [96].

For any new design concept, the most reasonable option to evaluate its performance would be a conjunction of mechanical testing and software based FEA analysis. By selection of appropriate material models, the design performance in different interaction scenarios can be effectively verified. Modifications can be predicted if the observed results are not at par with the set constraints.

CHAPTER II

2. ARMOR PLATE DEVELOPMENT, MATERIAL SELECTION AND DESIGN SPECIFICATIONS

It is evident from the literature in Chapter 1 that designing a particular energy absorber requires thorough understanding of: (a) the application requirements and constraints, (b) field of use or work environment, (c) developments in structures and materials for these applications - their function modes, properties, pros and cons (d) necessary test procedures to evaluate pre and post design performance. This helps the designer to make selections that provide maximum efficiency and refine the choices made by continual testing. The methodology involved is thus a closed looped process.

The current study aims at illustrating the designing and testing methodology of a Hybrid-Composite-Armor plate insert prototype that provides protection against a 7.62 mm ball (.308 WIN) projectile threat as per the level III specifications by NIJ (details in section 2.1). The study is a performance evaluation of a multilayered armor design concept (using a collapsible structure sandwiched between high strength fabric laminates). In the future, this insert combined with a front impact ceramic layer will provide protection comparable to the Enhanced Small Arms Protective Insert (ESAPI) worn by ground troops. When placed in the Outer Tactical Vest (OTV) pocket of the Multiple Threat Body Armor (MTBA), the insert will provide ballistic protection from specific 5.56 mm

and 7.62 mm ball and AP rounds (similar to the currently used Interceptor). It will also have options for multiple sizes as per the standards. The procedure that was followed to make the multilayered armor insert concept is a step wise execution in accordance to the basic principles suggested by Lu et al. [7], Hazell et al. [37] and Ashby et al. [105]. The key steps that briefly describe the procedure used are as below:

1. Review: Background study on armor inserts, specifications - NIJ level III standards.
2. Role identification: Evaluation of functions, objectives, component property limits.

    Functions: - Absorber Armor Insert to suffice for NIJ level III standard,

    - Multilayered to combine advantages of different components,
    - Fabric laminate and collapsible structure for energy dissipation.

    Objective: - Maximize energy absorbed per unit volume,

    - Minimize weight.

    Property limits: - Repeatability of deformation modes of each component,

    - Irreversible energy conversion mode,
    - Constant reaction force and maximum allowable stroke,
    - Ease of manufacturing and handling, durable construction.

3. Set parameters: Evaluation of Constraints, free variables and material indices.

    Constraints: - Must have Aerial density lower than 3.8 lb/ sq.ft,

    - Must have Back Fire Signature (BFS) less than 44 mm,
    - Must have V50 of close to reference velocity or better.

    Free variable: - Thickness of the insert.

    Material Indices: - Minimum mass, Energy absorbed per unit volume (KJ/m^3)

4. Build up: Material procurement, manufacture and assembly.

5. Testing and evaluation: Mechanical testing and FEA.

In this chapter, selection of design and materials are discussed based on the application requirements. Details of the above mentioned points and the actual design are in upcoming sections. The procedure followed for testing the design concept is illustrated in Chapter 3. FEA analysis procedure (in ABAQUS 6.8.2), to support the experimental testing, is presented in Chapter 5. With the intention of familiarizing with the ballistic test procedure and FEA with first hand experience, heat treated 4130 steel plates were used as test samples. Details of the tested 4130 steel plates are also presented in these chapters.

2.1. Threat Specifications and NIJ Standards - 0101.06

The standard 0101.06 was developed for ballistic resistance of body armors (against gunfire only) by National Institute of Justice (NIJ). It is a part of The Standards and Testing Program as a basic and applied research effort to set minimum performance standards for specific devices, commercially available equipment nationally and internationally, that form a part of the body armor system. It also specifies the methods that are to be used to test their performance. Body armor models that meet the minimum performance requirements are selected for inclusion on the NIJ Compliant Products List. The tests and methods prescribed by the standard are also used by other agencies for equipment selection according to their own requirements.

The standard classifies ballistic performance according the caliber and type of projectile threat that can be defeated. Table 6 illustrates different threat specifications for testing armor. For level III armor type, the test round is a 7.62 mm NATO FMJ, 9.6 g weight. A similar round currently used is the .308 WIN 7.62 mm, 9.8 g weight. The test reference velocity of the round is 838 m/s. As per the standard specifications, for a level III armor,

a minimum 4 panels have to be tested for measuring the Back Fire Signature (BFS). BFS is defined as the greatest extent of indentation in the backing material caused by a non perforating impact on the armor. It is the perpendicular distance between two planes, both of which are parallel to the front surface of the backing material. Maximum allowable BFS for level III panels is 44 mm.

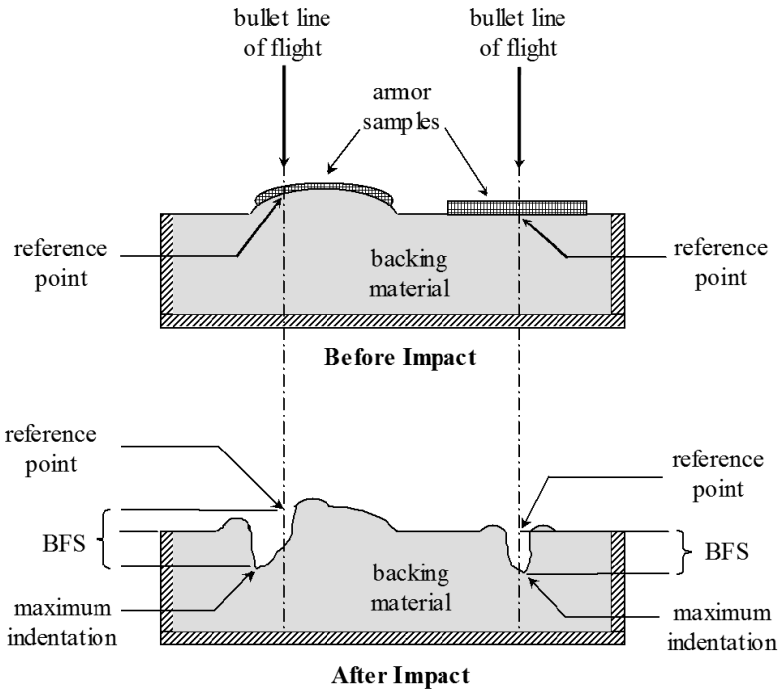

Figure 7 Measurement of BFS as stated by NIJ 0101.06.

Backing material is a substance that can closely resemble the mechanical resistance of a human body. The standard prescribes the use of Plastilina clay, a type of commercially available non-hardening oil based modeling clay generally used for ballistic testing, as a backing material. Similar materials that have seen experimental attention as backing materials for testing are as listed in Table 5. The most standard material used apart from ballistic clay is Gelatin. Being translucent, it is mostly preferred for tests where post-impact projectile investigation is a priority. Other NIJ specifications for multi-shot

testing of armor panels are: 51 mm (2 inches) shot-to-plate edge and shot-to-shot distance, test bullet velocity should be within 9.1m/s (30 ft/s) of reference (847 m/s), angle of incidence (angle between bullet line of flight and perpendicular axis to armor plate surface plane) is no greater than 5 degrees. Specifications on the test method and set up details are presented in Section 3.4 of Chapter 3.

Table 5 Comparison of commercially available backing materials [106-108].

Backer type	Materials	Elastic/plastic	Specific gravity	Relative hardness vs. Gelatin	Application
Roma Plastilina Clay #1	Oil/Clay mixture	Plastic	>2	Moderately hard	Back face signature measurement. Used for most standard testing
10% gelatin	Animal protein gel	Visco-elastic	~1 (90% water)	Baseline	Good simulant for human tissue, hard to use, expensive. Required for FBI test methods
HOSDB-NIJ Foam	Neoprene foam, EVA foam, sheet rubber	Elastic	~1	Slightly harder than gelatin	Moderate agreement with tissue, easy to use, low in cost. Used in stab testing
Silicone gel	Long chain silicone polymer	Visco-elastic	~1.2	Similar to gelatin	Biomedical testing for blunt force testing, very good tissue match
Pig or Sheep animal testing	Live tissue	Various	~1	Real tissue is variable	Very complex, requires ethical review for approval

Table 6 Threat Specifications and requirements, NIJ Standard 0101.06.

Armor Type	Test Round	Test Bullet	Bullet Mass	Conditioned Armor Test Velocity	Normal Hits per Panel	Maximum BFS Depth
II A	1	9 mm FMJ RN	8.0 g 124 gr	373 m/s 1225 ft/s	4	44 mm 1.73 in
	2	.40 S&W FMJ	11.7 g 180 gr	352 m/s 1155 ft/s	4	44 mm 1.73 in
II	1	9 mm FMJ RN	8.0 g 124 gr	398 m/s 1305 ft/s	4	44 mm 1.73 in
	2	.357 Mag. JSP	10.2 g 158 gr	436 m/s 1430 f/s	4	44 mm 1.73 in
III A	1	.357 SIG FMJ FN	8.1 g 125 gr	448 m/s 1470 ft/s	4	44 mm 1.73 in
	2	.44 Mag. SJHP	15.6 g 240 gr	436 m/s 1430 ft/s	4	44 mm 1.73 in
III	1	7.62 mm NATO FMJ	9.6 g 147 gr	847 m/s 2780 ft/s	6	44 mm 1.73 in
IV	1	.30 Cal. M2 AP	10.8 g 166 gr	878 m/s 2880 ft/s	1 - 6	44 mm 1.73 in

2.2. Ultra High Molecular Weight Poly Ethylene (UHMWPE)

After the evaluation of the Set parameters, the next step in the design procedure is the selection of materials. The focus of the design concept was to incorporate ballistic fabric laminate system to perform as a frontal absorber unit of the armor panel. Based on the literature review presented in Chapter 1, possible material choices were evaluated. As per the constraints mentioned, a fabric system having highest tenacity and in-plane stiffness, maximum energy absorption capacity per unit mass was needed.

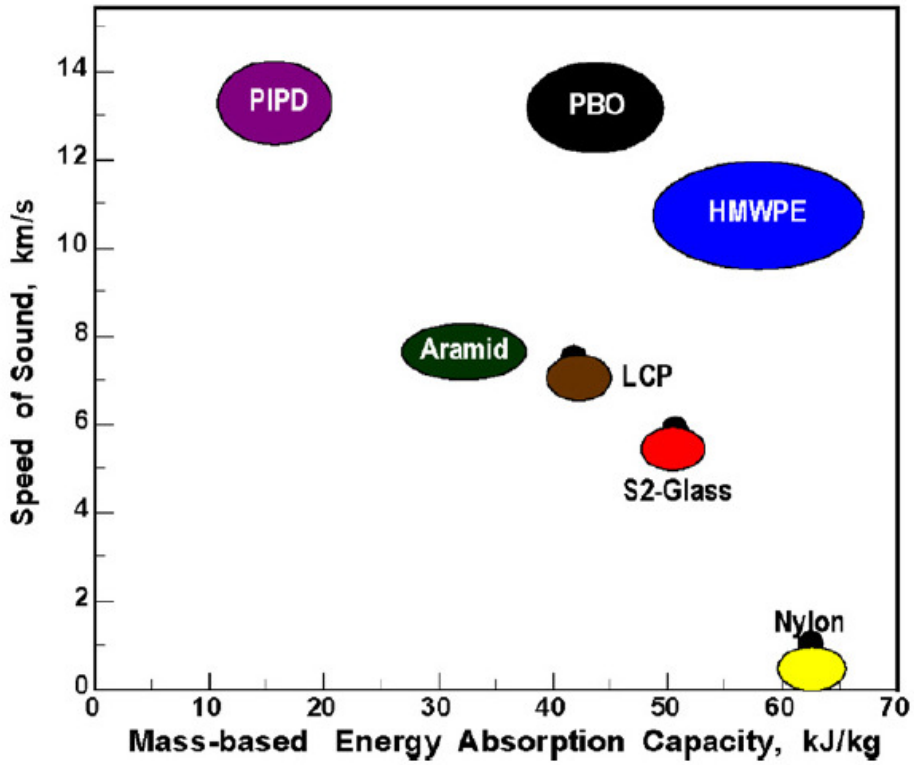

Figure 8 Comparison of material properties of fabric systems ideal for Ballistic applications, Grujicic et al. [25].

As stated by Grujicic et al. [25], the ballistic performance of these fabric systems is quantified with respect to their ability to: (a) absorb the projectile's kinetic energy locally; and (b) spread out the absorbed energy fast before local conditions for the failure are met. Numerically, energy absorption capacity per unit mass (E_{sp}) is directly proportional to failure stress (σ_{fail}) and strain (ε_{fail}) and inversely proportional to density (ρ).

$$E_{sp} = \frac{0.5\sigma_{fail}\varepsilon_{fail}}{\rho} \tag{6}$$

Also, the ability to spread out the absorbed energy is directly proportional to the speed of sound in the material and in turn to the material stiffness (E) and inversely to its density (ρ).

$$v_{\text{sound}} = \left(\frac{E}{\rho}\right)^{(1/2)} \tag{7}$$

As shown in Figure 8, the best choice of materials potentially viable for the current application would be PBO and UHMWPE. This can also be supported by the material property values presented earlier in Table 2, Table 3 and Table 4. Although PBO is a seemingly good material choice, research has shown drawbacks due to environmental degradation [109]. This favored the selection of UHMWPE fabric laminates. Commercially available brands of UHMWPE are Spectra (Honeywell Co.) and Dyneema (DSM Co.). Dyneema (SK66, HB1, and HB2) has been ballistic-tested with a proven performance [92-93, 99]. Energy absorptive capacity of Dyneema has been shown superior to Spectra Shield by Morye et al. at different temperature conditions [110]. Dyneema was chosen over Spectra for the current application. The latest available option for Dyneema as stated by DSM was HB 50. Two different sizes were procured (6 inch x 6 inch / 152 mm x 152 mm, 1 ft x 1 ft / 304 mm x 304 mm).

2.3. Amorphous Metals and Metallic Glass (MG) "Teardrop" Honeycomb

The second tier energy absorber unit for the current Hybrid-Composite-Armor plate insert prototype was selected as a collapsible cellular structure. Advantages and extensive use of collapsible structures as energy absorbing units has been discussed earlier in Section 1.1 of Chapter 1. With reference to the current application, the advantages are threefold. Firstly, due to high strength to weight ratio of these structures, considerable addition in strength along the thickness direction of the armor plate can be achieved with minimum addition in aerial density. Secondly, the collapsible structure would enable irreversible energy dissipation through plastic deformation. Thirdly, being of cellular

morphology, it enables to efficiently control the energy absorbed through a tailored plateau by governing porosity. Added advantage of tailored plateau stress is a control over reactive force and stroke. Inherent high strength, high elastic modulus, and achievable low density through porosity prompted the selection of amorphous materials as a base material for the cellular structure. Section 1.1 of Chapter 1 describes the benefits of these materials over traditional metal alloys. To further elucidate this point, consider Figure 9 which shows a plot of energy absorbed per unit volume vs. plateau stress for traditional metal foams by Ashby et al. The majority of commercially available metal foams lie in the region within 10 MJ/m^3 and 30 MPa limits.

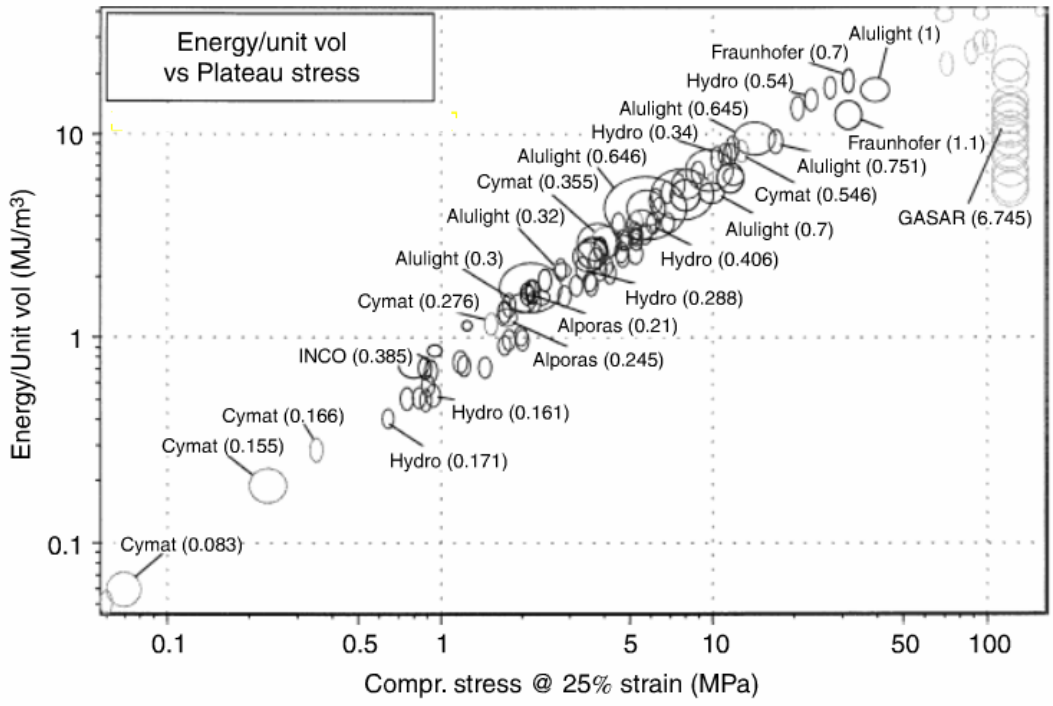

Figure 9 Comparison of energy absorbed per unit volume for commercially available metal foams, Ashby et al. [105].

As stated by Luo et al. [34] in the recent study of Pd based amorphous metal foam, the energy absorption capacity of 14.1 MJ/m^3 was achieved with a plateau of 35 MPa. Similar observation can be made from the stress strain curves of other amorphous metal

foams presented by Brothers et al. [111] proving the advantages of amorphous metals. The composition of the base amorphous metal alloy used for making the teardrop honeycomb lattice is MB2826 ($Fe_{45}Ni_{45}Mo_7B_3$). The precursor for the cellular structure was obtained as fully processed slip-cast ribbons from MetGlass Inc. The cells in the honeycomb were made from these 28 μm thick ribbons (8 mm wide) through a bottom-up manufacturing approach.

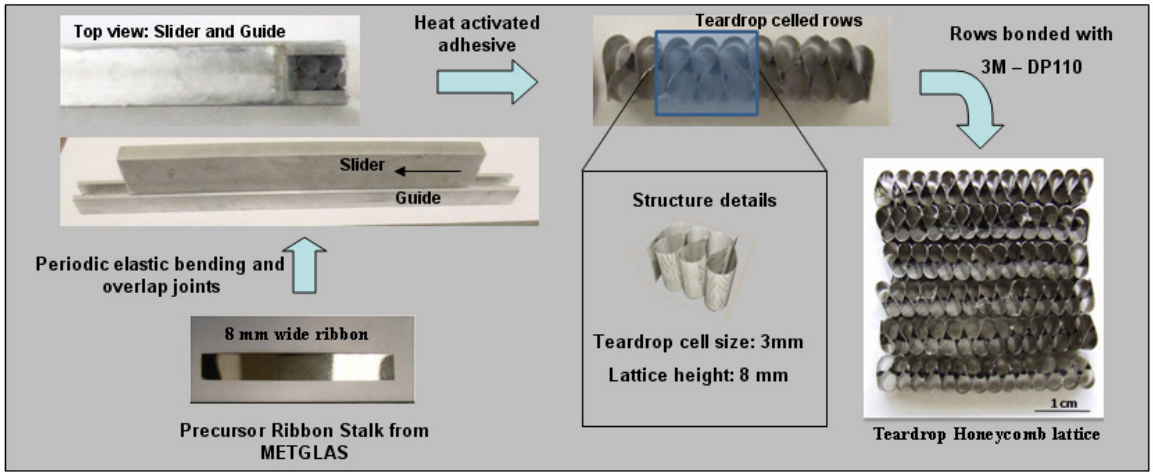

Figure 10 Schematic of step wise process to manufacture Teardrop honeycomb lattice.

Since this was the earliest attempt to incorporate an amorphous metal precursor in the manufacturing process, a thermal activated adhesive system had to be used for binding consecutive cell walls. The cell shape of a teardrop was achieved by periodic elastic bending and overlap-joints of the ribbon. Consecutive bonded cells result in a lattice row and consecutive lattice rows then bonded together using an industrial adhesive based bonding system 3M-DP110 formed the final honeycomb plate. Selection of this adhesive system was done through experimental testing of other bonding agents. Schematic of the manufacturing process is as shown in Figure 10.

The final structure has an average cell size of 3 mm with its height in out-plane direction equal to the ribbon width, 8mm. The surface area of one integrated teardrop honeycomb panel was 152 mm x 152 mm (6 inch x 6 inch).

2.4. Design Geometry

The current objective with the passive Hybrid-Composite-Armor design concept was multi hit protection against a 7.62 mm ball (.308 WIN) projectile threat as per the level III specifications by NIJ 0101.06. The key steps followed in making the insert have been stated at the start of the chapter. The ballistic insert design geometry was essentially inspired to combine advantages of collapsible energy absorbers and ballistic fabric armors that were discussed. The plate construction was envisioned as a Fabric laminate - honeycomb sandwich. Dyneema HB50 laminate was selected to intercept the projectile first (front absorber unit) and deform it, distributing the energy over a significantly large region to avoid local failures by force concentration. The function of sandwiched MG teardrop lattice was to act as an energy diffuser after partial penetration of Dyneema front layer, thereby reducing the back face deformation of the panel and resulting blunt trauma. As a final layer of protection against fragmentation, a thin laminate of Dyneema was to form the backing spall liner.

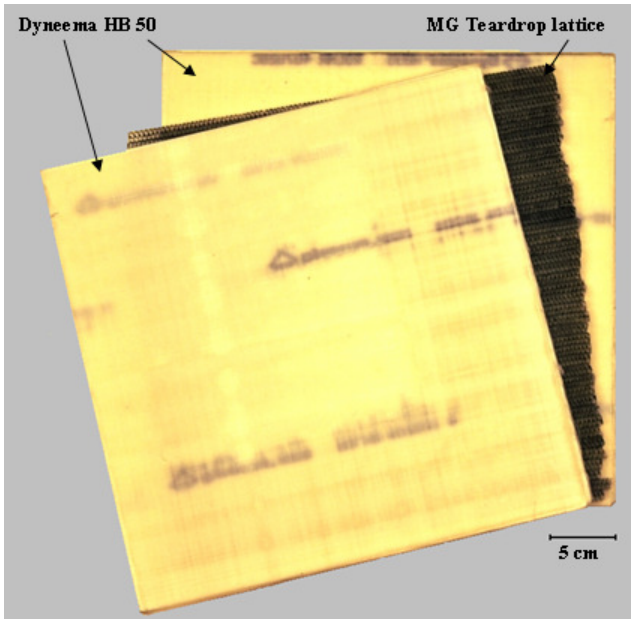

Figure 11 Sectional view of Composite armor plate construction.

The design hypothesis was: the front Dyneema layer in itself should have adequate areal density to significantly reduce the projectile kinetic energy with the remainder energy taken care of by the Teardrop lattice. This would help to limit the spread of fabric delamination damage over an area as compared to Dyneema by itself thus allowing an improved multi-hit capability. Since the thickness and other dimensions of MG lattice were fixed parameters at the initial design stage, it was decided to select the required aerial density Dyneema laminate panels based on previous research.

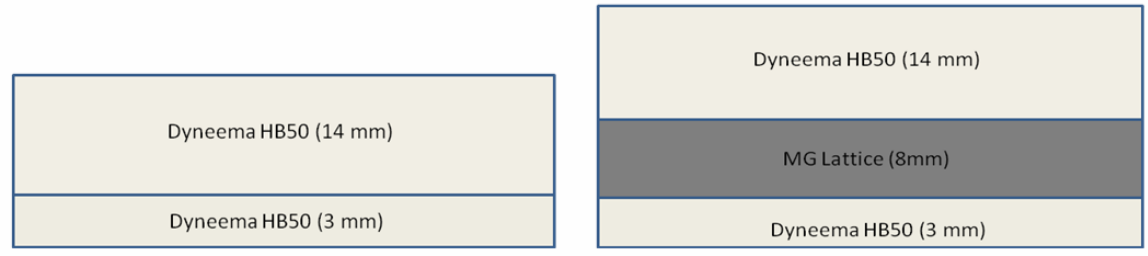

Figure 12 Schematic of cross sectional construction of Baseline plate (left) and Composite plate (right).

From ballistic test results presented by Jacobs et al. [92] on Dyneema HB2, a 16 kg/m^2 aerial density panel was able to stop a 830 m/s 7.62 NATO Ball round. In terms of thickness, a 12 mm thick Dyneema HB2 panel was capable of stopping the 830 m/s projectile. It indicated that superior quality Dyneema HB50 (12 mm thick) can also be estimated to stop it. It was decided to incorporate a factor of safety and the final front panel thickness was chosen to be 14 mm. In case of the backing spall liner layer, 3 mm thick laminate panel was selected. As mentioned, two sizes (6 inch x 6 inch / 152 mm x 152mm, 1 ft x 1 ft / 304 mm x 304 mm) were procured for both 14 mm and 3 mm thick laminates.

To bind the individual layers together 3M–DP110 adhesive system was used. Once cured the assembly was wrapped in Kevlar 49 outer liner. The Kevlar wrapping was not functionally involved in the energy dissipation process and served an aesthetic and transport convenience purpose. To compare the efficiency of energy dissipation by the Hybrid-Composite-Armor insert, a baseline plate with plain Dyneema 14 mm and 3 mm laminates was made for ballistic testing. The schematics of both these plates are as shown in Figure 12.

Figure 13 Perspective side view of the Composite plate with Kevlar wrap.

The functional areal densities of the two design plates are as mentioned in Table 7. It is to be noted that for the bigger plate (1 ft x 1 ft / 304 mm x 304 mm), 4 individual Teardrop honeycomb lattice layers had to be bonded with 3M – DP110 to form the final stage.

Table 7 Areal densities achieved post the manufacturing process.

Type of plate	Areal density (kg/m^2)	Areal density (lbs/ ft^2)
Baseline plate	15.22 +/- 0.2	3.09 +/- 0.04
Composite plate	17.37 +/- 0.16	3.53 +/- 0.03

2.5. Heat Treated 4130 Steel

Since there was no pre existing setup ready for the ballistic test of the armor panels, a new test fixture and test assembly was indigenously made (details in Section 3.4). It was necessary to ensure that the test method and the components involved for the same performed according the set standards by NIJ 0101.06. To test the efficiency of each of these components and their method of use, heat treated 4130 steel plates were used as dummy panels. Testing these plates was to provide an insight into how to calibrate the velocity measurement devices (Chronograph and High-speed camera) as well as to understand the effects of variations in test conditions on the observed results. The plates were 6 inch x 6 inch in size and were obtained in the cold rolled state from an engineering material supplier (18 in number). These plates were then subjected to a heat treatment. The objective of the heat treatment was to heat the plates above Austinizing temperature for a significant time and rapid quench to obtain the hardest Martensitic microstructure. Due to variations incurred during the heat treatment process, the end hardness values ranged from 5 HRC to 37 HRC. This had an indirect advantage since it

allowed gauging what magnitude hardness of steel was required for achieving minimum ballistic limits set by NIJ standard. Also areal density of that plate would serve as a comparison to illustrate the advantages of the Hybrid-Composite-Armor insert. Results from testing these plates would also serve a primary purpose of verifying the accuracy of FEA analysis carried out in ABAQUS 6.8.2. The material models considered for simulations were used for simulating the impact of projectiles on other steel targets by other research groups. Testing the 4130 steel plates provided key information on how to adapt the material codes and contact model parameters to map the deformation behavior of projectile materials as well other target materials that show anisotropy.

CHAPTER III

3. MECHANICAL TEST METHODS

The methods described in this section are the standard procedures recommended to test energy absorptive structures and their individual components. As described in Section 1.3 of Chapter 1, the nature of these tests varies with the end objective to be achieved. Three different tests are described: (a) Direct impact Ballistic tests of armor plates according to the pre stated NIJ standards with post impact NDT testing, (b) Quasi-static testing of the MG Teardrop honeycomb to evaluate its anisotropic properties and of a cylindrical section from bullet projectile to evaluate its bulk properties, (c) Dynamic testing to set up a standard method that can be followed to test MG Teardrop honeycomb for strain rate dependence. Results obtained from these tests are to serve as inputs for the FEA simulation material models in ABAQUS 6.8.2. The process of converting the observed stress strain response into material parameters is described in Chapter 4.

3.1. Ballistic Testing

The primary performance evaluation experiment undertaken to gauge the Hybrid-Composite-Armor plates was ballistic testing. As stated before, the test configuration and method was according to the standards specified for a level III armor insert in NIJ 0101.06. The tests were conducted over a span of 11 months, gradually, as the earlier

prototypes of the design concept were regularly improved with gain in experience. The tests were conducted at the courtesy of DSM testing range (North Carolina), US Shooting Academy (Tulsa, OK), Tulsa Fire Arms (Tulsa, OK), Stillwater Shooting range (Stillwater OK). In all, three different types of plates were tested. Namely: Heat treated 4130 steel plates, small baseline and composite plates (6 inch x 6 inch), big baseline and composite plates (1 ft x 1 ft). The projectile selected for testing the plates was a .308 WIN 7.62 mm FMJ round (9.8 g weight), equivalent of the 7.62 mm NATO FMJ (9.6 g weight) that NIJ suggests. Few tests were also conducted by a heavier version .308 WIN 7.62 mm FMJ Wolf round (Russian made). Being the first attempt to conduct ballistic testing, the entire set up was indigenously developed. Two separate fixtures were used in the first few tests. The later tests were conducted using a Plastilina ballistic clay backing.

The ballistic test arrangement was according to the details stated by NIJ for a valid test. Schematic of the arrangement followed in all of the ballistic tests that were carried out is as shown in Figure 14. The gun barrel to target distance was 15 m (49.2 ft). Velocity measurement was done using a standard CED M2 chronograph placed at a centre-to-target distance of 2.5 m (8.2 ft). For cross referencing the velocities and monitoring deformation, a high speed camera setup was placed at an angle to the target face at an approximate distance of 3 m. In situations of low visibility, high intensity lamps were used.

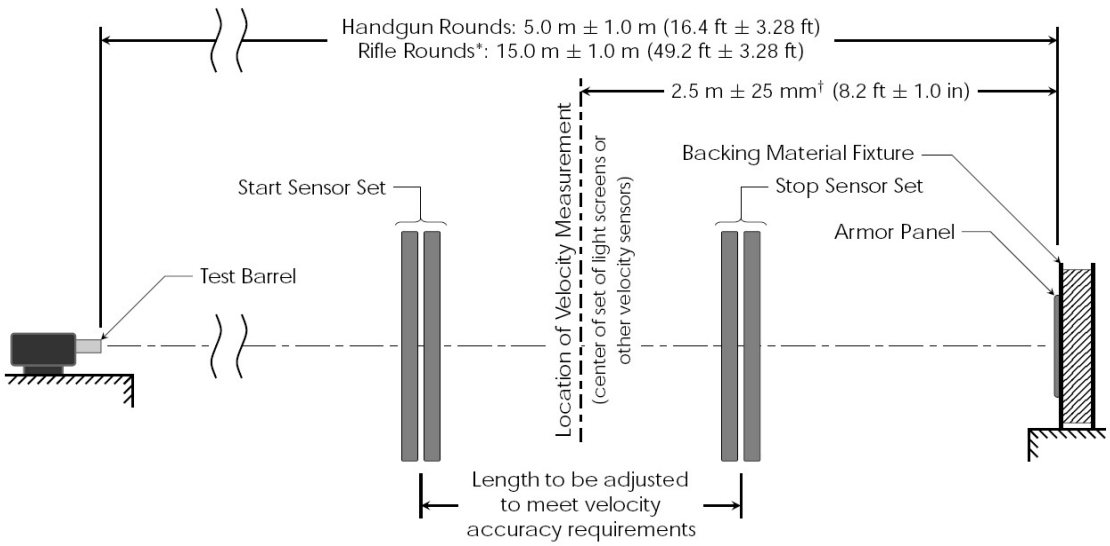

Figure 14 Schematic of test equipment arrangement used for ballistic testing as per NIJ 0101.06.

The backing layer clay box was fabricated as per the specifications mentioned in the NIJ standard 0101.06 with a wooden frame of 2 ft x 2 ft holding tightly packed ballistic Plastilina clay. The clay had to be thermally softened using ovens to give it adequate plasticity in order to achieve good dimensional tolerance. Mounting of the plates on this clay box backing layer was done using Velcro straps. The setup was adequately rigid to maintain uniformity and repeatability in tests. The images of the setup are as shown in Figure 15.

Figure 15 Mounting of plates on clay backing using Velcro straps.

Figure 16 shows the final assembly with the chronograph positions. The setup was again as per the NIJ standards (no specifications for camera placement). For testing small baseline and composite armor plates, a wooden rigid framework was used. The setup was modified to a steel framework for testing the heat treated 4130 steel plates essentially pinning the plate edges firmly (Figure 16).

Figure 16 Perspectives of Rigid steel frame setup to test 4130 plates with front and back chronograph.

BFS measurements were done on plates with partial penetration. For small plates, BFS measurements were based on the dimensions of the actual back bulge. For big plates, BFS readings were taken from the clay backing layer as mentioned in Section 2.1 of Chapter 2. No BFS readings were taken on 4130 steel plate targets.

V50 is another ballistic parameter that defines the plate performance. It is the velocity at which the armor panel can stop 50% of the bullets. From the later conducted ballistic tests at the DSM facility in North Carolina, where as per NIJ standards 4 similar composite plates were shot, velocity measurements for complete and partial penetration were plotted against probability of penetration (complete penetration: 0, partial penetration: 1). The V50 was calculated by plotting the corresponding velocity values with the probability of penetration in a Sigmoidal or Logistic function plot. The Armor

panels tested had the same configuration and thus the V50 calculated was based on the generic behavior. The curve equation can be defined by:

$$y = \frac{1}{1 + ce^{-kx}} \tag{8}$$

The time and location of all the ballistic tests that were conducted is presented in Table 8.

Table 8 Summary of ballistic tests conducted.

Date of testing	Testing venue	Types of plates	Total Number of plates	Ballistic test set-up
10/06/2008	US Shooting Academy Tulsa Oklahoma	Baseline and Composite Armor	3	No Ballistic Clay used
09/26/2008	US Shooting Academy Tulsa Oklahoma	Composite Armor	1	No Ballistic Clay used
04/03/2009	US Shooting Academy Tulsa Oklahoma	4130 Steel Plates	22	Rigid Steel Frame
06/19/2009	Tulsa Fire Arms Tulsa Oklahoma	Baseline and Composite Armor	2	Ballistic clay used as backing layer
07/17/2009	US Shooting Academy Tulsa Oklahoma	Baseline Plate insert	1	Ballistic clay used as backing layer
08/25/2009	DSM Testing Range North Carolina	Baseline and Composite Armor	5	Ballistic clay used as backing layer

Post ballistic testing, the shot plates were observed for deformation distribution and prediction of failure modes using a CT scan. Other motive for conducting the NDT was to categorize plate performance according to the extent on bulging resulting due to partial penetration. Numerical values obtained could then be used to gauge the accuracy of results obtained from FEA analysis in ABAQUS 6.8.2. Efficiency of the selected material models for simulations could also be checked from the extent of damaged zone from

NDT and from simulations. CT scans were carried out at Servant Medical Imaging in Stillwater, OK.

3.2. Quasi-static Behavior Evaluation

The objective of carrying quasi-static tests on servo hydraulic machines was to evaluate the elastic and plastic material properties of three materials, namely: MG Teardrop lattice, heat treated 4130 steel and lead core from the projectile used for testing. Evaluation of these properties would not only provide first hand information on the failure characteristics of each material but also serve a main objective of numerical input values for the desired material models in ABAQUS simulations.

Since the MG teardrop lattice is anisotropic in nature, separate tests to evaluate in-plane and out-plane properties had to be conducted. For out-of-plane compression tests, ASTM C365/C365M-05 ("Standard test method for Flatwise Compressive properties of Sandwich Cores") was followed. The tests were carried out on an UTS INSTRON series 5582 at a strain rate of 2×10^{-3} /s. The strain was measured from the cross head displacement of the machine and resultant data was corrected for the machine compliance. Sample sizes were in accordance to the standards by ASTM. Similarly, for the in-plane directions, ASTM C364/364M-07 – "Standard test method for edgewise compressive strength of Sandwich constructions" was used. Sample sizes were again as per the ASTM specifications. Tests were conducted at the same strain rate. The results were corrected for compliance. Elastic modulus, Poisson's ratio, Yield stress and fracture stress - strains were evaluated from the stress - strain curves.

Quasi-static properties of heat treated 4130 steel were to be evaluated in accordance to the methodology and theory specified by Johnson and Cook [100]. The procedure of the

tests involves tensile testing of non-notched and notched specimen of the desired material at an arbitrary set strain rate which is constant for all tests. By testing the non-notched specimen, values of strain hardening constants *B* and *n* can be evaluated from the stress - strain curve. The value of failure strain from this test would correlate to a stress triaxiality ratio of 0.333. The notched samples were machined to incorporate circular radial notches of varying diameters. The sample dimensions were in proportion to those specified by Borvik et al. [81]. An artificial notch produces an initial triaxiality different from that in the smooth specimen where triaxiality initiates only after necking. Correlation of notch radius and resulting maximum stress triaxiality ratio σ^*_{max} is given by Bridgman's relation:

$$\sigma^*_{\max} = \frac{1}{3} + \ln\left(1 + \frac{a}{2R}\right) \tag{9}$$

where, a is the radius of specimen in the neck region and R is the notch radius. Three notch radii were considered for test, namely 2, 0.8 and 0.4 mm. The sample geometries are as illustrated in Figure 17. From the results obtained in the form of stress strain curves, failure strains are to be correlated with the corresponding triaxiality ratio. The resulting stress triaxiality vs. failure strain plot is used to evaluate the D_1, D_2, D_3 and D_4 parameters of the Johnson-Cook dynamic failure equation. Since adiabatic effects are neglected for the current study, D_5 is assumed to be zero.

To evaluate material properties of the impacting projectile, compression test was conducted on a cylindrical sample cut from an actual round using a diamond saw. The sample dimensions were 13.8 mm length and 7.62 mm diameter. The compression test was carried out at a strain rate of 5 x 10^{-3} /s. The results from the test were compliance

corrected and the elastic modulus and the Johnson-Cook strain hardening coefficients were calculated from the stress - strain response.

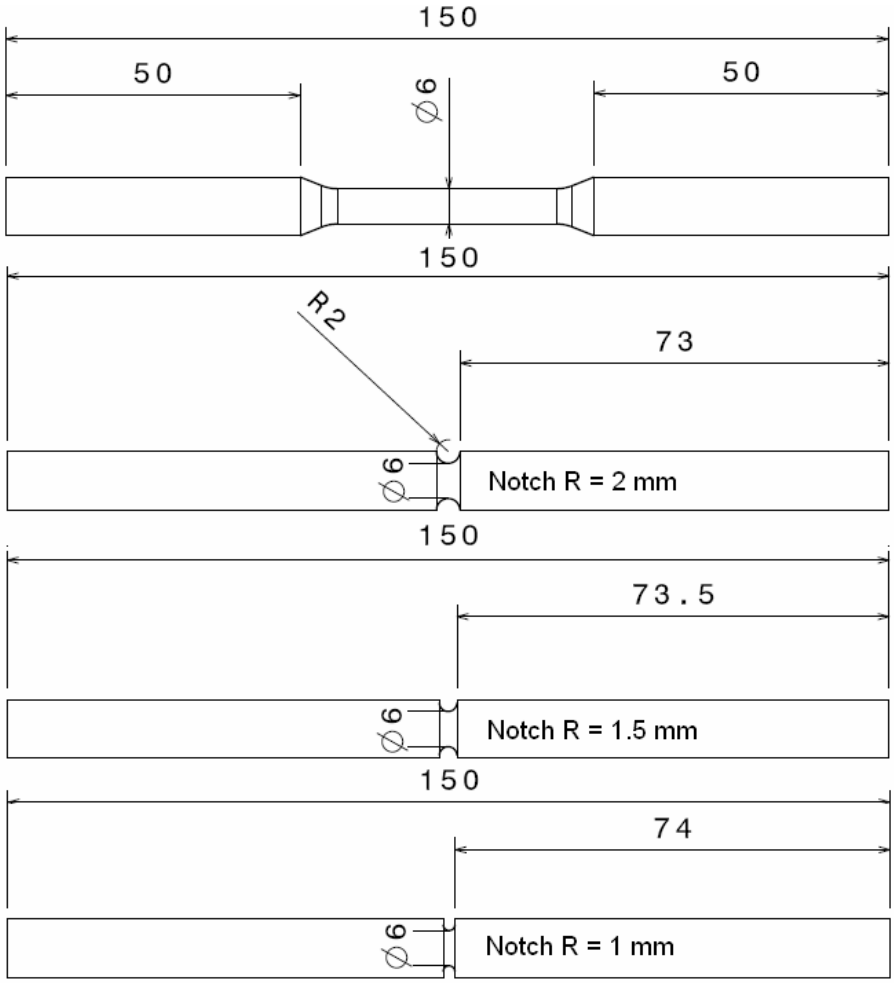

Figure 17 Tensile specimen geometries for evaluation of Johnson-Cook parameters.

3.3. Dynamic Behavior Evaluation

The objective of dynamic tests was to test the strain rate effects in low impedance materials like amorphous cellular structures and to establish a process for testing the same. Unlike traditional quasi-static tests, dynamic tests carried out using Kolsky bar / SHPB are very material specific. Hence no standards are available that can be followed to carry out tests. It is thus imperative that a test method had to be verified so it could be applied to similar nature materials and set individual standards for all components

involved in the test. A dynamic compression test was carried out for this purpose was on 82% porosity amorphous metal foam. The composition of the skeletal amorphous alloy used to make the foam samples was $Pd_{43}Ni_{10}Cu_{27}P_{20}$. It is envisioned that the test standards set by this experiment can also be applied to test the 82% porosity Teardrop honeycomb lattice to evaluate its dynamic properties. The literature review behind selection of individual components listed here for the test are presented in detail by Luo et al [34]. Test samples were cylindrical with diameter of 17.3 mm and height of 8 mm. The schematic diagram of the SHPB apparatus used is shown in Figure 18.

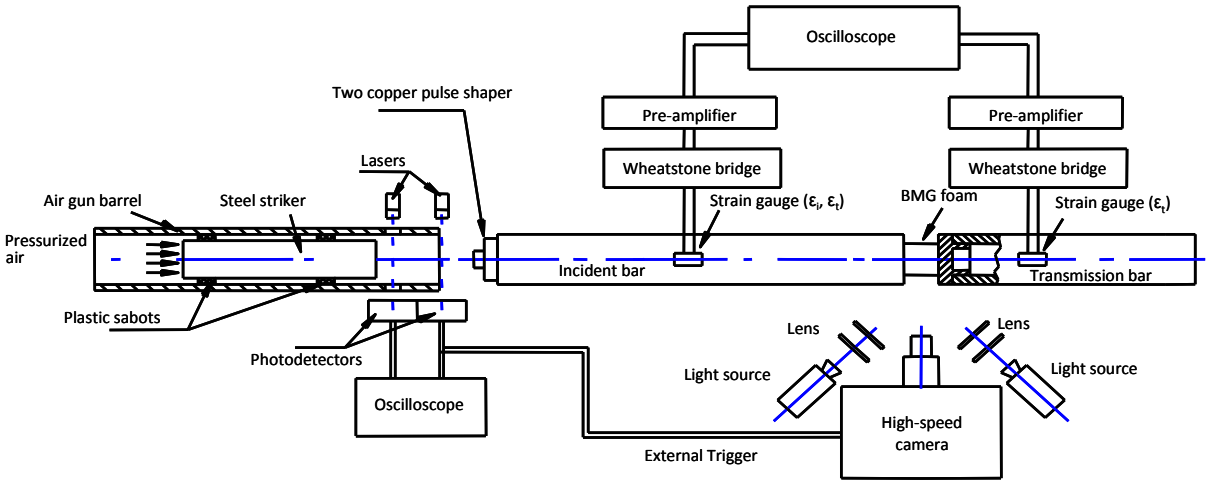

Figure 18 Split Hopkinson Pressure Bar setup used to test amorphous metal cellular structures.

A hollow transmission bar was used to obtain a better signal-to-noise ratio for the low impedance material with a reduced cross sectional area. The incident, transmission bars and striker bar were made from 304L steel and had lengths 7514 mm, 4049 mm, and 1219 mm for, respectively. The common outer diameter was 19 mm and inner diameter for the transmission bar was 14.1 mm. A pneumatic valve was used to control the compressed air to launch the striker bar. Confinement was performed using a copper tube

to contain otherwise coated material in order to simulate the effect of an infinite plate. The inner diameter of the confining copper tube was 19.9 mm. The 1.45 mm gap between the inside of copper tube and foam was filled by epoxy bonded alumina powder composite (mixture elastic modulus was 2 GPa approximating to the observed foam modulus from the quasi-static tests). A strain gage was mounted on the center surface along the hoop direction to measure the confinement pressure for strain history as platen displacements could not be measured by direct vision high speed camera method. However, since the Teardrop honeycomb sample can be made bigger, this test setting can be modified and measurements can be taken with a Cordin 550-62 high speed camera (62 color frames, 4 million frames per second maximum, 10-bit resolution CCD with 1000×1000 pixel frame) with a rubber speckle pattern on the sample side.

At the end of the transmission bar, in contact with the specimen, a hard tool steel end cap was press-fit into the hollow tubing to support the specimen. Two copper pulse shapers stacked together were used to facilitate dynamic stress equilibrium and a constant strain rate over a sustained period. Similar pulse shaping method can be incorporated for the Teardrop honeycomb however their dimensions would have to be re-evaluated. Two WK-13-125BZ-10C strain gages (2.08 gage factor) were mounted on opposite faces at the same longitudinal location of the two bars. A Nicolet Sigma-30 digital oscilloscope (12-bit resolution and 10Ms/s sampling rate) was used to acquire the strain signals on incident and transmission bars through a Wheatstone bridge and a Vishay 2310A signal conditioning amplifier.

The compressive stress, σ_s, in the specimen sandwiched between the incident and transmission bars was calculated from the transmission bar signal using:

$$\sigma_s(t) = \frac{A_t}{A_s} E_0 \varepsilon_t(t) \tag{10}$$

where, As and At are the cross sectional area of the specimen and transmission bar, respectively; E_0 is the Young's modulus for the bars and ε_t is the strain of the transmission bar. The strain rate was deduced from both the incident signal and the reflected signal on the incident bar:

$$\dot{\varepsilon}_s(t) = \frac{c_0}{L_s}\left[\left(1 - \frac{A_i}{A_t}\right)\varepsilon_i(t) - \left(1 + \frac{A_i}{A_t}\right)\varepsilon_r(t)\right] \tag{11}$$

Where, c_0 is the bar wave speed; L_s is the length of the specimen; the subscripts *i* and *r* represent incident and reflected, respectively. Integration of strain rate with respect to time gives the strain history. With the known stress and strain history, dynamic stress-strain curves were obtained. The most important step in the experiment was to check if the dynamic stress equilibrium was achieved. Also care was taken to verify no dispersion effects took place and frictional losses were minimal. Similar steps are extremely important for testing Teardrop honeycomb lattice.

CHAPTER IV

4. EXPERIMENTAL RESULTS AND DISCUSSION

The motivation for conducting the mechanical test experiments have been discussed in the previous chapter. In this chapter, based on the observed results from these tests, inferences are drawn and numerical parameters are evaluated. Comparisons between these parameters are presented and discussed in detail. Based on the information obtained, possible future steps are described.

4.1. Observed Results from Ballistic Tests

Details of all the ballistic tests and locations are mentioned in Table 8. The initial tests were carried out on small plates (152 mm x 152 mm / 6 inch x 6 inch) of both baseline and composite armor configurations (conducted on 6/10/08 and 9/26/08). The plates were tested using a rigid wooden frame work for support with no clay backing. Both testes resulted in complete penetration in all the plates. These earlier tests were conducted to validate the proof of the proposed concept and were not conducted under comprehensively equipped testing conditions. It is estimated that the smaller size of the plates and non complaint backing resulted in edge effects and caused complete penetration. However, these tests yielded useful information on test conditions like temperature, humidity, perfectly scale projectile velocity, and calibration of measurement

equipments. The next test was carried out using a ballistic clay backing layer as per standards (conducted on 6/19/09). The plate size was big (304 mm x 304 mm / 1 ft x 1 ft). The plates showed complete penetration for both configurations. Velocities recorded from chronograph indicated a faster round (similar to .308 WIN 7.62 mm Wolf). This indicated that several factors severely affected the accuracy of the conducted tests and control on conditions was very imperative.

The tests carried out on 7/19/09 resulted in a successful test with a baseline big plate configuration successfully defeating the projectile. This test was conducted with clay backing and customized rounds with measured charge quantities to accurately travel at selected velocities. The recorded velocity was 2560 ft/s / 805 m/s by the chronograph. The averaged out BFS reading from the clay was 32.5 mm. NDT analysis was conducted on this plate (details in section 4.2). Similar tests were carried out on 5 other plates (1 baseline, 4 composite) of big size at DSM range in North Carolina. The observed results for successfully defeated shots are as shown in Table 9 and Table 10.

Table 9 Observed results from ballistic test of Baseline plate at DSM range.

Baseline plate **Shot number**	**Recorded Velocity** **(ft/s)**	**Observed BFS** **(mm)**
1	2598	48.5
2	2637	42.4
3	2663	45.3
4	2586	35
Average	**2621**	**42.8**

Table 10 Observed results from ballistic test of Composite plate at DSM range.

Composite plate Shot number	Recorded Velocity (ft/s)	Observed BFS (mm)
1	2703	36.5
2	2716	28.0
3	2600	36.3
4	2733	34.5
5	2741	35.0
6	2775	34.8
7	2602	33.6
8	2594	33.3
9	2648	33.2
10	2615	31.0
Average	**2672**	**33.6**

As stated earlier, the big plates were made by adhesively bonding four 152 mm x 152 mm quadrants, which results in a seam running transversely from one edge centre to another. All of the shots listed in Table 10 were on the central or close to central zone of the honeycomb lattice quadrants and hence successfully defeated. It was seen that all shots that were near the seam zone were not stopped and resulted in complete penetration. Clear difference in the non seam shots and seam shots is seen in the NDT analysis presented in section 4.2. The 16.8 kg/m^2 average areal density baseline plates resulted in an average BFS of 42.8 mm for 2621 ft/s average velocity. In comparison, for a higher average velocity of 2672 ft/s, the composite plates exhibited a reduced average BFS of 33.6 mm. The difference is as shown in Table 11.

Table 11 Difference in average ballistic performance between baseline and composite plates.

Type of Plate	Areal density (Kg/m^2)	Average Velocity (ft/s)	Average BFS (mm)
Baseline plate	16.80	2621	42.8
Composite plate	18.98	2672	33.6
Difference	**2.1**	**51**	**9.2**

It is evident that for a 13 % increase in areal density by incorporation of Teardrop honeycomb layer between Dyneema HB 50 laminates, a 24% reduction in BFS can be achieved. This clearly projects the advantages of the current design concept where in a collapsible structure combined with a high strength ballistic fabric laminate can improve the ballistic performance. As per the NIJ standards stated in Table 6, a total of 4 Hybrid-Composite-Armor design plates were subjected to ballistic testing for a level III setup and resulted in an average BFS of 33.6 mm (< required 44 mm). To estimate the reference velocity, a V_{50} calculation was done with the details from all seam and non seam shots. The information was graphically represented using a Sigmoidal function discussed earlier. The resulting plot is as shown in Figure 19. From the plot for a 50 % probability of penetration, the corresponding velocity is 832 m/s. This V_{50} velocity is fairly close to the desired 838 m/s for a .308 WIN 7.62 mm, 9.6 g projectile.

The Hybrid-Composite-Armor insert can thus be stated to have passed the requirements for the level III armor plate standards. Combination of this insert with a SiC ceramic front impact face is a viable choice for future tests.

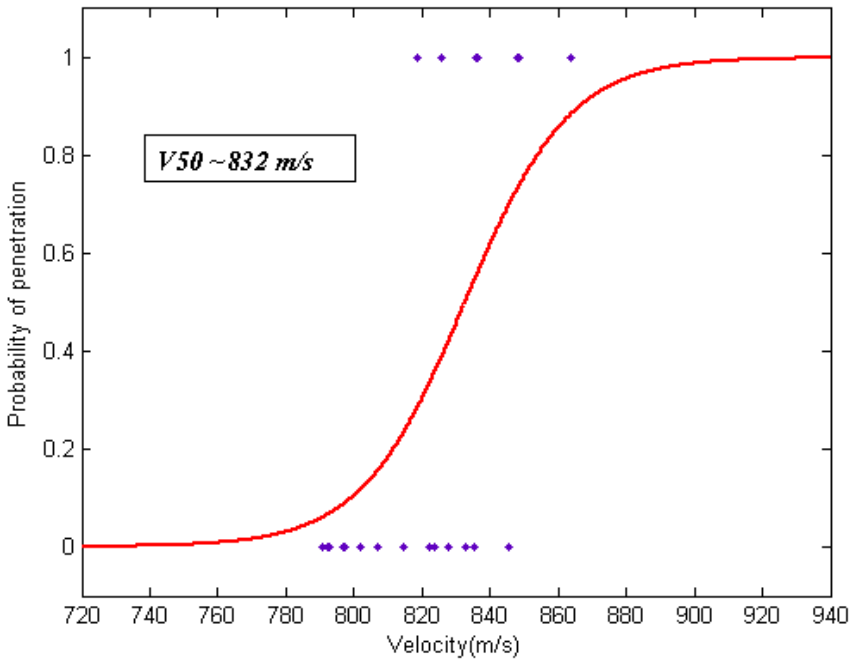

Figure 19 Calculation of V50 velocity for the composite armor plate.

From the tests carried out on heat treated 4130 steel plates, a low success rate was observed. Out of the 18 tested plates, only 4 were capable of defeating the projectile. From the information presented in Table 12, it is clear that majority of the plates lying in the surface hardness range of 20 HRC - 30 HRC were not successful in stopping the bullet. Amongst the 4 plates that stopped the bullet, the average impact velocity was 2645 ft/s with average surface hardness of 32 HRC. The heat treatment used to for these plates involved heating the plate to 900 °C for an average 1 hour and then rapid quenching in an ice - water mixture at roughly 5 ° C. Similar procedure would be applied for heat treating the notched and the non-notched 4130 tensile samples to evaluate Johnson-Cook parameters. These parameters would be then used to simulate an FEA model of projectile impacting steel plate at 2645 ft/s and test results would be used to compare the FEA response of simulations.

Table 12 Observed ballistic results for heat treated 4130 steel plates.

Plate Group	Surface Hardness (HRC)	Impact Velocity (ft/s)	Residual Velocity (ft/s)	Plate Group	Surface Hardness (HRC)	Impact Velocity (ft/s)	Residual Velocity (ft/s)
A	30	2668	1707	**J**	31	2668	-
B	22	2611	1604	**K**	21	2599	1519
C	19	2618	1506	**L**	37	2684	-
D	25	2631	1604	**M**	35	2600	-
E	24	2666	1723	**N**	5	2670	1305
F	25	2631	1604	**O**	18	2612	1686
G	20	2587	1669	**P**	36	2645	1367
H	25	2653	1637	**Q**	22	2598	1536
I	31	2655	1469	**R**	23	2626	-

4.2. Post Impact NDT and Damage Evaluation

The baseline plate shot on 7/19/09 and other plates shot on 8/25/2009 were taken to Servant Medical Imaging for conducting CT scans. The scanning was done to determine the extent of damage and failure modes observed in Dyneema HB50 from the baseline plate. Composite plates were scanned to evaluate the intrinsic damage sustained by the Teardrop honeycomb for weak zone identification. Bulge heights from shots with partial penetration were calculated to compare the plate performance. Following sequence of cross-sectional CT images in Figure 20 illustrate the scan results through the thickness of the baseline plate. The sequence initiates with the outermost slice on the top continuing progressively downwards as we move towards the point of impact on the plate.

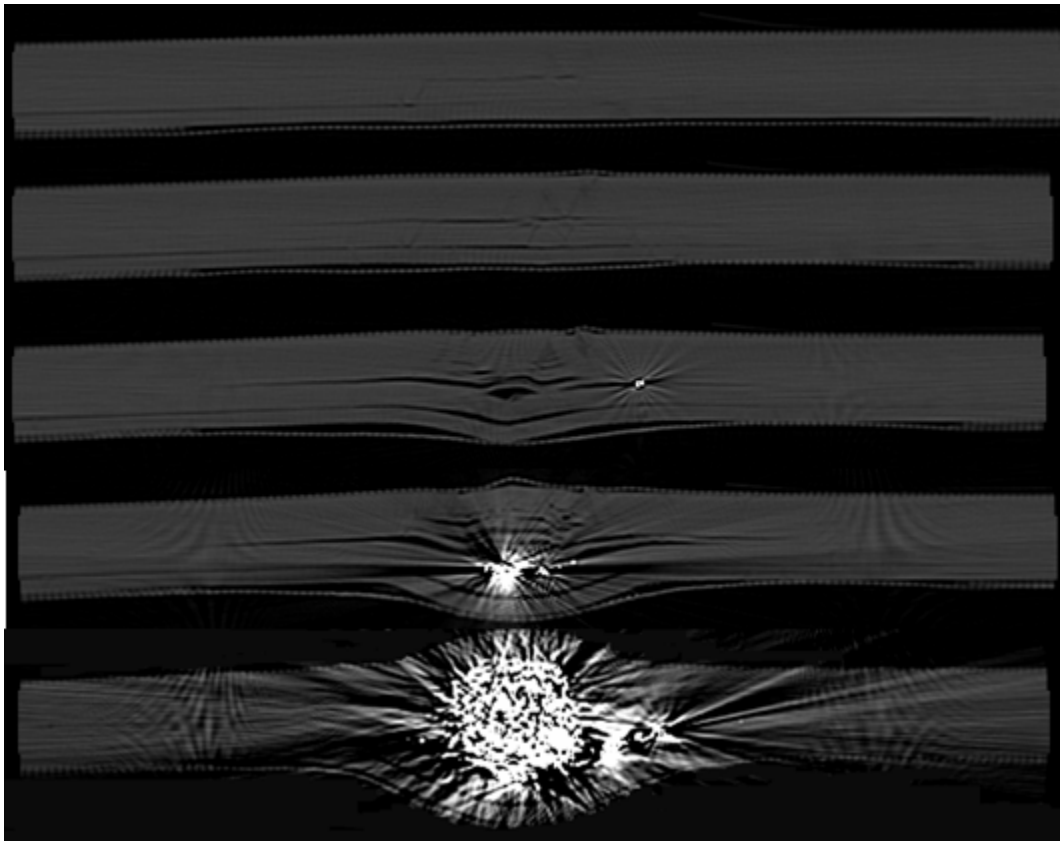

Figure 20 Cross - sectional slices showing progressive damage traversing along the length towards the point of impact from the outermost edge (top to bottom).

The slices clearly indicate the pattern of delamination whose magnitude increases as we move towards the impact zone. Transverse layer separation is primarily seen approximately at the centre of the 14 mm Dyneema plate and also at the interface zone of the 14mm and the 3 mm Dyneema layers. General observation and the CT scan imaging suggests the fracture and damage modes that are generally observed for fabric composites, (i) brittle shear at contact surface due to force localization (ii) sequential delamination in the successive layers, (iii) combined fiber elongation / pullout and fiber tensile failure. In the cross-plied laminates, fibers in the top plies are typically found to shear along the edges of the projectile. Similar observations have also been stated by

Grujicic et al [25]. Lowermost fabric layers located in the back layers of the laminates give a slight indication of generator strip failure mode. Image slice 4 from the top roughly indicates that the bullet was trapped within the 14 mm Dyneema layer itself. This proves that the hypothesis considered while selecting the thickness of front Dyneema HB 50 laminate was correct. The 3 mm backing Dyneema layer had no actual contact with the projectile and hence the damage in that layer is purely of the tensile and accompanied delamination type.

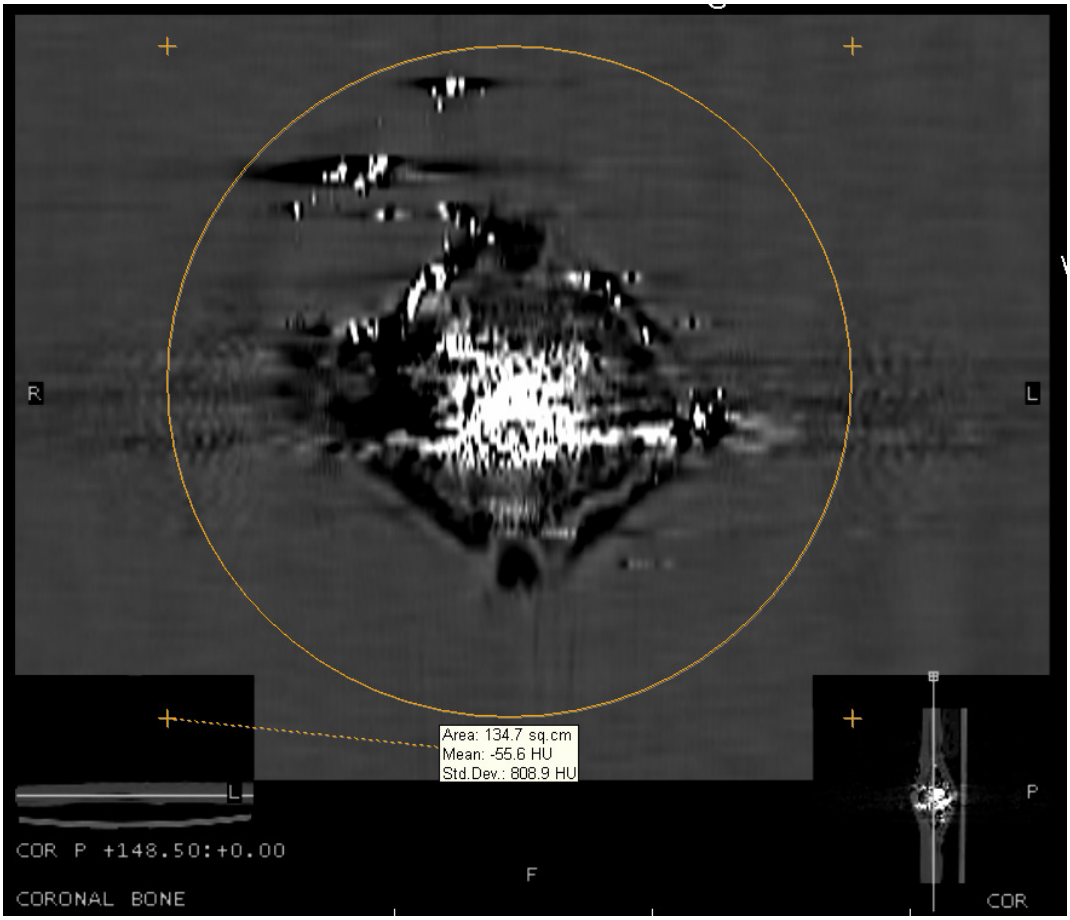

Figure 21 Extent of damage observed in the baseline plate with images on the lower right and left showing the position of this slice in the plate.

Another motive was to evaluate the actual spread or extent of bullet fragmentation within the plate to give an approximately estimate of damage distribution. Figure 21 illustrates

the maximum spread of the damaged region. The scan is at a cross ply approximately 7 mm from the plate base. The spread of the bright spots indicates the zone within the plate where bullet fragmentation is evident. The fragmentation was in an approximate circular region of radius 65.4 mm (approximate area: 134.7 cm^2).

From the observation of the back face bulge dimensions it was observed that it matched very closely with the recorded BFS of 32.5 mm. The 3D volumetric reconstruction of the plate is shown in Figure 22.

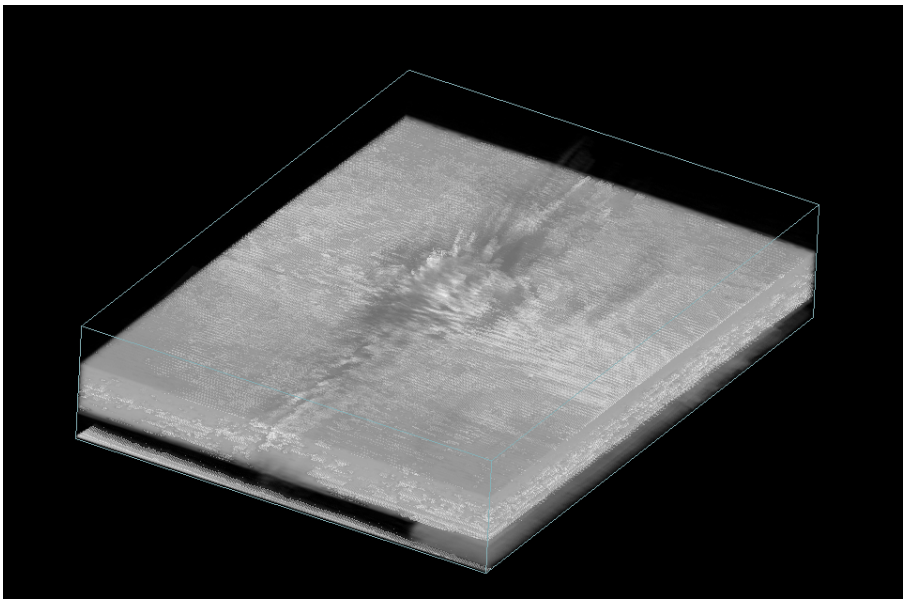

Figure 22 3D volumetric reconstruction of the baseline plate from CT scan slices.

In order to have a comparison with results from ABAQUS simulations in the future, the volume was cropped to a symmetric quadrant (Figure 23). The extent and nature of damage observed in the cropped quadrant will help to analyze the accuracy of the material parameters and input variables in the future ABAQUS simulations and also help to predict the necessary modifications. Test methods used to obtain these parameters can thus also be verified.

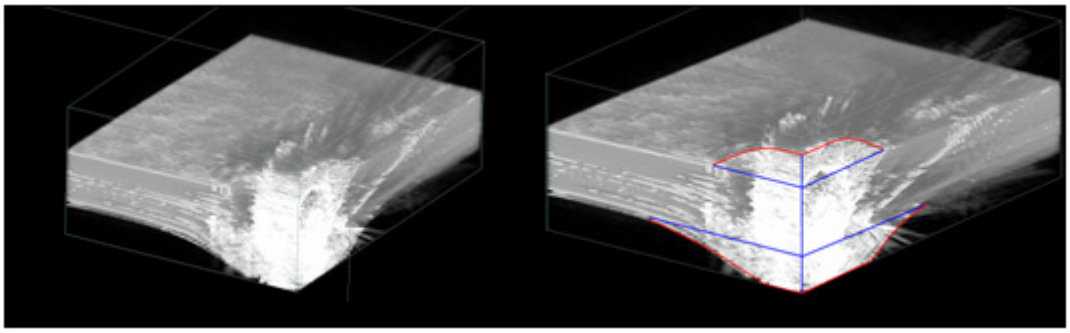

Figure 23 Cropped quadrants to be used for comparison with simulation results in the future.

CT scanning of composite armor plates was also done similar to the baseline plates. Figure 24 shows the reconstructed 3D volume of a composite plate that was shot 9 times. The plate was capable of defeating 4 shots all of which were deduced to be in the non seam region. The 5 shots close to the seam of the Teardrop honeycomb resulted in complete penetration.

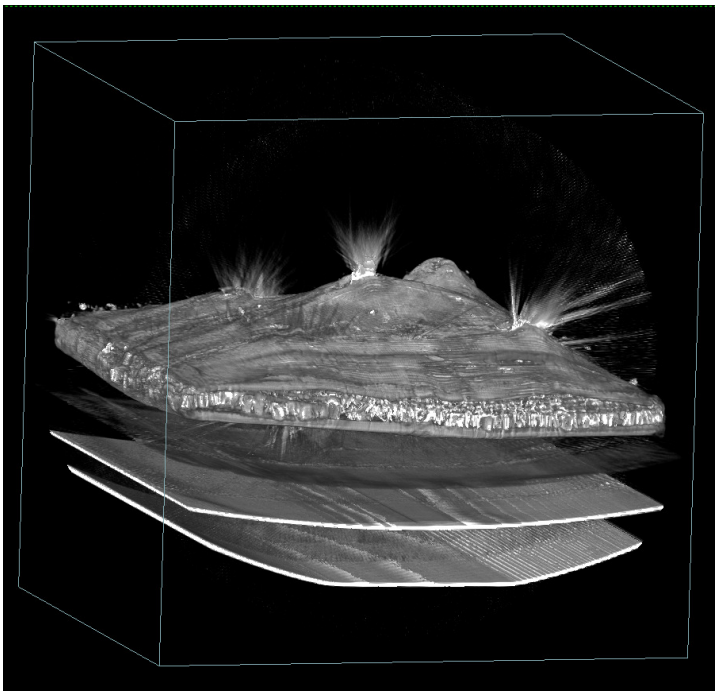

Figure 24 Volumetric Image constructed from a Computer Tomography showing 9 bullet shots.

To estimate the area influenced directly by bullet fragmentation, a transverse pan was done along the reconstructed images. Using an area map tool, sizes of the damaged zones were estimated. Figure 25 illustrates a transverse slice along a composite plate that was shot 4 times at the centre of each honeycomb quadrant. It was seen that the average size of the damage zone was less than 134.7 cm^2 which was measured in the baseline plate. This also proves the design hypothesis of delamination damage reduction in fabric laminate plate by shared energy dissipation with the Teardrop lattice.

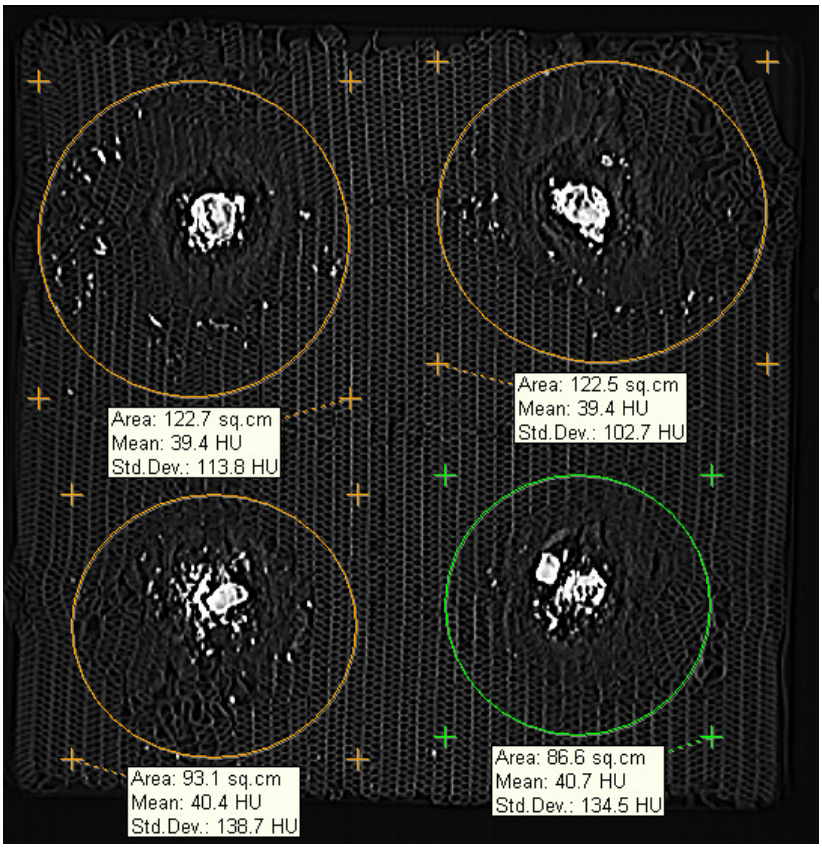

Figure 25 Extent of damage observed in a composite plate by bullet fragmentation.

The maximum BFS was observed in the composite plate that was shot the 9^{th} time. In order to estimate the maximum damage the composite plate could handle a cross section slice along the centre of the shot was chosen for measurement.

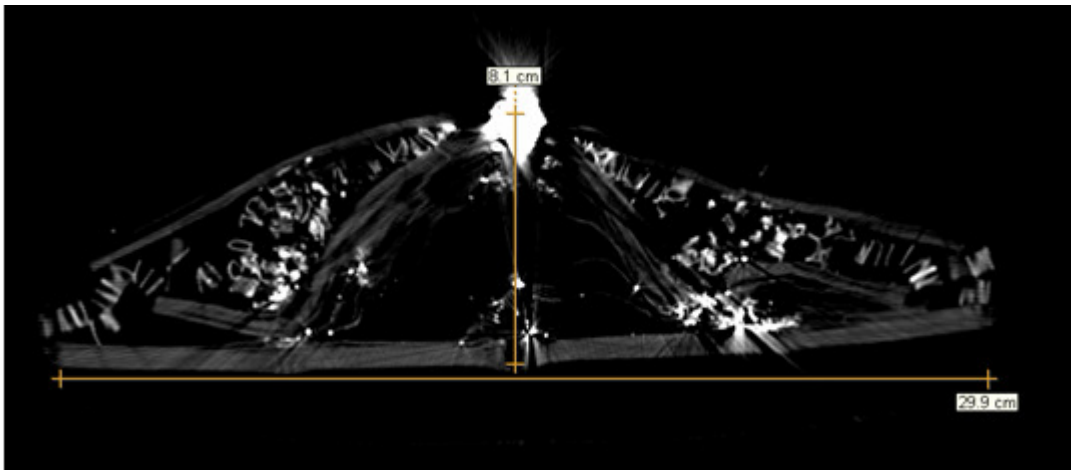

Figure 26 CT image slice of maximum shot composite plate showing the damage pattern of shot 9.

The excessive damage taken by the plate is clearly seen through Figure 26. Even after eight shots the plate was able to defeat the next round which adds to the positive attributes of the design concept in terms of reliability. The strike face to backing layer distance as measured from the CT image was 8.1 cm which was highest recorded in all the shot plates.

4.3. Quasi-static Test Results

The quasi-static compression tests were conducted for in-plane and out-plane directions for the MG Teardrop honeycomb. The objective of these tests was to evaluate the elastic and plastic properties of this honeycomb structure and experimentally measure it energy absorption capacity through plastic deformation. The results obtained as stress - strain curves were compliance corrected. The observed results are shown in Figure 27.

Evaluation of these properties was to provide first hand information for the main objective of numerical input values for the desired material models in ABAQUS simulations.

MG teardrop lattice showed significant anisotropy in its compressive behavior. The in-plane and out-plane properties of the honeycomb are listed in Table 13.

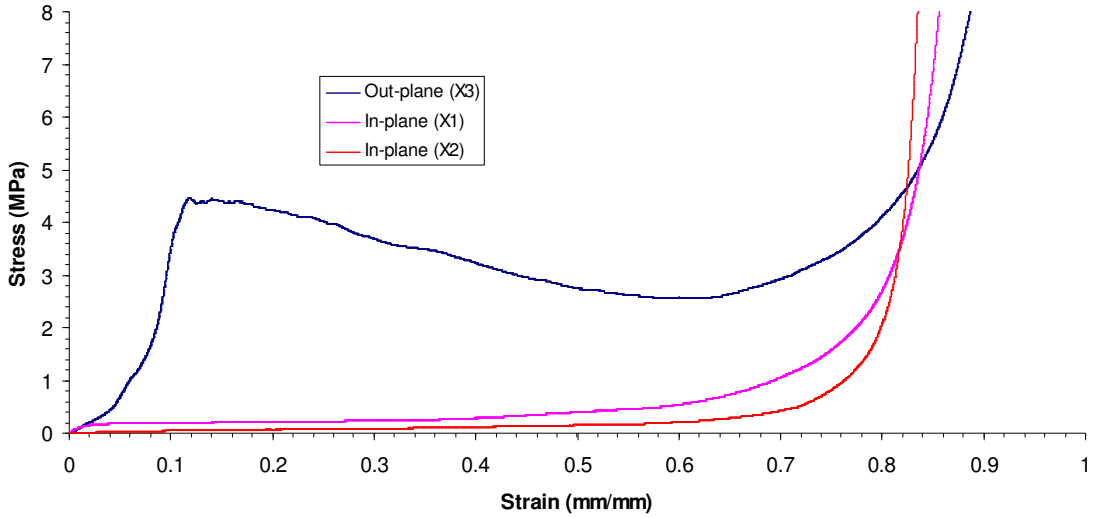

Figure 27 Quasi - static stress strain curves for the MG Teardrop Honeycomb.

It was seen that the modulus for the out-plane direction was about ten times of that in both the in-plane directions. The magnitude of collapse stress, as expected was highest in the out-plane direction. Owing to the construction of the honeycomb the collapse stress magnitude varied even for the in-plane directions. Data on the elastic modulus and stress - strain values obtained from the out-plane direction were used as input values for simulations in ABAQUS.

Table 13 Anisotropic compressive material properties exhibited by MG Teardrop Honeycomb.

	Young's Modulus (GPa)	Collapse Stress (MPa)
Out-of-plane(X_3)	0.05	4.6
In- plane(X_1)	0.005	0.06
In-plane(X_2)	0.004	0.1

The energy absorbed per unit volume for the Teardrop Honeycomb as calculated from the out-plane (X3) stress strain curve was 6.66 J/mm^3.

The desired quasi-static tensile tests on the notched and un-notched 4130 samples were not conducted as the heat treatment process details had variations. Since the tensile test samples had a smaller cross section, it was expected that the end hardness post the heat treatment would be higher than what was seen in the plates. It is necessary to calibrate the heat treatment duration and temperature so that the end hardness values of the plate and the samples matched thus ensuring accuracy of the results. This process is prone to errors and requires detailed investigation. In future, this study would be carried forward and the Johnson-Cook parameters would be evaluated.

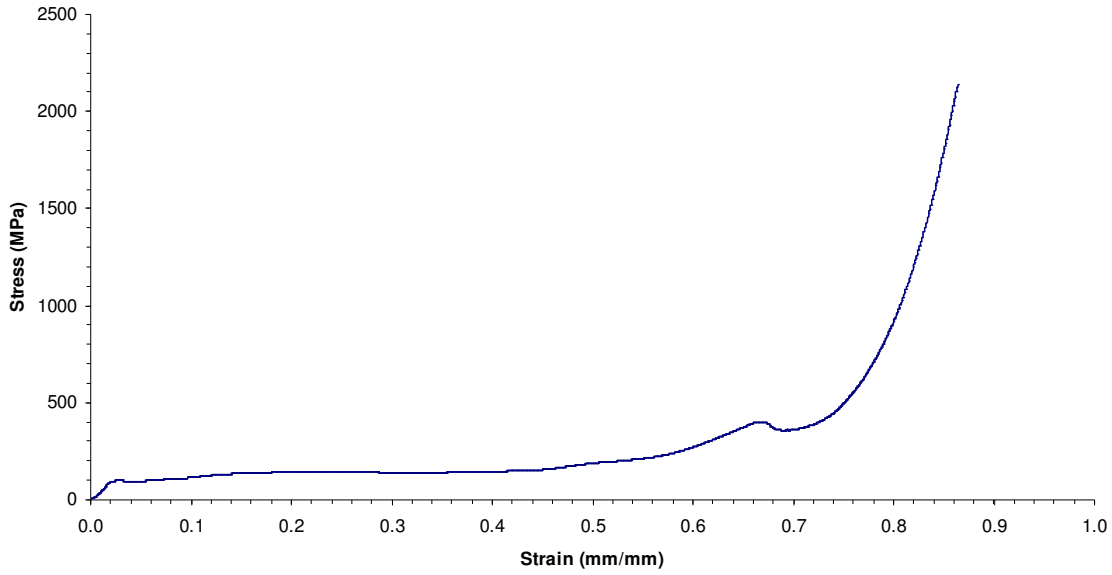

Figure 28 Compressive Stress - Strain response for the cylindrical sample from 7.62 mm bullet.

To evaluate material properties of the impacting projectile, compression test was conducted on a cylindrical sample cut from an actual .308 WIN 7.62 mm FMJ round. The cylindrical sample dimensions were 13.8 mm length and 7.62 mm diameter. The

compression test was carried out at a strain rate of 5 x 10^{-3} /s. The results from the test were compliance corrected. The observed stress - strain plot is as shown in Figure 28.

The observed elastic modulus was 4.916 GPa and a yield stress of 95.4 MPa. The elastic and plastic properties were used to simulate a homogenous material that was assigned to the projectile in Generation 2 FEA models in ABAQUS (Appendix A).

4.4. Dynamic Test Results

The objective of the dynamic test was to establish a standard procedure for testing low impedance amorphous metal high porosity cellular structures. Accordingly a Kolsky bar / SHPB compression test setup was designed to test 82% porosity $Pd_{43}Ni_{10}Cu_{27}P_{20}$ foam.

For validation of SHPB experiment, it was necessary to verify the dynamic stress equilibrium on the specimen using the 1-wave, 2-wave method. Figure 29 demonstrates the dynamic stress equilibrium check, as well as strain rate history.

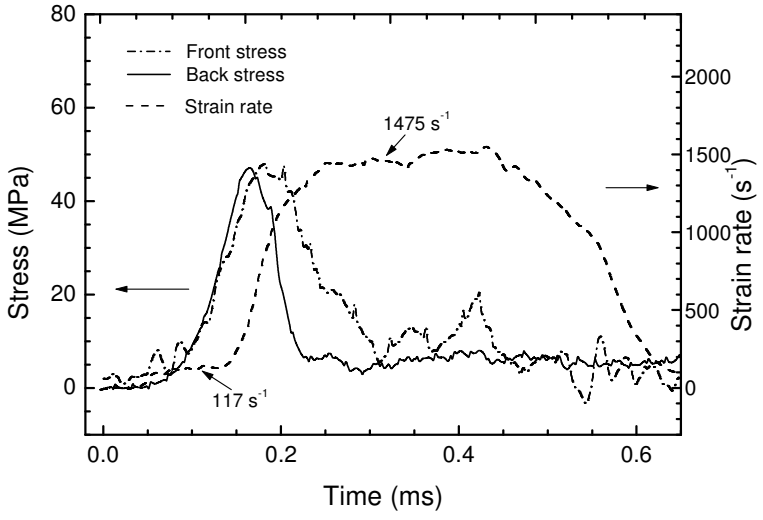

Figure 29 Dynamic equilibrium check conducted to validate the SHPB experiment.

The front stress was very close to the back stress during loading, indicating that the dynamic equilibrium condition was established and the specimen was uniformly

deformed. The basically flat phase in strain rate history indicates that a constant strain rate was achieved. The slight variation (2.5%) in the flat stage of the strain rate history during the loading indicates that the specimen was deformed at nearly a constant strain rate.

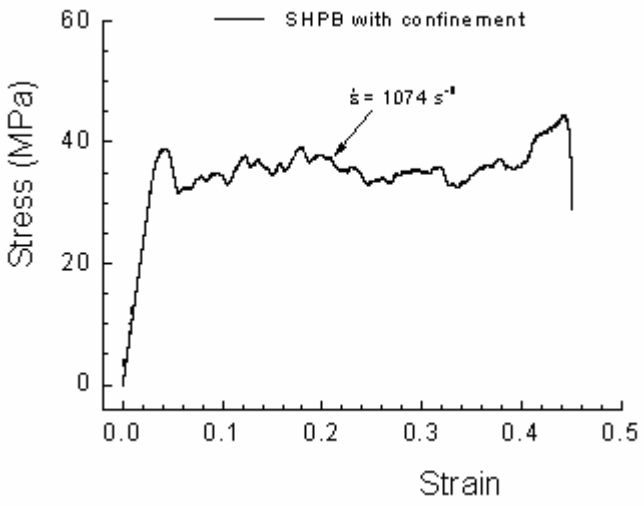

Figure 30 Dynamic Stress - strain curve for the amorphous metal foam.

The dynamic stress strain curve of BMG foam under confinement is shown in Figure 30. The curve show typical characteristics of brittle material. The stress-strain curve shows a steady plateau stress of average 35 MPa with yield stress of 39 MPa. The strain rate for the stress plateau was 1074 s^{-1}. The energy absorbed by the foam sample as calculated from the stress-strain response was 14.1 MJ/m^3, indicating the effectiveness of amorphous metal cellular structures. The mechanical properties of BMG foam were found to show slight sensitivity to the strain rate after comparison with other strain rate tests conducted on the same foam [34]. It was evident that a similar process could yield results for the honeycomb sample. Similar strain rate sensitivity can be observed and stress - strain response can be evaluated. This result would prove valuable in the future as the derived properties can then be used as inputs for FEA simulations.

CHAPTER V

5. FINITE ELEMENT MODELING IN ABAQUS 6.8.2

The aim of conducting dynamic FEA simulations was to closely model and compare the behavior of the plates that were tested using the direct impact ballistic experiments with NIJ level III standards. The simulations were to be designed to provide an alternate means to validate the ballistic test results and recommend structural modifications if necessary. The primary aim was to verify if the current Hybrid-Composite-Armor plate dimensions and construction were capable of withstanding the projectile impact with minimal possible BFS. Visual results obtained from simulations could also be used to compare the damage distribution pattern and evolution of temporal back face bulge observed through the CT scans. The numerical results would help to determine and compare the V_{50} and ballistic limit of each experimentally tested plate. These comparisons can then confirm the effectiveness of the material models currently available and used in the numerical analysis. Like other dynamic tests, FEA simulations are situation specific implying that there are not set procedures that can be followed to ensure positive results. The current effort will help to set a guideline for future impact simulation testing in ABAQUS 6.8.2 and suggest a brief outline of a plausible method to test isotropic and anisotropic materials.

Impact problems have been modeled with these basic objectives of numerically deriving ballistic limits of structures and also to visualize and compare their damage distribution patterns [25, 46, 83, 89, 96]. Referring to these listed publications as guidelines, the dynamic explicit simulations in ABAQUS 6.8.2 were designed for the current study. Similar to software codes used by above referred research groups, the explicit code in ABAQUS works by direct computation of the dependent variables in terms of known quantities or provided inputs. An explicit dynamic analysis was also selected for the reason that it was computationally efficient and consistent for large models with relatively short dynamic response times, comparatively larger deformations and large number of small time increments (the exact circumstances pertaining to the current application). This analysis system was also quite flexible and allowed for fixed or automatic time incrementation depending upon the requirement.

To formulate the contact between the impacting projectile and the armor plates two algorithms were used: General Contact algorithm and Contact Pair algorithm. Both these algorithms were used by modeling contact through element based surfaces that allowed for material degradation. The classic erosion model in ABAQUS was used to simulate the material damage response by individual element deletion as the damage parameter D reached unity. The software also allowed selection of post-damage-initiation material response and also how failure evolved. Details on these selections are presented in the upcoming sections.

All simulation models were built up following a basic sequence of steps. The chronological order is as below:

- Part Generation.
- Material property assignment and Section generation.
- Section allotment and Section Control selection.
- Element selections, Part mesh generation and creating Mesh parts.
- Surface creation, Assembly generation, set creation.
- Constraint assignment (Surface Tie, Dynamic Contact, explicit)
- Step formulation with predefined fields and boundary conditions.
- Selection of field output.
- Job generation.
- Inputs file modification for erosion model.
- Job run

Modifications in this general sequence were liable based on immediate requirements. Contact models generated were 2D and 3D for impact formulation between different materials like Steel, Copper, Lead, Dyneema and MG Teardrop lattice. Development in Material model selection for each material with assigned properties and parameters is listed in section 5.2. Being the first attempt to indigenously develop Simulation models, sequential adaptations were done in the earlier prototypes by incorporating newer factors learnt through experience. Earlier models failed due to issues of excessive distortions, convergence problems, node penetrations, warping of elements during the dynamic contact. Section controls, mass scaling, material modeling options were explored to solve the problem leading to the current status of modeling. Details of this development are listed in Appendix A with illustration of obtained results. In the upcoming sections, details of the current modeling method are described. Application of this method for

impact modeling is listed in Section 5.4 with derived results and discussion in Section 5.5.

5.1. Model Geometry, Meshing, and Boundary Conditions

The basic procedure of modeling any simulation initiates by creation of individual parts that are involved in the analysis. Usually the sizes of these parts are exact match of the real time objects or their scaled /cropped portions as per the requirement. In this study, from the first model creation to the current version, the geometric specifications selected for modeling each component of the tested plates (Dyneema HB 50 laminates, MG Teardrop honeycomb lattice and Steel plates) were to exactly match their actual square surface area and thickness. The geometry of the impacting projectiles was also modeled to exactly match the volumetric attributes (for example .308 WIN 7.62 mm FMJ round). 3D dynamic FEA procedure is computationally extensive due to the large number of elements and node points involved. For faster execution of the analysis procedure and solution computation time reduction, only a quadrant of the actual volume was considered for all FEA owing to the axisymmetric nature of the problem (Refer Figure 31 and Figure 32).

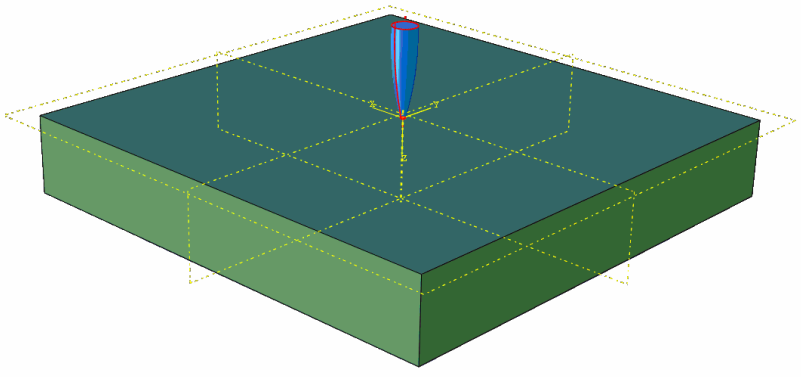

Figure 31 3D representation of the projectile - plate impact problem showing axisymmetry about out-plane axis.

Similar consideration has been made by other research groups investigating projectile-plate impact problems [25, 46]. As it was needed to further reduce the computation time in later models, circular outer surface geometries were selected instead of the initial square (Figure 32). As the total time duration of the dynamic impact is in the order of 2 - 4 x 10^{-4} seconds, the change to circular geometry does not affect the solution by wave propagation issues. Part meshes were then created using hexagonal or hexagonal dominated elements (C3D4) and then structured and sweep mesh construction was done as per requirement. Section controls were assigned to these elements in all the later models to control excessive distortion. Mesh was generated in discrete zones or parts (denser in contact region, coarser at the far edge to improve result quality without severely increasing computation time). The element sizes varied across the length of the plate model. Meshed parts were created to enable mesh surface generation required for Tie function to be used to join the discrete mesh zones.

Once the individual meshed parts were created and assigned material section, they were put together in the assembly module. Necessary boundary conditions had to be evaluated and assigned to accurately model the actual tests. As only a quadrant of the entire volume was considered for analysis, the inside edge surfaces of the model were subjected to symmetry conditions along the X and Y axes. For the outer edge surfaces, their motion being completely restricted due to the test setup, Pinned boundary condition was chosen. Details are represented in Figure 32. Initial velocity assignment to the projectile was done by regulating the predefined field values.

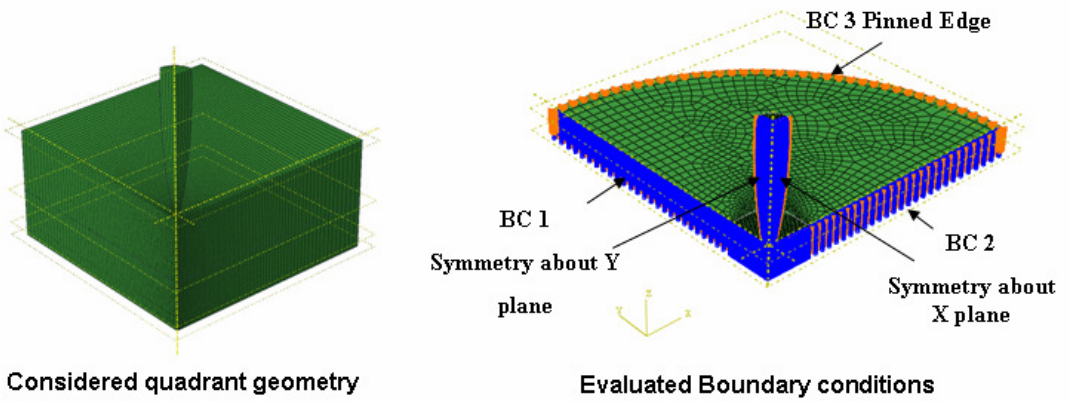

Figure 32 Schematic of the considered quadrant volume for analysis (left) and the applied boundary conditions (right).

5.2. Material Modeling

Material model selection and assigned properties govern the nature of the final output that can be seen through simulation analyses. Accurate input of values is thus of high importance as errors in assigned properties reflect in incorrect visual and numerical response seen from the simulations. The models that have been used for impact simulations are listed in Section 1.3 of Chapter 1. Property assignment for any material can be segregated into 4 basic inputs: (a) Elastic property inputs (b) Plastic property inputs (c) Damage initiation input (d) Damage evolution inputs.

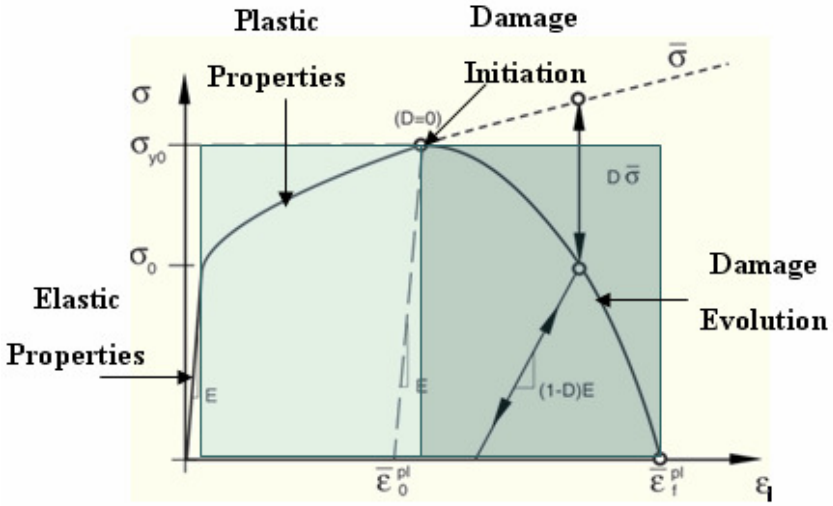

Figure 33 Material Property Inputs for simulations shown on a sample Stress - Strain curve [112].

ABAQUS allows for individual models and their combinations to be simultaneously used for any of the listed inputs. The elastic and plastic inputs can be directly derived from stress strain curves for the selected materials. The software allows for inclusion of anisotropy for elastic properties by using the stiffness matrix as input. Similarly, Hill's criterion is available to include anisotropic yield behavior for materials. As seen from Figure 33, for any ideal material the stiffness steadily increases till it reaches a maximum point beyond which there is a steady degradation in the values. This point maximum is considered as the material damage initiation stage (when damage parameter considered for erosion, D =0). The progress from maximum stiffness stage to no stiffness is defined as damage evolution (D = 0 to D = 1).

The different materials considered in the simulations required individual material models. For first generation models, isotropic material properties were considered for all materials (Dyneema, MG Teardrop lattice and Lead). Tabulated property inputs from stress strain curves were used for plastic properties of Lead and MG lattice. Damage was simulated using simple shear and tensile failure. Substitution of these properties resulted in inaccurate results. For second generation models these properties were re-evaluated. High strain rate properties for Spectra cross ply laminates published by Koh et al [56] were used. The out-plane properties for MG lattice were used similar to the earlier case. The newly evaluated properties from compression of Lead core from actual bullet round were used. Damage models selected earlier were kept the same. The analyses failed to complete all iterations and resulted in no convergence.

The third generation simulations were carried out to simulate experiments similar to those conducted by Hazell [89] and Borvik [81, 83]. The materials used in these simulations

were steels, copper and lead. These models used more defined progressive damage models (by Hooputra [103] and Johnson-Cook [100]). For simulating experiments by Borvik (steel cylindrical rod impacting steel plate), the impacting projectile was made of Arne Tool Steel. The properties were directly used from those evaluated in the published literature (Table 14). An elastic-perfectly plastic model was used for this material as it had no inherent damage.

Table 14 Material properties for Arne Tool Steel [83].

E (MPa)	ν	ρ (kg/m^3)	σ_0 (MPa)	E_t (MPa)	Mean ε_f (%)
204000	0.33	7850	1900	15000	2.15

The plates considered in the experiment were made from high strength Weldox E steel. The properties for this material were also used from those published in the literature. Johnson-Cook plasticity model and dynamic failure model were used to model plastic and damage initiation response. Damage evolution was based on the failure strain listed in the literature. The properties used are as listed in Table 15.

Table 15 Material properties for Weldox E Steel [83].

Elastic constants and density			Yield stress and strain hardening			Strain-rate hardening		Damage evolution	
E (GPa)	ν	ρ (kg/m^3)	A (MPa)	B (MPa)	n	$\dot{p}_0, \dot{r}_0$ (s^{-1})	C	D_C	p_d
200	0.33	7850	490	807	0.73	$5 \cdot 10^{-4}$	0.0114	0.30	0

Adiabatic heating and temperature softening							Fracture strain constants				
C_p (J/kgK)	χ	α (K^{-1})	T_m (K)	T_0 (K)	m	K	D_1	D_2	D_3	D_4	D_5
452	0.9	$1.1 \cdot 10^{-5}$	1800	293	0.94	0.74	0.0705	1.732	−0.54	−0.015	0

For the experiments involving copper and steel bullets impacting steel plates, properties from the ABAQUS user's manual [112] were used for steel as well as copper. The steel properties were taken from the example problem for steel rod impacting steel block. Extended Shear and Ductile damage by Hooputra was used to model this steel while the copper was modeled using Johnson-Cook model. Strain based damage evolution criteria

were used for both these materials. Material properties for Johnson-Cook plasticity model were evaluated for the simulations with lead core. The stress-strain curve used for property evaluation was an extrapolation of data from Atlas of stress-strain curves [113]. The properties were found to be similar to those used are similar to those reported by Borvik et. al [96]

Table 16 Material properties evaluated for Lead.

Elastic constants and density			Yield stress and strain hardening		
E (GPa)	ν	ρ (kg/m^3)	A (MPa)	B (MPa)	n
16	0.44	11350	23	11.59	0.2604

5.3. Contact Formulation and Element Section Controls

Out of the two algorithms available in ABAQUS to model dynamic contact (General Contact Algorithm and Contact Pair Algorithm), the General Contact Algorithm is used in all 3D models due to its simple definition and comparatively less restrictions. Since this option was not available in 2D simulations, Contact pair algorithm had to be used instead. The General Contact method is advantageous over its counterpart since its efficiency is better in enforcing contact conditions with three dimensional surfaces which is the requirement of the current simulation. Results presented in the later section clearly show the difference between the two methods proving General Contact as a better option. The General Contact algorithm requires specification of the contact domain during its definition to specify the regions of the model that can potentially come into contact with each other. A convenient method of specifying the contact domain is using automatically defined element-based all-inclusive surfaces derived from element sets. For the current

study an element set “erode” was generated to define the contact domain for derivation of all-inclusive element based surface (Refer Figure 34). The all-inclusive surface then defines the self-contact mode of interaction. Surfaces used in the General Contact algorithm are allowed to span multiple unattached bodies, so self-contact in this algorithm is not limited to contact of a single body with itself. Hence, self-contact of an all-inclusive surface generated from the set “erode” that spans two bodies (projectile and the plate) implies contact between the bodies as well as contact of each body with itself.

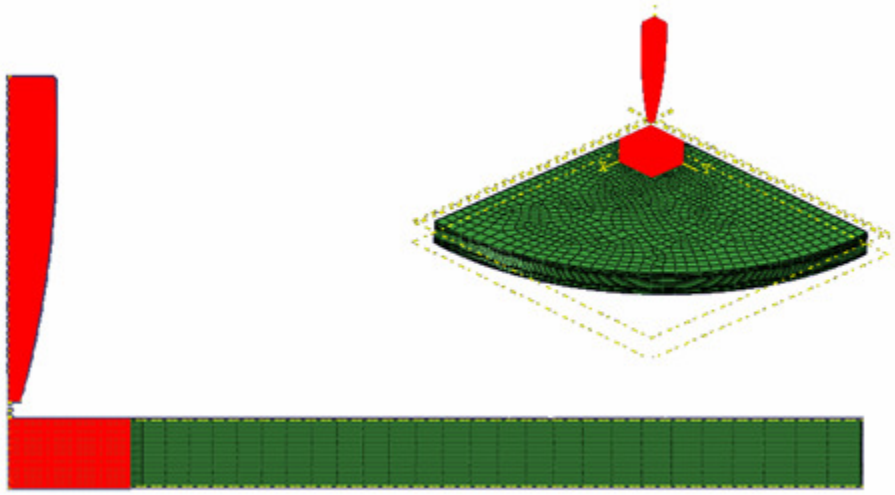

Figure 34 Element set “erode” created to model contact and erosion behavior.

This all-inclusive element-based surface defined from set “erode” also functions to model surface erosion for analyses (element surface based algorithm as described earlier). Post the interior surface definition from the earlier steps, the surface topology evolves to match the exterior of elements that have not failed as the steps progress and the two solids erode. The General Contact algorithm modifies the list of contact faces and contact edges that are active in the contact domain based on the failure status of the underlying elements. It considers a face only if its underlying element has not failed and it is not

coincident with a face from an adjacent element that has not failed; thus, exterior faces are initially active, and interior faces are initially inactive. Once an element fails, its faces are removed from the "erode" contact domain, and any interior faces that have been exposed are activated. A contact edge is removed when all the elements that contain the edge have failed. New contact edges are not created as elements erode. Based on this algorithm, the active contact domain evolves during the analysis as elements fail. Topology of an eroding contact surface is demonstrated in Figure 35.

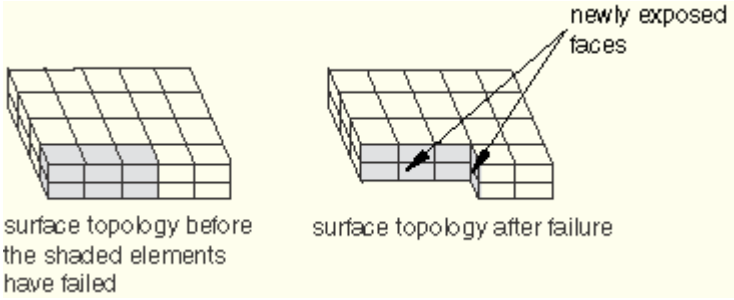

Figure 35 Surface topology evolution resulting from element erosion [112].

The contact nodes from failed elements remain in the contact domain as free floating point masses and contribute significant momentum transfer. The contact algorithm also generates contact forces to resist node-into-face, node-into-analytical rigid surface, and edge-into-edge contact penetrations. This helps to maintain the solid nature of objects during progressive iterations by preventing unreal intersections between two different materials. The primary mechanism for enforcing contact is node-to-face contact.

Section controls in ABAQUS can be used for multiple options and are specified when element types are assigned to particular mesh regions. Use of section controls is generally done for hourglass control formulation and scale factor control for all general purpose

elements. The primary objective for manually selecting section controls was to improve computational efficiency, enable element deletion and most importantly control excessive distortion due to the extremely dynamic contact condition. The section control options used in the later models of this study are: (a) Maximum stiffness degradation control, (b) Hourglass control, (c) Distortion control, (d) Kinematic split control, and (e) Variable mass scaling.

The maximum stiffness degradation option was used to choose the behavior upon complete failure of an element. Once the material stiffness was fully degraded, by use of progressive damage material models, this option enabled the removal of failed elements from the mesh.

The current simulations considered only the linearly varying part of the incremental displacement field in the element for the calculation of the increment of physical strain. The remaining part of the displacement field is the hourglass field and may lead to severe mesh distortion, with no stresses resisting the deformation. “Hourglass control” attempts to minimize these problems and hence was chosen for later models. Several methods are available in ABAQUS for suppressing the hourglass modes. The integral viscoelastic approach generates more resistance to hourglass forces early in the analysis step where sudden dynamic loading is more probable. It is the most computationally intensive hourglass control method. The Kelvin-type viscoelastic approach has pure stiffness and pure viscous hourglass control as limiting cases. When the combination is used, the stiffness term acts to maintain a nominal resistance to hourglassing throughout the simulation and the viscous term generates additional resistance to hourglassing under

dynamic loading conditions. Hence the "Combined Hourglass control" option was chosen for all models which combined the positive attributes of both earlier methods.

"Distortion control" was used to prevent solid C3D4 elements from inverting or distorting excessively for these cases under large compressive and shear deformations. The constraint method prevents each node on an element from punching inward toward the center of the element past a point where the element would become non-convex. Constraints are enforced by using a penalty approach, and the associated distortion length ratio can be controlled. This control reduces the chances of analyses failing prematurely when the mesh is coarse relative to strain gradients and the amount of compression. This option was specifically developed for analyses of energy absorbing, volumetrically compacting materials and can be used with any material model.

A noticeable reduction in computational cost can be obtained by using the "Kinematic split" orthogonal formulation which is based on the centroidal strain operator. This strain operator requires three times fewer floating point operations than the uniform strain operator and works well on refined mesh. It also performs well for large rigid body motions and hence was chosen to make the current analyses more efficient.

During an impact analysis, elements near the impact zone typically experience large amounts of deformation. The reduced characteristic lengths of these elements result in a smaller global time increment. Scaling the mass of these elements as required throughout the simulation can significantly decrease the computation time. "Variable mass scaling" was thus used to scale the mass of elements periodically during a step. To use this type of

mass scaling, a desired minimum stable time increment was defined. Mass scaling factors were calculated automatically and applied, as required, throughout the step.

5.4. Evolution of Simulation Models

The first generation of FEA models was developed to understand the basics of the model development sequence in ABAQUS. Their execution helped to identify necessary modules and algorithms that could be used to improve the observed result qualitatively (visual stress and damage variation response) and quantitatively (numerical outputs: change in velocity). These models also helped to find methods of trouble shooting errors incurred and software options for better efficiency leading to second generation models. These second generation models helped to identify drawbacks in meshing, material modeling and established the need for better material inputs and progressive damage models. Details of the third generation models are discussed in this section. These models were developed after incorporating all modifications learned through the model development process (details of development and evolution of models in Appendix A) that helped in successful execution.

The following objectives were set for these models to improve understanding of the FEA and modeling:

- Validate the effectiveness of the current third generation models through the simulation run of a referred literature experiment by result comparison with those from other software.
- Verify if a 2D model was more effective than a 3D model by comparing end results with published experimental values.

- Prove that the current modeling procedure was capable of predicting ballistic limits for any particular impact scenario.
- Check the influence of size of the impacted plate made in the observed results.
- Confirm if modeling the projectile with separate materials (e.g. core with lead and casing with copper) provided results closer to experimental ones from ballistic testing of 4130 steel plates.

Achieving these set objectives would provide useful information that can be incorporated into future models and help in establishing a standardized procedure which was a primary aim to initiate simulation work. This procedure can be modified for future dynamic impact simulations. A step wise execution plan was decided to carry out simulation experiments that could answer the questions posed above.

To establish the effectiveness of current third generation model, problem description for impact on high strength Weldox steel plates by Borvik et al. [83] was used. 2D and 3D models were created to match the dimensions of the tested plates (12 mm thickness, 500 mm diameter). The impacting object in this simulation was an Arne tool steel cylinder (20 mm diameter, 80 mm length). Material properties for both these steels have been listed in section 5.2. Velocities for impact were chosen to match those in the literature. The minimum element size considered for the 3D model was 0.5. For the 2D model, two element sizes were considered: 0.2 and 0.3 to verify mesh sensitivity. Parts for the 3D model were discretely meshed with varying mesh size. Mesh size for the 2D model was kept constant. Boundary conditions, contact formulation and section controls derived from the second generation model were used (details in earlier sections). Variable mass scaling was used to regulate incrementation. The element-by-element incrementation

option was used. The simulation run time for 2D analysis was 50 minutes and for 3D analysis was 11 hours in ABAQUS 6.8.2. Results from these models are discussed in the next section.

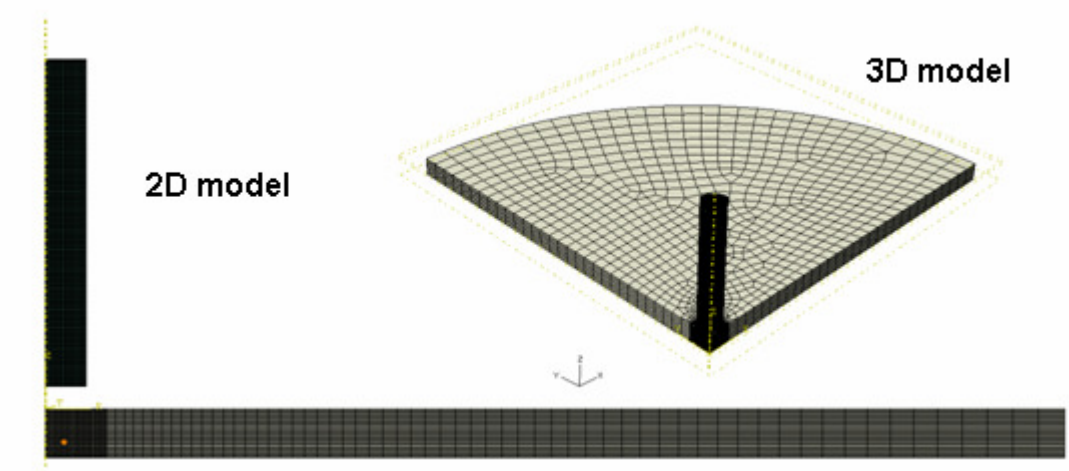

Figure 36 2D and 3D models created to verify performance of current modeling procedure.

To prove that the current modeling procedure was capable of predicting ballistic limits for different scenarios, a steel bullet impacting a steel plate simulation was run. The model was an extension of the earlier considered generation 2 models 4 and 5 (Refer Appendix A). The plate and the projectile were modeled using steel properties from the ABAQUS users manual [112]. Two plate sizes were considered to see if the size change affected the results. The big plate was considered as 152 mm diameter and 6 mm thick (similar to the heat treated 4130 plates that were shot). The smaller plate was considered as 110 mm diameter and 6 mm thick. The bullet geometry was considered same as that of a .308 WIN 7.62 mm FMJ round. Three different velocities were considered for comparing the plate size effect (800 m/s, 838 m/s and 850 m/s). The velocities for the big plate simulations were further reduced till the ballistic limit was achieved. Other simulations controls were kept similar to the earlier 3D model.

To get closer to the actual ballistic test carried out on steel plates, copper material properties were considered for the impacting bullet. Properties for this material (as mentioned in Section 5.2) were taken from the ABAQUS User's manual [112]. The dimensions of the plate were kept similar to the 152 mm diameter big plate. All the simulation conditions were kept same as earlier runs for ease of conformation. Results from these simulations are presented in the next section.

For achieving the last objective, lead was incorporated in the projectile as per the actual bullet geometry. The Johnson-Cook model parameters were used for lead (details in Section 5.2). Initial velocities were considered similar to the earlier model with copper and steel bullets. All simulation conditions were again kept similar to earlier models.

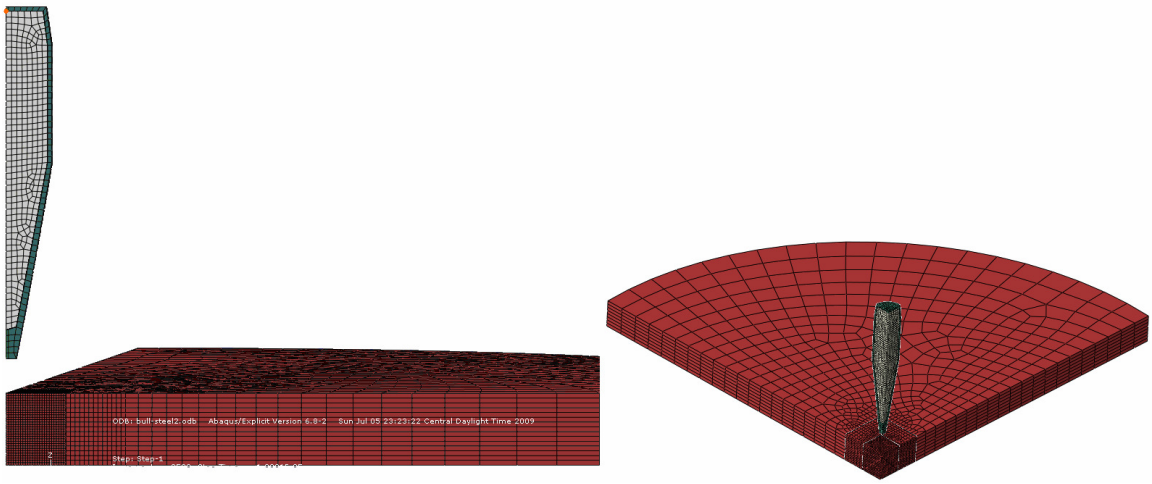

Figure 37 Model geometry considered for simulating an actual 7.62 mm Ball bullet impact on a steel plate.

5.5. Simulation Results and Discussion

The run time for the 3D simulation model to replicate the experiment of a tool steel cylinder impact on a Weldox plate was 11 hours. At the end of the simulation a node point at the centre of the cylinder was chosen to obtain velocity outputs for the negative Z direction. These outputs stated the change in velocity of the node with time. Assuming

the volume centre of the cylinder to be the node average of the entire cylinder solid, its velocity change with time was plotted to represent the whole solid. Three different initial velocities were considered to replicate the experimental conditions. The change-in-velocity plots thus obtained are shown in Figure 38.

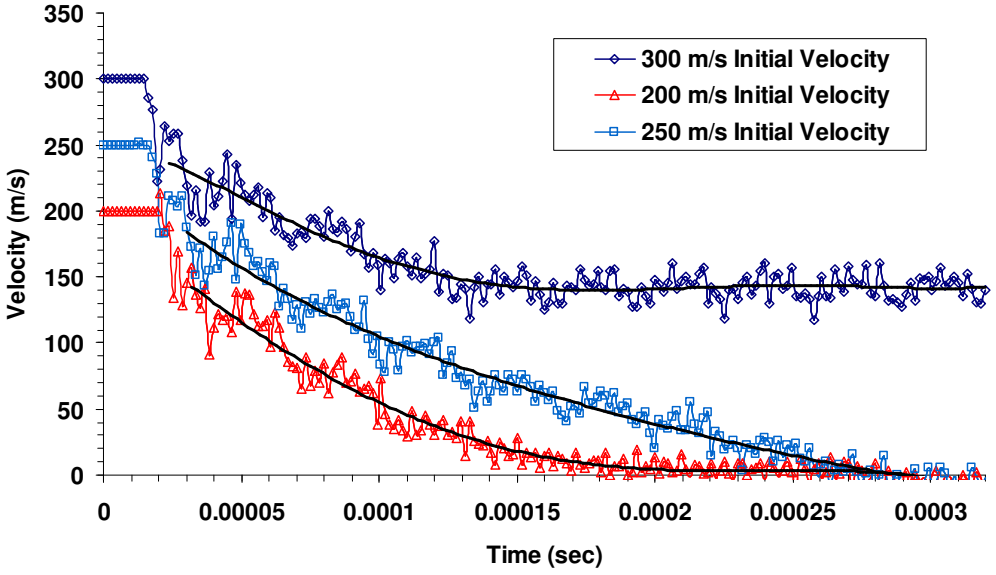

Figure 38 Comparison of change in projectile velocities with time for the 3D model.

As per the experimental results for the 12 mm plate, a ballistic limit of 185 m/s was seen. Using the current modeling procedure in ABAQUS, a ballistic limit of 250 m/s was observed. With the current mesh size of 0.5 used for this simulation, the ballistic limit prediction was higher by 35.1 %. Predictions by LS-DYNA for the ballistic limit were 220 m/s (coarse mesh, size 0.4) and 193 m/s (fine mesh, size 0.2). The coarse mesh result from DYNA was 18.9 % higher from the experimental value while the fine mesh result was 4 % higher. However, the current results are comparable to those seen for LS-DYNA 0.5 size coarse mesh. The current modeling procedure for 3D model can be thus expected to match the results from LS-DYNA with a similar refined mesh, validating its effectiveness.

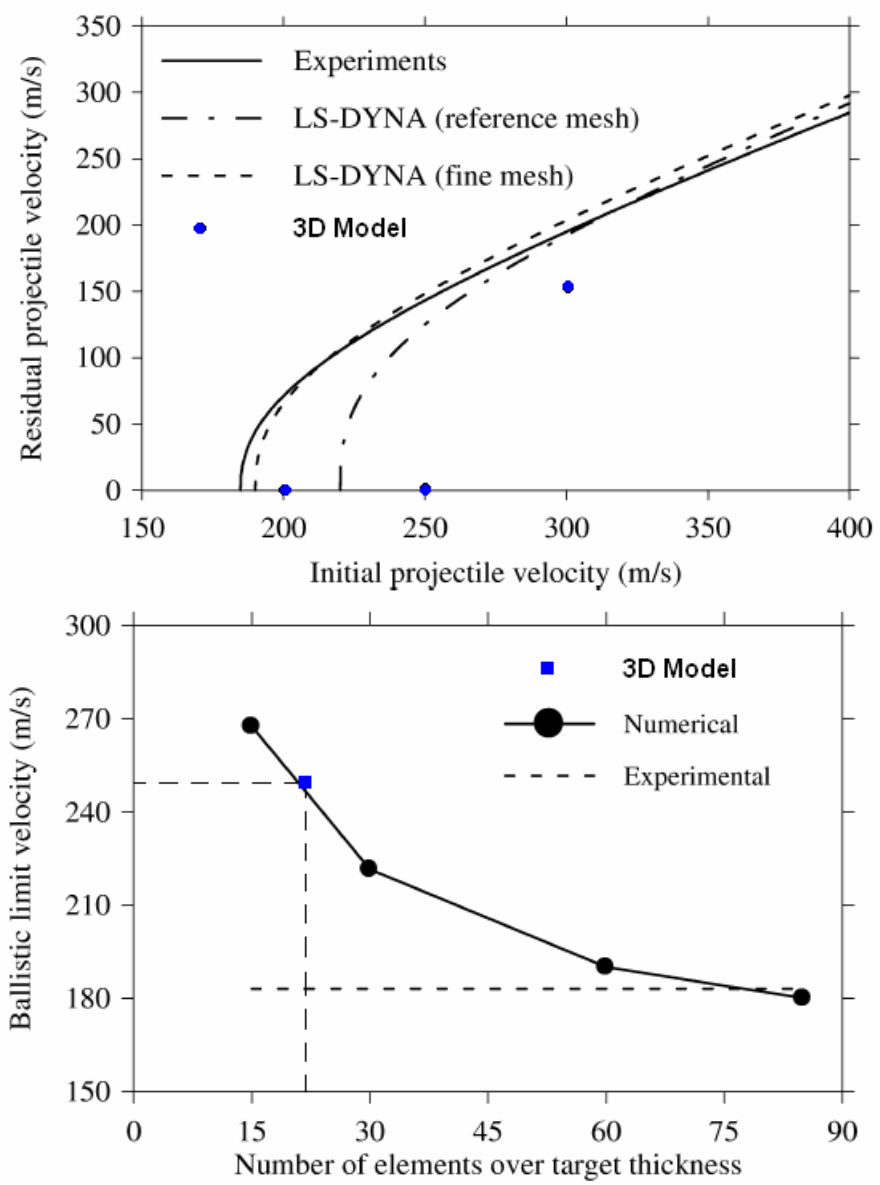

Figure 39 Observed results from Borvik et al. [83] and comparison with those from the current 3D model

The same simulation scenario was run with a 2D mesh to evaluate if the faster model could give similar results as the 3D model. Change-in-velocity plots for the same reference central node were plotted (Refer Figure 40).

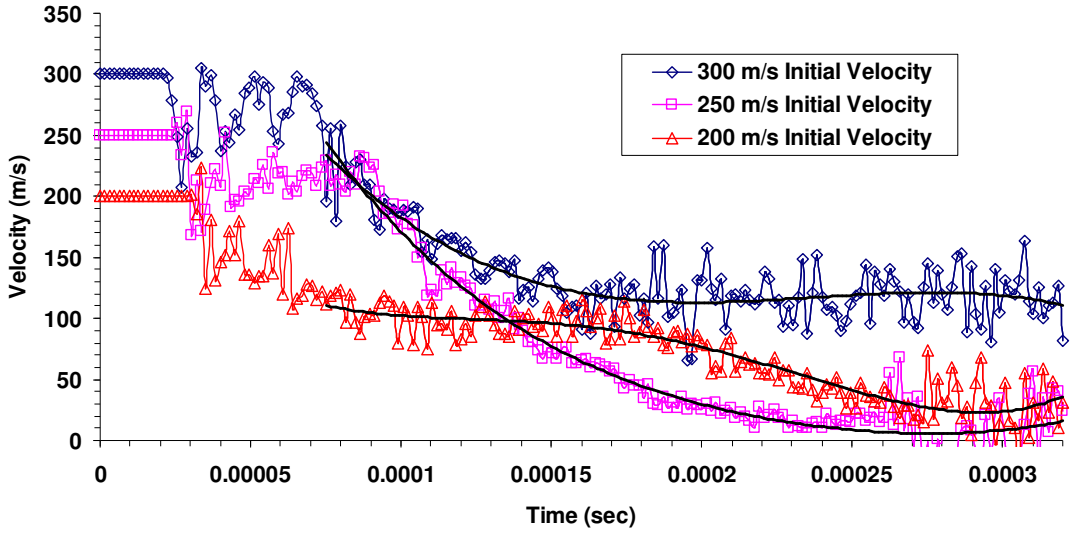

Figure 40 Comparison of change in velocities with time for 2D model (0.2) element size.

It was seen that the modeling procedure for the 2D model gave results that were inconsistent with the experimental values. Even after refining the mesh size from initially used 0.3 to 0.2 (matching that of the DYNA fine mesh model), the solution was not in agreement with the experimental observations.

The change-in-velocity plots for a 300 m/s initial velocity for 0.2 and 0.3 mesh size 2D simulations plotted with the result from a 0.5 mesh size 3D simulation is shown in Figure 41. The residual velocity comparison indicated that a coarser 3D mesh was a more accurate option for simulating dynamic contact behavior (198 m/s residual velocity observed experimentally, also shown in Figure 41). This can be attributed to the contact algorithms and modeling schemes available for 2D models. The General Contact algorithm traditionally used for all earlier simulations could not be used for the 2D model as it was restricted to only 3D geometries. The erosion model in 2D was thus proving to be a less accurate choice in the ABAQUS software for the current study.

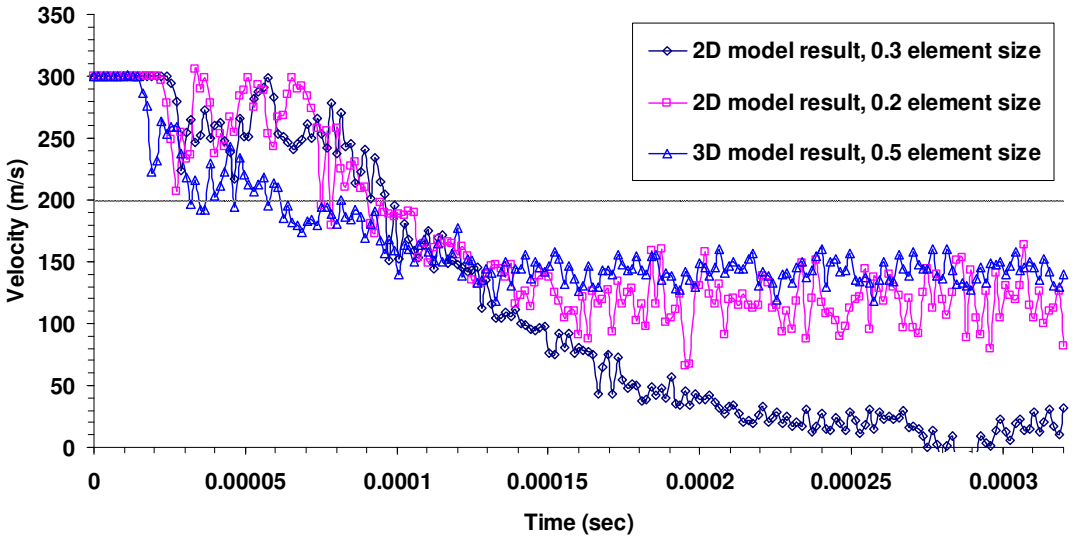

Figure 41 Change in velocity plots for comparison between 2D and 3D models.

To further check the solution stability of both 2D and 3D models, results from an 838 m/s initial velocity were compared. Figure 42 shows that solution convergence was better in the 3D model with General Contact algorithm as the observed amplitude of solution oscillations was lower than the 2D model.

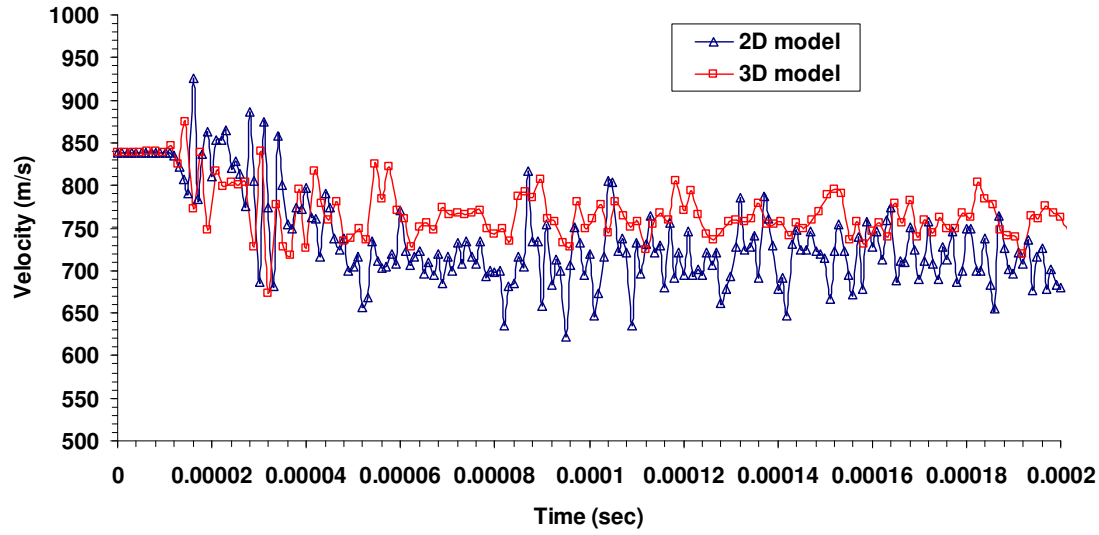

Figure 42 Change in velocity plots for 838 m/s initial velocity.

Next analyses were focused on using actual bullet geometries for projectiles instead of cylinders to get closer to the actual ballistic testing. The projectile was modeled with steel and copper material properties. The properties considered for the steel plate were similar to that of the projectile in the first simulation. As mentioned, two plate sizes were used to verify if any size effects were observed. The results obtained as change in velocity plots for both plate sizes are as shown in Figure 43. The readings were taken from a central representative node similar to the earlier case.

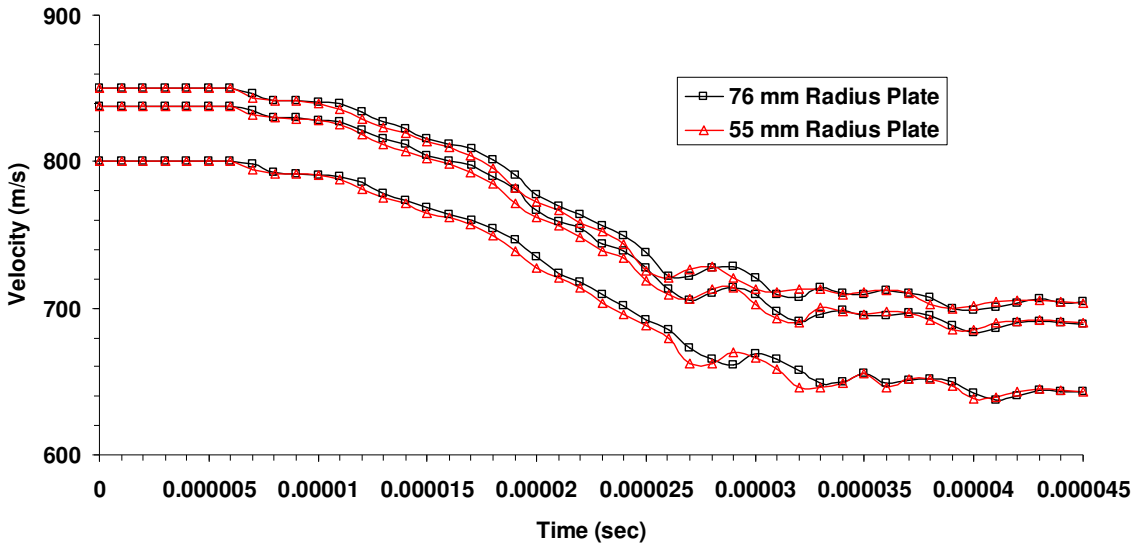

Figure 43 Change in velocity comparison for 55mm and 76 mm steel plates.

A slight change is observed in the velocity trends however the results are within 5% velocity difference of each other at any give time. A 21 mm change in plate length did not significantly affect the solution. This again can be attributed to the relatively short time interval within which the dynamic impact occurs. The reflection of stress wave fronts from the edges of both plates is almost identical and hence solutions for both cases do not vary significantly from one another.

Simulations for a copper bullet impacting a 76 mm plate were run and the change in velocity with time was plotted from the same reference node. The observed results are as shown in Figure 44. It can be seen that as expected, the exit velocity for a copper projectile drops significantly as compared to that for a steel projectile. Copper being a softer material, the steel plate resistance against impact is better. Initial velocities for this model were continually reduced from 850 m/s until a zero residual velocity was observed.

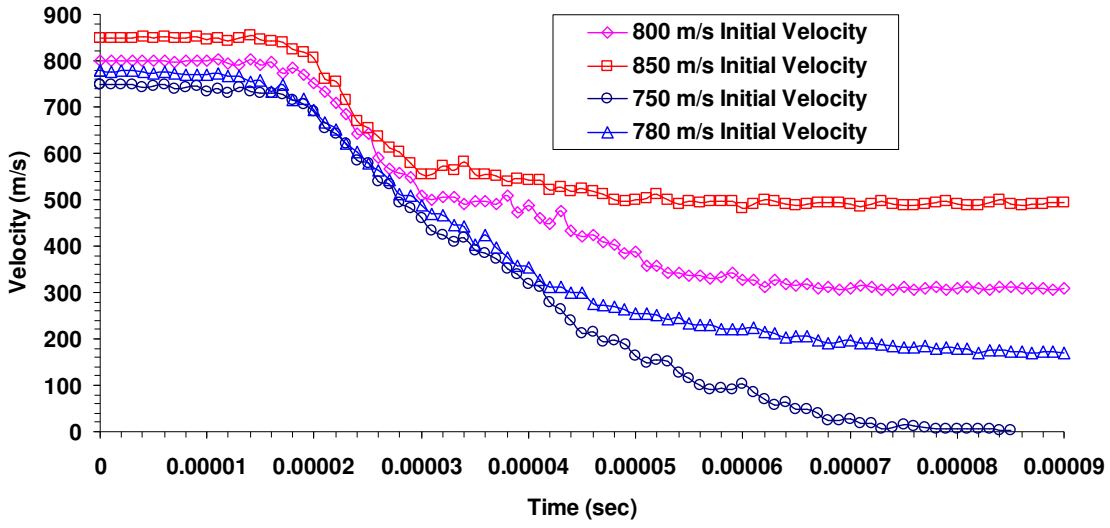

Figure 44 Change in velocity plot for Copper bullet impacting steel plate.

This minimum initial velocity that does not result in a complete penetration can be considered to set the ballistic limit for this impact scenario. Similar results for a steel bullet impacting steel plate were obtained. Figure 45 shows the comparison of the observed ballistic limits for both cases.

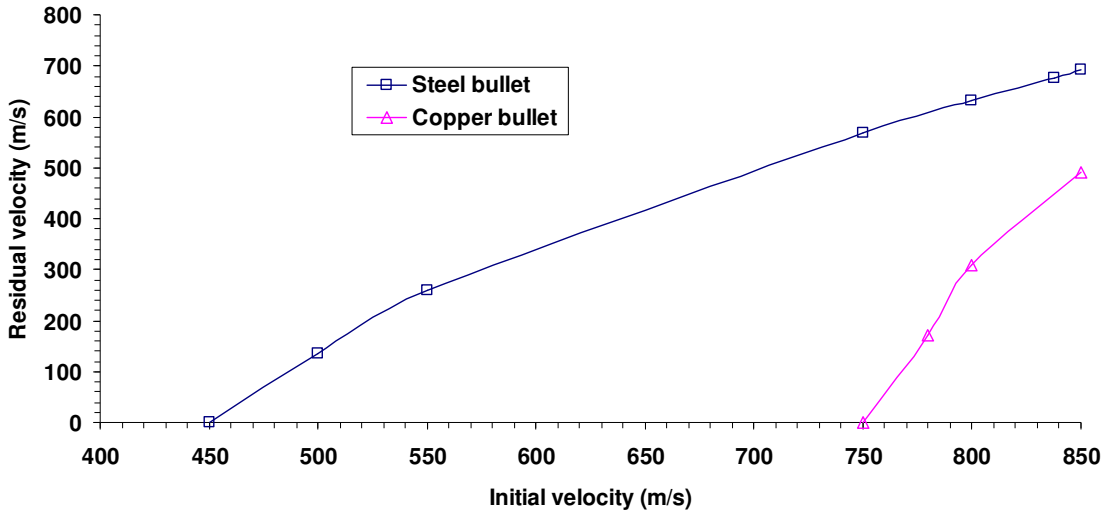

Figure 45 Ballistic limit estimate for Steel bullet and Copper bullet impact simulation.

A hypothesis can thus be made that an actual bullet with a lead core and copper jacket of same geometry as considered for these simulations will have a ballistic limit between these two curves. The hypothesis is based upon the fact that the lead core, being of least hardness will definitely result in a higher ballistic limit as compared to steel. When compared to a full copper bullet, being heavier, the actual projectile will have a higher momentum of penetration owing to the higher density of the lead core. However, the role of degree of hardness vs. density is undetermined, so verification by actual results is needed to predict the real case.

To model the actual ballistic test, the impact of a copper jacketed lead core bullet on steel plate was modeled with exactly similar conditions as earlier described models. Upon running the simulation, the software was unable to compute beyond a second iteration as the material deformations and the contact overclosures exceeded the calculation capacity. The primary reasons stated by the software suggested that the ratio of deformation speed to wave speed exceeds 1.0 in at least one element of the bullet lead core. The probable

reason for this would be the lower elastic modulus of lead with a higher density as compared to that of steel. Mesh dependency might also lead to this error. As a way to rectify this error, refined mesh sizes were implemented for both the plate and the projectile. However the software was still unable to proceed beyond the first iteration. Problems were faced in the first and second generation models as well due to inaccuracies resulting from use of lead properties.

Upon researching possible ways to solve the problem, it was observed that lead had not been considered for modeling bullets [104]. Earlier simulations had focused on using steel cores to simulate armor piercing non-deformable rounds. As stated by Borvik et al. [96], the composition for the lead core significantly varied for bullets. By using PMI measurements, the composition of the bullet core was found to be 87% Lead and 13% Antimony. This contradicts the composition considered in the present study (98% Lead and 2% Antimony). Antimony addition makes the core stronger. For the composition considered by Borvik, the alloy strength was 36 MPa with a 24 MPa yield stress. These properties for the current consideration were 45 MPa and 23 MPa. The overview presented in the referred literature describes the variations in the material constants and most properties being rough estimates. This numerical investigation carried out in LS DYNA was unable to effectively model the impact simulation due to severe mesh distortion similar to that observed in the current study. Attempts were made to use Lagrangian - Eulerian integration codes in GRALE software to model fluidity of the lead core. It was found that even this method did not give a good description of the perforation process as global target deformation was too large.

For the current study, options like adaptive meshing, mesh refinement and section control modification did not significantly alter the output. Problems of modeling lead have also been encountered by Schwer [114]. Research in solving the lead core deformation problem has been limited. As stated by Borvik [96], as an alternative, soft lead core has been replaced by a soft steel core by the majority of research groups. Steel cores being easier to simulate by standardized FEA tools, these materials are bound to replace lead in all future work in this area of ballistic simulations. It is imperative that similar considerations be made for the current study as well to solve the excessive deformation problem.

CHAPTER VI

6. CONCLUSIONS

A composite ballistic insert for a level III NIJ 0101.06 ballistic vest standard was designed and tested. Literature review was conducted to understand the phenomenon of energy absorption and basic functioning of energy absorbers. For creation of a successful design, the available literature of ballistic armors was studied and the latest trends in composite armors were identified. The objectives to be achieved by the ballistic insert were studied by thorough understanding of the standard 0101.06 and accordingly a novel Hybrid-Composite-Armor (HCA) design concept was envisioned and manufactured. This multilayered passive armor prototype consisted of a sandwich structure (Metallic Glass (MG) Teardrop celled honeycomb layer between Dyneema HB50 laminates).

Methods to test the structure and its components were discussed and detailed experiments were conducted. Through quasi-static compressive testing, anisotropic properties of MG Teardrop honeycomb were evaluated. The structure exhibited Young's modulus of 50 MPa in the out-plane direction and an average of 4.5 MPa in the in-plane directions. The observed collapse stress was 4.6 MPa for the out-plane direction and an average of 0.08 MPa for in-plane directions. The energy absorbed per unit volume was 6.66 J/mm^3.

A standard SHPB test method that could be used for dynamic property evaluation of this low impedance Teardrop celled honeycomb structure was identified and it's functioning

was verified by compression experiment on a Pd based amorphous metal foam. Standards were set for the setup construction, to check its equilibrium and methodology of generating output. Observed results from this compression experiment suggested higher energy absorption capacity of amorphous metal cellular structures with noticeable strain rate sensitivity.

Performance of the HCA insert was verified through ballistic tests. Comparison of observed results with those from similar tested Baseline plates show improvement in ballistic performance by incorporation of collapsible MG Teardrop celled honeycomb layer. Reduction in BFS by 24% was observed for a 13% increase in areal density due to inclusion of this layer. BFS of 33.6 mm and a V_{50} of 832 m/s validated successful compliance of the HCA to the NIJ level III standards, thus proving the design hypothesis to be effective. Post impact evaluation and NDT carried out on the tested inserts revealed reduction in damage zones for the HCA in comparison to the Baseline (134 cm^2 for Baseline and 122 cm^2 or lower for HCA), validating improved multi hit capability. Test method used in all these tests was standardized for repeatability and accuracy by experiments on heat treated 4130 steel plates.

An FEA modeling procedure for dynamic impact in ABAQUS 6.8.2 was investigated and methodology of conducting simulations was perfected. The experiment setup conditions from steel plate testing served as a guideline for this FEA modeling procedure. Results obtained from 2D and 3D models were compared with experimental values published by Borvik et al. [83]. The accuracy of a coarse mesh 3D model with General Contact algorithm was found to be better and more stable than even a fine mesh 2D model. This 3D model was also capable of predicting dynamic impact FEA results comparable to

those from LS-DYNA validating the efficiency of the current modeling procedure. Minimal size effect influence was observed in these 3D models. Simulations with actual bullet geometries were conducted using copper and steel material properties for impacting projectiles. The model was efficient in predicting variations in projectile velocities post impact as a function to time. These results also verified that the modeling procedure developed was very flexible and capable of predicting ballistic limits for different impact scenarios as per requirement. Although simulations with copper jacketed lead core projectile were not a success, observations made during the process exactly corroborated the deficiencies in Lead modeling reported by Borvik et al. [96] and Schwer et al. [114].

The current study was thus successful in demonstrating a design methodology wherein mechanical testing and software based FEA analysis could be used in conjunction to evaluate performance of any energy absorber design concept.

CHAPTER VII

7. FUTURE WORK

- Dynamic and shear properties for Dyneema HB50 need to be evaluated.
- Johnson-Cook parameters for heat treated 4130 steel need to be evaluated.
- Possible use of Hill and Hashin model for individual crossply creation can be done and bonding with cohesive elements can be explored for simulation of delamination.
- Possible use of other base amorphous alloys to improve honeycomb strength can be made.
- Testing of absorber HCA unit when combined with front ceramic layer using armor piercing rounds and comparison with ESAPI insert needs to be done.
- Methods to evaluate properties for extended shear and ductile failure model by Hooputra model need to be explored.
- Possible uses of MG Teardrop honeycomb can be considered for Aerospace applications.

REFERENCES

1. Johnson, W. and A. Walton, *An experimental investigation of the energy dissipation of a number of car bumpers under quasi-static lateral loads.* Int J Impact Engg, 1983. **1**(3): p. 301 - 8.
2. Reid, J.D. and D.L. Sickling, *Design and simulation of a sequential kinking guardrail terminal.* Int J Impact Engg, 1998. **21**(9): p. 761 - 72.
3. Kanae, Y., T. Sasaki, and S. Shimamura, *Experimental and analytical studies on the drop-impact test with lead-shielded scale model radioactive shipping casks.* Structural imapct and crashworthiness, 1984: p. 343 - 54.
4. Alghamdi, A.A.A., *Protection of Saudi descent roads using metallic collapsible energy absorbers.* Final report KACST 98 - 2- 74, April, 2000.
5. Alghamdi, A.A.A., *Collapsible impact energy absorbers: an overview.* Thin-Walled Structures, 2001. **39**(2): p. 189-213.
6. Johnson, W. and S.R. Reid, *Metallic energy dissipating systems.* Appl Mech Rev, 1978. **31**(3): p. 277 - 88.
7. Lu, G. and T. Yu, *Energy absorption of structures and materials.* 2003.
8. Carney, J.F. and S. Pothen, *Energy dissipation in braced cylindrical shells.* Int J Mech Sci, 1988. **30**(3/4): p. 203 - 16.
9. Alexander, J.M., *An appropriate analysis of the collapse of thin cylindrical shells under axial loading.* Quart J Mech Appl Math, 1960. **13**(1): p. 10 - 5.
10. Langseth, M. and O.S. Hopperstand, *Static and dynamic crushing of square thin-walled aluminum extrusions.* Int J Impact Engg, 1996. **18**(7/8): p. 949 - 68.
11. Langseth, M., O.S. Hopperstand, and T. Berstad, *Crashworthiness of aluminum extrusions: validation of numerical simulation, effect of mass ratio and impact velocity.* Int J Impact Engg, 1999. **22**(8): p. 829 - 54.
12. Mamalis, W. and W. Johnson, *The quasi-static crumpling of thin-walled circular cylinders and frusta under axial compression.* Int J Mech Sci, 1983. **25**(9/10): p. 713 - 32.
13. Harris, J.A. and R.D. Adams, *An assessment of the impact performance of bonded*

joints for use in high energy absorbing structures. Proceedings of the Inst of Mech Engg, 1985. **199**(C2): p. 121 - 31.

14. Wierzbicki, T., *Crushing analysis of metal honeycombs.* Int J Impact Engg, 1983. **1**(2): p. 157 - 74.
15. Reddy, T.Y. and R.J. Wall, *Axial compression of foam-filled thin-walled circular tubes.* Int J Impact Engg, 1988. **15**(2): p. 151 - 60.
16. Nahas, M.N., *Impact energy dissipation characteristics of thin-walled cylinders.* Thin-Walled Structures, 1993. **15**(2): p. 81 - 93.
17. Reddy, T.Y. and S.T.S. Al-Hassani, *Axial crushing of wood-filled square metal tubes.* Int J Mech Sci, 1993. **35**(3/4): p. 231 - 46.
18. Khondker, O.A., et al., *Impact and compression-after-impact performance of weft-knitted glass textile composites.* Composites: Part A, 2005. **36**: p. 638 - 48.
19. Kang, T.J. and C. Kim, *Impact energy absorption mechanism of largely deformable composites with different reinforcing structures.* Fibres and Polymers, 2000. **1**(1): p. 45 - 54.
20. Grujicic, M., et al., *Ballistic-protection performance of carbon-nanotube-doped poly-vinyl-ester-epoxy matrix composite armor reinforced with E-glass fiber mats.* Matl Sci and Engg, 2008. **A**(479): p. 10 - 22.
21. Ifju, P.G., *Textile composite materials.* Handbook of Experimental Solid Mechanics, 2008: p. 114 -117.
22. Karger-Kocsis, J., T. Czigany, and J. Mayer, *Fracture behaviour and damage growth in knitted carbon fibre fabric reinforced polyethylmethacrylate.* Plast Rubber Compos Process Appl, 1996. **25**(3): p. 109.
23. Huysmans, G., B. Gommers, and I. Verpoest, *Mechanical properties of 2D warp knitted fabric composites: An experimental and numerical investigation.* Conf Proceedings: 17th Intl SAMPE Europe Conf Basel, Switzerland, 1996: p. 97 - 108.
24. Verpoest, I., *Advanced three-dimensional textile sandwich composites.* Course notes, CRC-ACS, Melbourne, Australia, 1997: p. 29 - 31.
25. Grujicic, M., et al., *A ballistic material model for cross-plied unidirectional ultra-high molecular-weight polyethylene fiber-reinforced armor-grade composites.*

Matl Sci and Engg, 2008. **498**(A): p. 231 - 241.

26. Evelin, R., et al., *Energy absorption behaviour of austenitic and duplex stainless steels in a crash box geometry.* Steel research international, 2006. **77**(9/10): p. 692 - 697.
27. Thornton, P.H., *Energy absorption by structural collapse in dual phase steel tubes.* Metall. and Matl. Transactions A, 1979. **10**(8): p. 1199 - 1201.
28. Wynne, R.C., *US Patent 5804757: Flexible, lightweight, compound body armor.* Sept. 8, 1998.
29. Ponnambalam, V., S.J. Poon, and G.J. Shiflet, *Fe-based bulk metallic glasses with diameter thickness larger than one centimeter.* Journal of Matl Res, 2004. **19**(5): p. 1320.
30. Brothers, A.H. and D.C. Dunanad, *Plasticity and damage in cellular amorphous metals.* Acta Materialia, 2005. **53**: p. 4427 - 40.
31. Demetriou, M.D., et al., *High porosity metallic glass foam: A powder metallurgy route.* Appl Physics Letters, 2007. **91**.
32. Demetriou, M.D., et al., *Yielding of metallic glass foam by percolation of an elastic buckling instability.* Adv Materials, 2007. **19**: p. 1957 - 72.
33. Yang, B., C.T. Liu, and T.G. Nieh, *Unified equation for the strength of bulk metallic glasses.* Appl Physics Letters, 2006. **88**(221911).
34. Luo, H., et al., *Dynamic compressive behavior of Pd-based amorphous metal foam.* Proceedings of Society of Experimental Mechanics Annual Conf., 2009.
35. Dunstan, S. and R. Volstad, *Flak jackets: 20th Century Military Body Armour, Osprey Publishing Ltd., London.* 1984.
36. Ogorkiewicz, R.M., *Technology of Tanks, Jane's Information Group, Coulsdon.* 1991.
37. Hazell, P.J., *Ceramic armour: Design and defect mechanisms, Argos Press, Canberra, Australia.* 2006.
38. Roberson, C., *Ceramic materials and their use in lightweight armour systems.* Proceedings of Lightweight Armour systems symposium, Shrivenham, UK, 1995: p. 28 - 30.
39. Bart, R.K. and J.C. Lindberg, *Ceramic bodygaurds.* Adv Matl and Processes inc

Metal Progress, 1987. **9**: p. 69 - 72.

40. Montgomery, J.S. and E.S. Chin, *Army materials research: Transforming land combat through new technologies.* AMPTIAC Quarterly, 2004. **8**(4): p. 15 - 20.
41. Armellino, R.A., *US Patent 3,971,072: Lightweight Armor and method of fabrication.* July 27,1972.
42. Machalaba, N.N. and K.E. Perepelkin, *Heterocyclic Aramide Fibers - Production principles, properties and application.* Journ of Indust textiles, 2002. **31**(3): p. 189 - 204.
43. Cunniff, P.M., et al., *High performance "M5" fiber for ballistics/structural composites.* 23rd Army Sci Conf, Orlando, Florida, 2002.
44. Lee, B.L., et al., *Penetration Failure Mechanisms of Armor-Grade fiber composites under impact.* Journ of Comp Matl, 2000. **35**(18): p. 1605 - 1633.
45. Cheeseman, B.A. and T.A. Bogetti, *Ballistic impact into fabric and compliant composite laminates.* Composite Structures, 2003. **61**: p. 161 - 173.
46. Grujicic, M., et al., *Material modeling and Ballistic-resistance analysis of Armor-grade composites reinforced with High-performance fibers.* Journ of Matl Engg and Performance, 2009.
47. Grogan, J., et al., *Ballistic resistance of 2D and 3D woven sandwich composites (vol 9, pg 283, 2007).* Journal of Sandwich Structures & Materials, 2007. **9**: p. 597-597.
48. Decker, M.J., et al., *Stab resistance of shear thickening fluid (STF)-treated fabrics.* Composites Science and Technology, 2007. **67**(3-4): p. 565-578.
49. Ramesh, K.T., *High Rates and Impact Experiments.* Handbook of Experimental Solid Mechanics, 2008: p. 929 - 959.
50. Field, J.E., et al., *Review of experimental techniques for high rate deformation and shock studies.* International Journal of Impact Engineering, 2004. **30**(7): p. 725-775.
51. Wang, Y. and Y. Xia, *The effects of strain rate on the mechanical behavior of Kevlar fibre bundles: an experimental and theoretical study.* Composites Part A, 1998. **29**: p. 1411 - 1415.
52. Wang, Y. and Y.M. Xia, *Experimental and theoretical study on the strain rate*

and temperature dependence of mechanical behaviour of Kevlar fibre. Composites Part A, 1999. **30**: p. 1251 - 1257.

53. Shim, V.P.W., C.T. Lim, and K.J. Foo, *Dynamic mechanical properties of fabric armour.* Int J Impact Engg, 2001. **25**: p. 1 - 15.
54. Benloulo, I.S.C., et al., *Dynamic tensile testing of aramid and polyethylene fiber composites.* Int J Impact Engg, 1997. **19**(2): p. 135 - 146.
55. Huang, W., Y. Wang, and Y. Xia, *Statistical dynamic tensile strength of UHMWPE-fibers.* Polymer, 2004. **45**: p. 3729 - 3734.
56. Koh, C.P., et al., *Response of a high-strength flexible laminate to dynamic tension.* Int J Impact Engg, 2008. **35**: p. 559 - 568.
57. Subhash, G. and G. Ravichandran, *Split-Hopkinson bar testing of ceramics.* ASM Handbook, H. Kuhn D. Medlin ed., 2000. **8**: p. 497 - 504.
58. Wang, H. and K.T. Ramesh, *Dynamic strength and fragmentation of hot-pressed silicon carbide under uniaxial compression.* Acta Materialia, 2004. **52**(2): p. 355 - 367.
59. Subhash, G. and G. Ravichandran, *Mechanical behavior of hot pressed aluminum nitride under uniaxial compression.* Journ of Matl Sci, 1998. **33**: p. 1933 - 1939.
60. Chen, W., G. Subhash, and G. Ravichandran, *Evaluation of ceramic specimen geometries used in Split-Hopkinson pressure bar.* DYMAT Journ, 1994. **1**: p. 193 - 210.
61. Mukai, T., H. Kanahashi, and T. Miyoshi, *Experimental study of energy absorption in closed-cell aluminum foam under dynamic loading.* Script Metal, 1999. **40**: p. 921 - 927.
62. Dannemann, K.A. and J. Lankford, *Strain rate effects in porous materials.* Matl Research Soc Symp Proceedings, 1998. **521**: p. 103 - 108.
63. Dannemann, K.A. and J. Lankford, *High strain rate compression of closed-cell aluminum foams.* Matl Sci and Engg, 2000. **A293**: p. 157 - 164.
64. Deshpande, V.S. and N.A. Fleck, *High strain rate compressive behavior of aluminum alloy foams.* Int J Impact Engg, 2000. **24**: p. 277 - 298.
65. Ramamurty, U. and A. Paul, *Strain rate sensitivity of a closed-cell aluminum foam.* Matl Sci and Engg, 2000. **A281**: p. 1 - 7.

66. Baker, W.E., T.C. Togami, and J.C. Weydert, *Static and dynamic properties of high density metal honeycombs.* Int J Impact Engg, 1998. **21**: p. 149 - 163.
67. Wu, E. and W.S. Jiang, *Axial crush of metallic honeycombs.* Int J Impact Engg, 1997. **19**: p. 439 - 456.
68. Goldsmith, W. and J.L. Sackman, *An experimental study of energy absorption in impact on sandwich plates.* Int J Impact Engg, 1992. **12**(2): p. 241 - 262.
69. Goldsmith, W. and D.L. Louie, *Axial perforation of aluminum honeycombs by projectiles.* Int Journ of Solids and Struct, 1995. **32**(8/9): p. 1017 - 46.
70. Liaghat, G.H., et al., *Dynamic crushing of honeycomb panels under impact of cylindrical projectiles.* Amir Kabir Univ Journ, 2003. **14**(53): p. 68 - 79.
71. AlaviNia, A., S.B. Razavi, and G.H. Majzoobi, *Ballistic limit determination of aluminum honeycombs - experimental study.* Matl Sci and Engg, 2008. **488**: p. 273 - 280.
72. Abramowicz, W. and T. Wierzbicki, *Crushing analysis of metal honeycombs.* Int J Impact Engg, 1983. **1**(2): p. 157 - 174.
73. HooFatt, M.S. and K.S. Park, *Perforation of honeycomb sandwich plates by projectiles.* Composites Part A, 2000. **31**: p. 889 - 899.
74. Liaghat, G.H., et al., *Ballistic limit evaluation for impact of cylindrical projectiles on honeycomb panels.* Thin-Walled Structures, 2010. **48**: p. 55 - 61.
75. Corran, R.S.J., P.J. Shadbolt, and C. Ruiz, *Impact loading of plates - an experimental investigation.* Int J Impact Engg, 1983. **1**(1): p. 3 - 22.
76. Levy, N. and W. Goldsmith, *Normal impact and perforation of thin plates by hemispherical tipped projectiles - II. Experimental results.* Int J Impact Engg, 1984. **2**(4): p. 299 - 324.
77. Wingrove, A.L., *The influence of projectile geometry on adiabatic shear and target failure.* Metall Trans A, 1973. **4**: p. 1829 - 1833.
78. Othe, S., et al., *Impact strength of steel plates struck by projectiles.* Bull JSME, 1982. **25**(205): p. 1226 - 1231.
79. Camacho, G.T. and M. Ortiz, *Adaptive Lagrangian modelling of ballistic penetration of metallic targets.* Comput Meth Appl Mech Engg, 1997. **142**: p. 269 - 301.

80. Borvik, T., et al., *Numerical simulation of plugging failure in ballistic penetration.* Int Journ of Solids and Struct, 2001. **38**: p. 6241 - 6264.

81. Borvik, T., et al., *Perforation of 12 mm thick steel plates by 20 mm diameter projectiles with flat, hemispherical and conical noses Part II: numerical simulations.* Int J Impact Engg, 2002. **27**: p. 37 - 64.

82. Gupta, N.K., M.A. Iqbal, and G.S. Sekhon, *Experimental and numerical studies on the behavior of thin aluminum plates subjected to impact by blunt and hemisperical nosed projectiles.* Int J Impact Engg, 2006. **32**: p. 1921 - 1944.

83. Borvik, T., et al., *A computational model of viscoplasticity and ductile damage for impact and penetration.* Eur Journ Mech A/ Solids, 2001. **20**: p. 685 - 712.

84. Arias, A., J.A. Rodriguez-Martinez, and A. Rusinek, *Numerical simulations of impact behaviour of thin steel plates subjected to cylindrical, conical and hemispherical non-deformable projectiles.* Engg Frac Mech, 2008. **75**: p. 1635 - 1656.

85. Tan, V.B.C., C.T. Lim, and C.H. Cheong, *Perforation of high-strength fabric by projectiles of different geometry.* Int J Impact Engg, 2001. **28**: p. 207 - 222.

86. Naik, N.K., P. Shrirao, and B.C.K. Reddy, *Ballistic impact behavior of woven fabric composites: Formulation.* Int J Impact Engg, 2006. **32**: p. 1521 - 1552.

87. Parga-Landa, B. and F. Hernandez-Olivares, *An analytical model to predict impact behaviour of soft armours.* Int J Impact Engg, 1995. **16**(3): p. 455 - 466.

88. Ben-Dor, G., A. Dubinsky, and T. Elperin, *The optimum arrangement of the plates in a multi-layered shield.* Int J Impact Engg, 2000. **37**: p. 687 - 696.

89. Hazell, P.J., *Numerical simulations and experimental observations of the 5.56 mm L2A2 bullet perforating steel targets of two hardness values.* Journ of Battlefield Tech, 2003. **6**(1): p. 1 - 4.

90. Grujicic, M., et al., *Ballistic performance of Alumina/S-2 glass-reinforced polymer-matrix composite hybrid lightweight armor againt Armor Piercing (AP) and non -AP projectiles.* Multidiscipline Modeling in Matl and Struct, 2006(1 - 28).

91. Tanoglu, M. and A.T. Seyhan, *Investigating the effects of a polyester preforming binder on the mechanical and ballistic performance of E-glass fiber reinforced*

polyester composites. Int Journ of Adhesion & Adhesives, 2003. **23**: p. 1 - 8.

92. Jacobs, M.J.N. and J.L.J. VanDingenen, *Ballistic protection mechanisms in personal armour.* Journ of Matl Sci, 2001. **36**: p. 3137 - 3142.
93. Iremonger, M.J. and A.C. Went, *Ballistic impact of fibre composite armours by fragment-simulating projectiles.* Composites Part A, 1996. **27**: p. 575 - 581.
94. Lim, C.T., V.P.W. Shim, and Y.H. Ng, *Finite-element modeling of the ballistic impact of fabric armor.* Int J Impact Engg, 2003. **28**: p. 13 - 31.
95. Larsson, F. and L. Svensson, *Carbon, polyethylene and PBO hybrid fibre composites for structural lightweight armour.* Composites Part A, 2002. **33**: p. 221 - 231.
96. Borvik, T., S. Dey, and A.H. Clausen, *Perforation resistance of five high-strength steel plates subjected to small-arms projectiles.* Int J Impact Engg, 2009. **36**: p. 948 - 964.
97. Fawaz, Z., W. Zheng, and K. Behdinan, *Numerical simulation of normal and oblique ballistic impact on ceramic composite armours.* Composite Structures, 2004. **63**: p. 387 - 395.
98. Mahfuz, H., et al., *Investigation of high-velocity impact on integral armor using finite element method.* Int J Impact Engg, 2000. **24**: p. 203 - 217.
99. Iremonger, M.J., *Polyethylene composites for protection against high velocity small arms bullets.* Proceedings: 18th Int Symp on Ballistics, San Antonio, Texas, Nov 1999: p. 946 - 953.
100. Johnson, G.R. and W.H. Cook, *A constitutive model and data for metals subjected to large strains, high strain rates and high temperatures.* Proceedings of 7th Intl Symp on Ballistics, Hague, Netherlands, April 1983: p. 541 - 547.
101. Hill, R., *A theory of the yielding and plastic flow of anisotropic metals.* Proceedings of Royal Soc of London, Series A, Math and Phy Sci, 1947. **193**: p. 281 - 297.
102. Hashin, Z., *Failure criteria for unidirectional fiber composites.* Journ of Appl Mech, 1980. **47**: p. 329 - 334.
103. Hooputra, H., et al., *A comprehensive failure model for crashworthiness simulation of aluminum extrusions.* Int Journ of Crashworthiness, 2004. **9**(5): p.

449 - 464.

104. Kurtaran, H., M. Buyuk, and A. Eskandarian, *Ballistic impact simulation of GT model vehicle door using finite element method.* Theo and Appl Frac Mech, 2003. **40**: p. 113 - 121.

105. Ashby, M.F., et al., *Metal foams: A design guide, Butterworth - Heinemann publication.* 2000.

106. Jussila, J., *Preparing ballistic gelatin - review and proposal for a standard method.* Forensic Sci Intl, 2004. **141**(2/3): p. 91 - 98.

107. Kenedi, R.M., et al., *Tissue Mechanics.* Phy in Med and Bio, 1975. **20**(5): p. 699 - 717.

108. Song, B., et al., *Dynamic and quasi-static response of porcine muscles.* Journ of Biomech, 2007. **40**(13): p. 2999 - 3005.

109. Walsh, P.J., et al., *Environmental effects on poly-p-phenylenebenzobisoxazole fibers. I. Mechanisms of degradation.* Journ of Appl Polymer Sci, 2006. **102**(4): p. 3517 - 3525.

110. Morye, S.S., et al., *A comparison of the properties of hot compacted gel-spun polyethylene fibre composites with conventional gel-spun polyethylene fibre composites.* Composites Part A, 1999. **30**: p. 649 - 660.

111. Brothers, A.H. and D.C. Dunand, *Amorphous metal foams.* Scripta Materialia, 2006. **54**: p. 513 - 520.

112. *ABAQUS – Version 6.7, User Documentation, Dassault Systems, 2007.*

113. Boyer, H.E., Atlas of Stress- Strain curves, ASM international, Metals park, Ohio, 1987: p. 623.

114. Schwer, L.E., K. Hacker, and K. Peo, *Perforation of metal plates: laboratory experiments and numerical simulations.* Proceedings of 2nd Intl Conf on Design and Analysis of protective structures (DAPS 2006) Singapore, Nov 2006: p. 13 - 14.

APPENDIX A

ARMOR PLATE DYNAMIC IMPACT SIMULATION TIMELINE

The aim of conducting dynamic simulations in ABAQUS 6.8.2 was to closely model and compare the behavior of the Hybrid-Composite-Armor insert according to a NIJ standard level III ballistic test (7.62 mm Copper jacketed Lead projectile). Different models with varying mesh properties, material properties and section controls were simulated. The timeline elaborates on the variations brought about in the simulation parameters till considerable result stability was observed. This process led to the development of Generation 1, Generation 2 and the most efficient Generation 3 models.

Generation 1 Models:

These models were the first attempts at generating FEA simulations and understanding the modeling procedure. The procedure of generating meshed parts, creating material models and selecting boundary conditions was familiarized. Being the first stage in this work, a conservative approach was used regarding inclusion of software options. Homogenous isotropic material models were used for all materials involved. Data available through literature review, then conducted experiments and their extrapolations were used. Simplest tensile and shear failure model was used to simulate material damage and erosion. General contact algorithm was used to model dynamic contact through element set “erode”.

Model 1: *(Analysis time duration: 1 hour 17 minutes)*

The model geometry is as shown in Fig 1. The multilayer composite model had (152 mm x 152 mm x 25.4 mm (6" x 6" x 1") dimensions and comprised of a 8mm Metallic Glass Teardrop honeycomb layer sandwiched between Dyneema HB50 layers (14 mm front impact layer and 3 mm backing layer). The model was a divided quadrant for simulation simplicity and faster analysis. The lead bullet (assigned with a velocity of 838 m/s) was also considered to be in 1/4th volume.

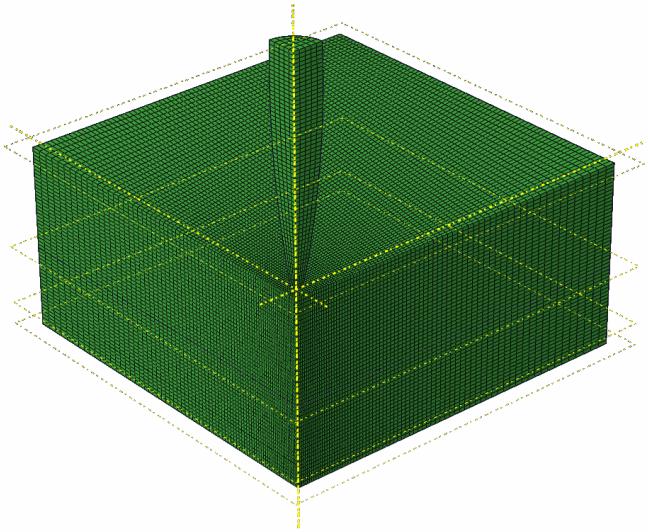

Figure1 Model geometry (Each layer of the composite plate is marked with the datum planes).

Boundary conditions were chosen to model symmetry about X and Y axes with outer edges with pinned condition. The time period was chosen to be 0.0002, proportional to the bullet velocity. Global automatic time step estimation was selected. It was seen from the analysis run that the simulation was not capable of completing all required iterations. The initial and final images of the simulation are shown in Figure 2. The results were not in accordance to those seen in the actual test. However the front damage zone and penetration was similar to the shear failure seen in actual test (approximate zone size 1" x 1" / 25.4 mm x 25.4 mm).

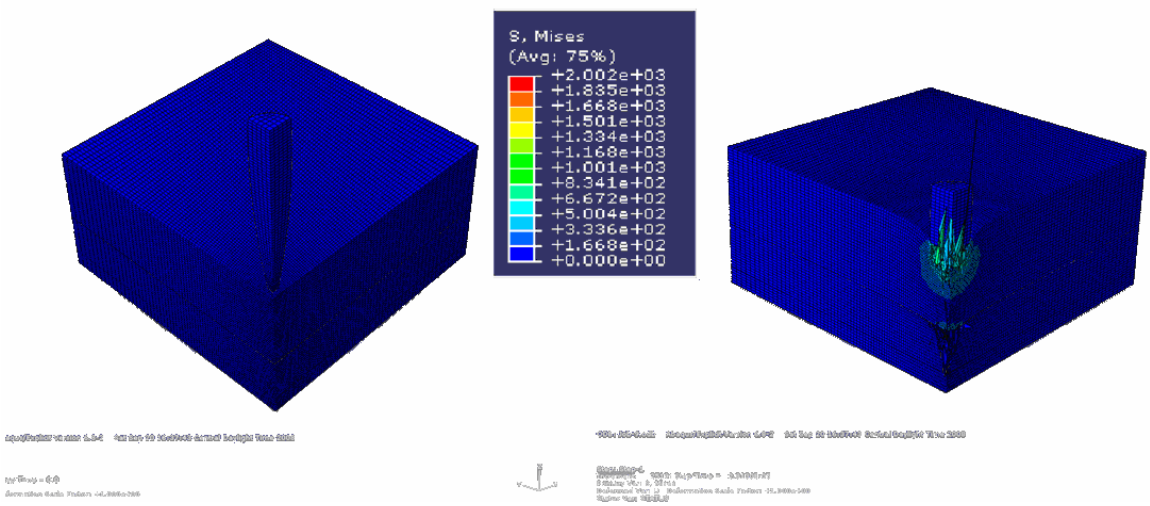

Figure 2 Initial and final images from simulation of Model 1.

The possible reasons for the discrepancies were evaluated. The details are as stated below:

- The material properties considered for the simulation did not correspond to the actual ones. The simulation being dynamic, it was essential to input the high strain rate properties of each of the materials used.
- The precision of the analysis needed to be improved indicating the mesh size had to be further refined. However, a highly refined mesh takes longer time for computation and analysis. Optimum mesh size had to be predicted with more tries.
- The precision could also be improved by reducing the analysis time step factor or varying the time period.

Model 2: *(Analysis Time duration: 7 ½ days approximately)*

Based on the results from Model 1, the material properties were scrutinized. Dynamic properties were not available for selected materials. The units used for the simulation

were found to be different from the standards (SI mm scale recommended to be used instead of SI m). Corrections were made accordingly. The basic numbers for the properties were kept the same. The mesh size was refined to an element size of 0.5 from initial 1.2. Multiple tries were made to adjust this parameter as well as the meshing geometry was modified. The time period was varied from 0.0025 to 1 keeping the time step factor constant. The time step factor was then changed to 0.01 from the initial 1 to give more iteration. This significantly increased the analysis time. The basic quadrant geometry was kept the same as that of Model 1. The results obtained are as shown below:

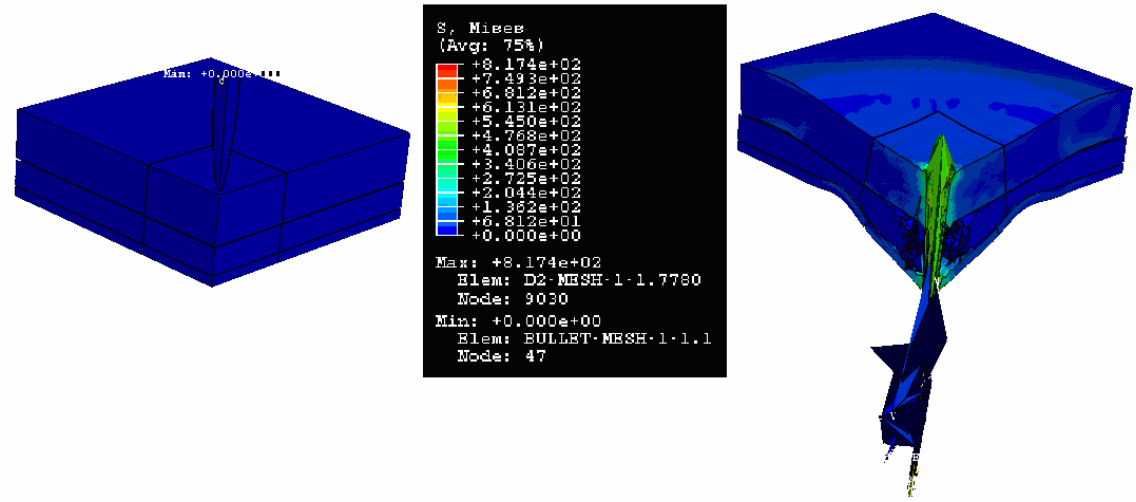

Figure 3 Initial and Final Image from simulation of Model 2.

The results obtained from this model were very close to those seen from the actual test. It was seen from the final simulation images that the front and back face damage key features were relatively close to actual results. Since the model considered Dyneema layers to be homogenous, delamination was not seen in within the layers. The model however failed to display individual material sections in the viewport. This loss of information was a hindrance to predict material loss and which material layer thickness had to be modified and by what magnitude. The model completed all desired iterations.

Developing a new model to incorporate this visual data in the viewport was necessary which led to the creation of Model 3. This would help to identify the material resulting in excessive deformations seen earlier. It would be then possible to make modifications accordingly to ensure better solution convergence.

Model 3: *(Analysis time duration: 9 days approx.)*

The previous model was modified to include improved mesh parts that retained the material sections view in the assembly view port. Mesh size was modified to a size 0.4. The failure criteria for the simple shear and tensile failure were modified with an objective of curtailing excessive projectile deformation seen in Model 2. For trial purpose the size of the element set "erode" was increased to see if affected the end solution.

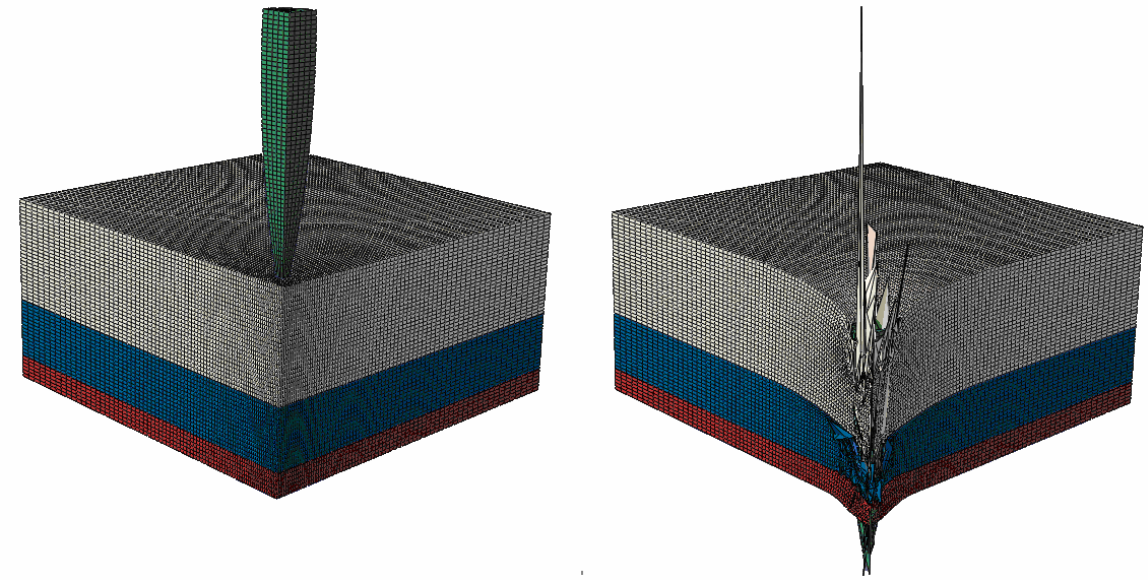

Figure 4 Initial and Final image from Materials section view from the simulation of Model 3.

Model 3 showed a significant change in the back face deformation as compared to Model 2 due to change in material parameters. The model had to be further optimized to reduce the analysis time. It was seen that modifying the time scale factor to 0.1 from 0.01 did not

make a significant difference in the end solution. Also the time period change was not effective and only penalized the total simulation run time. A complete fine meshing of all parts did not serve the desired purpose of improvement is solution. Most important observation was material property variations were seen to significantly change the output in all the models. It was clear that simple assignments of elastic and plastic material properties were not enough to govern the behavior of the impacting solids. Being a dynamic impact scenario strain rate dependence had to be incorporated. The simple shear and tensile failure damage model used in these analyses was not capable of closely modeling the progressive damage seen in materials. This intensified the need for better material property approximations and other progressive damage models.

Generation 2 Models:

Generation 1 models established a platform from which further improvements could be made to the modeling procedure. It was evident that the entire part need not be of the same mesh size throughout. Generation 2 models thus involved discrete mesh parts that could be combined together using Tie function to form an entire plate. These models also incorporated sets of axial nodes along Z axis that were used to measure the projectile velocity change with time in that direction. The reduction in number of nodes for output generation significantly reduced the computation time. Velocity variations in X and Y directions were minimal and hence neglected. For further reduction in computation time duration, instead of a square quadrant, model geometries were modified with a circular outer edge.

Model 4: *(Analysis time duration: 5 hours approximately)*

Literature review on progressive damage models for dynamic impact simulations in ABAQUS User's Documentation [111] led to the finding of extended shear and ductile failure model by Hooputra [102] for steel. The example problem of steel cylindrical rod impacting a steel block was presented. Model 4 was made by using the input file for this example problem as-is to verify the efficiency of this progressive damage model. The results obtained from the simulation are as shown in Figure 5. It was clearly seen that this progressive damage model was very efficient in exactly reproducing the extent of damage and the failure patterns seen in the dynamic impact scenario. The model was also capable of simulating material fragmentation and particle separation phenomenon.

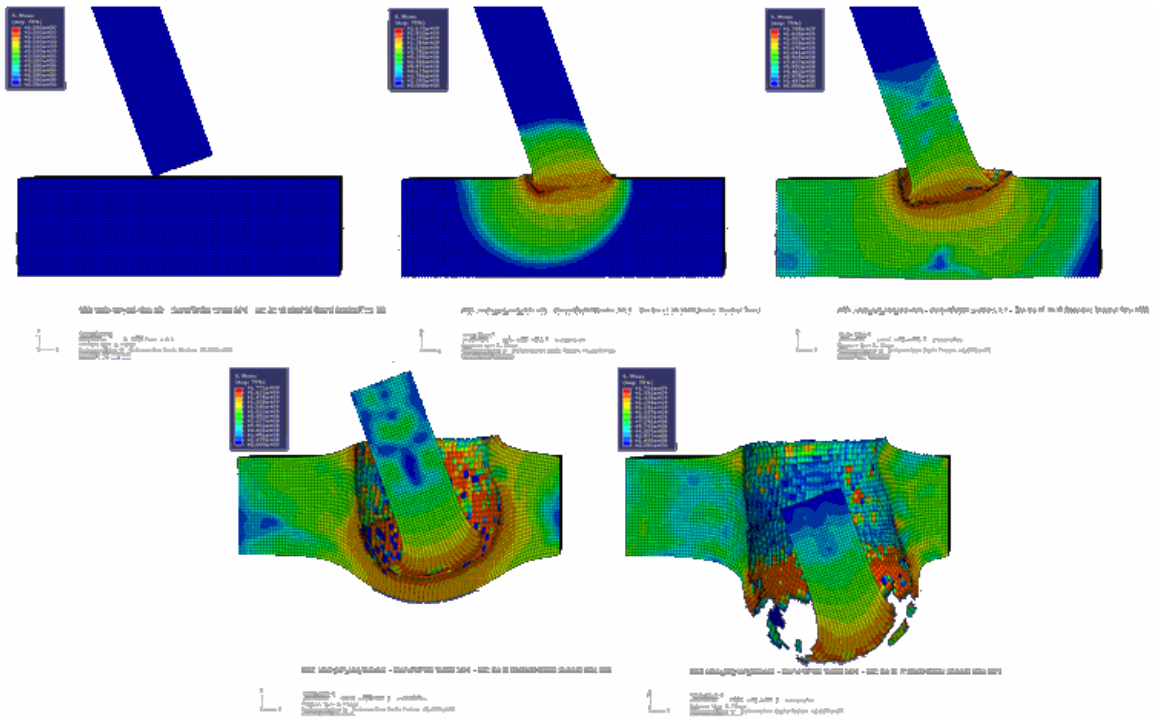

Figure 5 Simulation result images from simulation run of Steel rod impact on steel block example input file [111].

The next objective post successful simulation run of the example problem was to verify if the stated material properties for steel from Model 4 could be applied to vertical steel rod impact on steel plate problem. Model 5 was developed to achieve this objective.

Model 5: *(Analysis time duration: 5 hours approximately)*

Model 5 was developed to simulate dynamic impact of a cylindrical steel rod (diameter 7.62 mm) on a steel plate (110 mm diameter, 6 mm thickness). The impacting rod was assigned a velocity of 838 m/s. The regular Dynamic Contact algorithm was used to model the impact between the projectile and the plate. Other conditions like boundary conditions were kept similar to those from Generation 1 models. Figure 6 shows the results obtained from the simulation run of this model.

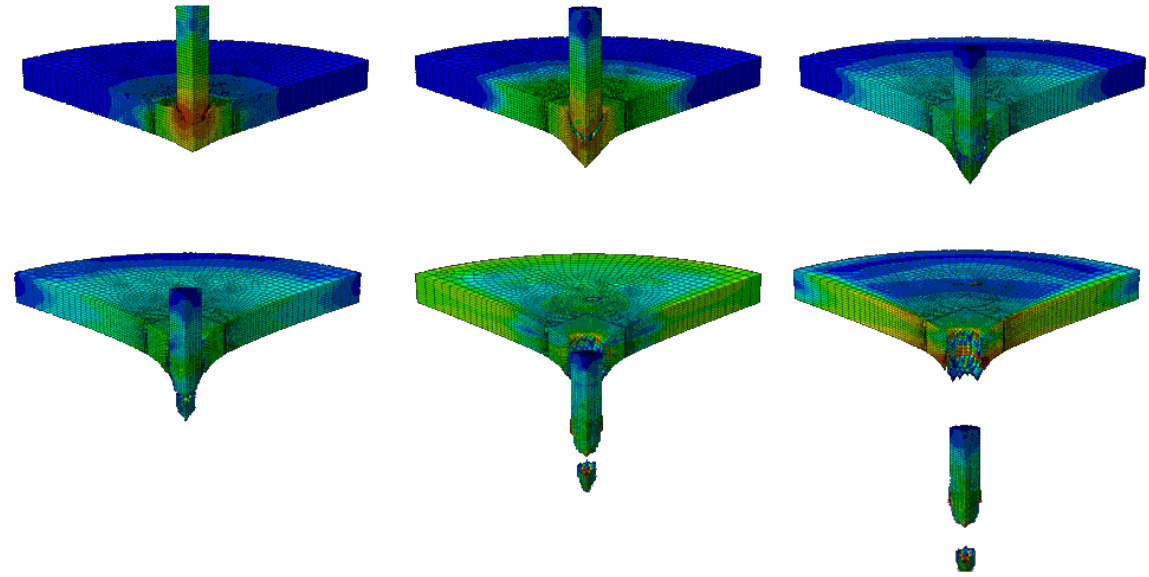

Figure 6 Simulation results from Model 5 showing the typical plug-out behavior seen in steel plate impact experiments.

The results were in good conformation with the physiological changes seen during a dynamic impact of a cylindrical projectile on a metal plate reported by Borvik et al. [83]. The effectiveness of the current progressive damage model was evident. The propagation of shear waves through the plate structure was axisymmetrical illustrating that the current

boundary conditions were precise. The steel material properties considered in this model were effective in high strain rate dynamic impact scenarios. To verify if the success from this model could be extended further to a Lead cylinder impacting steel plate, Model 6 was developed.

Model 6: *(Analysis time duration: 45 minutes approximately)*

Lead properties from the earlier Generation 1 models demonstrated a predominant brittle cracking in early stages with unrealistic deformations. To evaluate more accurate properties, compression test was done on an actual bullet cylindrical cut-section sample (section 3.2, chapter 3) and the results were used to model the cylindrical projectile. The dimensions and other properties were exactly identical to Model 5. For an 838 m/s initial velocity, the simulation runs ceased prematurely at the first iteration owing to excessive deformation resulting in the Lead cylinder. Methods to correct these errors were sought and method of using section controls was identified from ABAQUS User's Documentation [111].

The initial velocity of the projectile was reduced to 300 m/s to check if it assisted in successful completion of all iterations. Only first 5 iterations were successful after which the software quit owing to excessive deformation in lead. The velocity was further reduced to 100 m/s to check the maximum velocity the software can handle for a complete simulation run. All other parameters were kept identical to the initial runs. The results are as shown in Figure 7. Variable mass scaling was explored to counter the problems faced due to excessive deformation seen in Lead. This method was carried forward in simulations run in Generation 3 models as well.

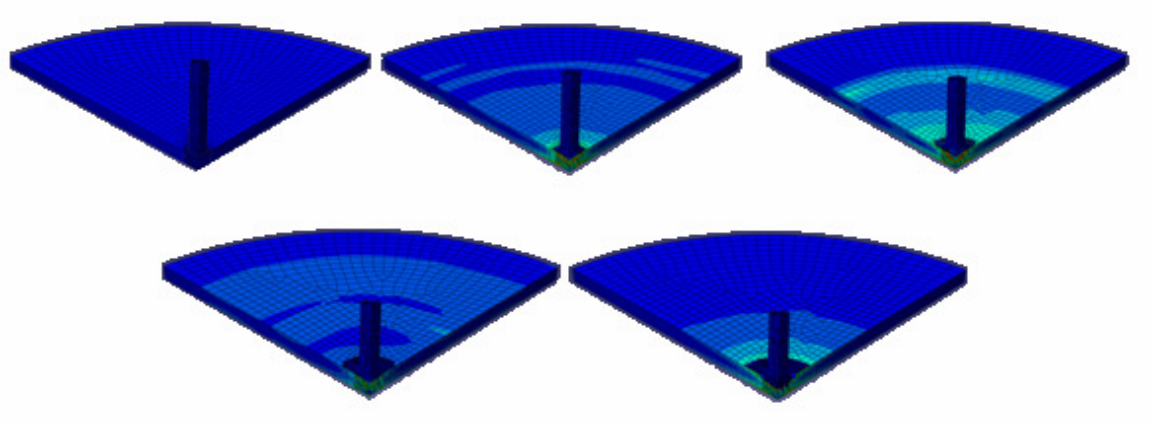

Figure 7 Simulation results from Lead cylinder impact on steel at 100 m/s.

Using online support resources provided by ABAQUS, possible solutions for the problem were sought.

- Manual over ride of wave cut off ratio. (Ratio of deformation wave speed to the transmitted stress wave speed)
- Variation in the bulk viscosity parameters.
- Reduction in the time step and using manual input instead of using the one calculated by the automatic algorithm.

Other suggestions involved reduction in the impact velocity or considering a stiffer material instead of lead but these approaches were not a consistent choice since verification of simulation results was not possible by comparison with experimental ones. Each suggested method was incorporated in the simulation model one at a time. Manual over ride of cut off ratio was done in steps. The default value selected by ABAQUS for this ratio is 1. Manually ratios 2, 3, and 4 were considered in input. However no significant variation in the results was observed. Next the bulk viscosity parameters were varied from the default values of 0.06 and 0.14 to 0.08 and 0.16 to increase the viscous

resistance to the deformation wave. This method too was not successful in giving any significant variations in the observed results. Stepwise reduction in time step from initial 2×10^{-8} to 2×10^{-9} was considered. No significant change was observed even after manual input of the time step during simulation.

The Generation 1 and 2 models helped to set standards on different options that ABAQUS 6.8.2 offered for use in Dynamic impact problems. Since method of evaluating material parameters for the extended shear and tensile failure model by Hooputra were not available a simpler progressive damage model proposed by Johnson-Cook was investigated. Considered to be a special case of the former extended shear and tensile failure model, effectiveness of this model had already been verified by comparison with experimental results (Refer section 1.3 of chapter 1). Generation 3 models were developed by incorporating all the positive attributes from each of the modules used in the dynamic impact simulations. Johnson-Cook model was used to model copper and lead in Generation 3 model runs. Steel properties from Model 4 and 5 were also used.

As progressive damage models for Dyneema HB50 and MG Teardrop structure were not available, these materials were not used in any further models.

APPENDIX B

SAMPLE KEYWORDS FROM SIMULATION INPUT FILE

```
*Heading
** Job name: Copper3 Model name: Model-2
** Generated by: Abaqus/CAE Version 6.8-2
*Preprint, echo=NO, model=NO, history=NO, contact=NO
**
** Constraint: Constraint-1
*Tie, name=Constraint-1, adjust=yes
ST2-mesh-1-1.Slave, ST1-mesh-1-1.Master
*Surface, type=element, name=surf1
,
erode, interior
*End Assembly
**
** ELEMENT CONTROLS
**
*Section Controls, name=EC-1, DISTORTION CONTROL=YES, ELEMENT
DELETION=YES, kinematic split=ORTHOGONAL, hourglass=COMBINED
1., 1., 1.
**
** MATERIALS
**
*Material, name=Copper
*Damage Initiation, criterion=JOHNSON COOK
 0.54,  4.89, -3.03, 0.014,  1.12, 1058.,   25.,    1.
*Damage Evolution, type=DISPLACEMENT
 0.2,
*Density
 8.96e-09,
*Elastic
124000., 0.34
*Plastic, hardening=JOHNSON COOK
90., 292., 0.31, 1.09,1058.,  25.
*Rate Dependent, type=JOHNSON COOK
 0.025,1.
*Material, name=Lead
*Density
 1.135e-08,
*Elastic
16000., 0.44
*Plastic, hardening=JOHNSON COOK
23.,  11.59, 0.2604,     0.,   328.,    25.
*Rate Dependent, type=JOHNSON COOK
 0.025,1.
```

```
*Material, name=Steel
*Damage Initiation, criterion=DUCTILE
  2.31,   -3.33,   0.001
  2.31,  -0.333,   0.001
  2.18,  -0.267,   0.001
  2.06,    -0.2,   0.001
  1.95,  -0.133,   0.001
  1.85, -0.0667,   0.001
  1.76,      0.,   0.001
  1.67,  0.0667,   0.001
  1.59,   0.133,   0.001
  1.52,     0.2,   0.001
  1.46,   0.267,   0.001
   1.4,   0.333,   0.001
  1.35,     0.4,   0.001
   1.3,   0.467,   0.001
  1.26,   0.533,   0.001
  1.23,     0.6,   0.001
   1.2,   0.667,   0.001
  1.15,    0.73,   0.001
  1.06,   0.851,   0.001
 0.945,    1.02,   0.001
 0.816,    1.24,   0.001
 0.685,    1.51,   0.001
 0.202,    3.33,   0.001
*Damage Evolution, type=DISPLACEMENT
 0.2,
*Damage Initiation, criterion=SHEAR, ks=0.03
  0.86,  -10., 0.001
  0.86,   1.7, 0.001
 0.859,  1.72, 0.001
  0.86,  1.73, 0.001
 0.865,  1.75, 0.001
 0.874,  1.77, 0.001
 0.886,  1.78, 0.001
 0.901,   1.8, 0.001
 0.921,  1.81, 0.001
 0.944,  1.83, 0.001
  0.97,  1.85, 0.001
    1.,  1.86, 0.001
  1.04,  1.88, 0.001
  1.08,  1.89, 0.001
  1.12,  1.91, 0.001
  1.17,  1.92, 0.001
  1.22,  1.94, 0.001
  1.28,  1.96, 0.001
  1.34,  1.97, 0.001
  1.41,  1.99, 0.001
  1.48,    2., 0.001
  1.56,  2.02, 0.001
  1.56,   10., 0.001
*Damage Evolution, type=DISPLACEMENT
 0.2,
*Density
 7.8e-09,
*Elastic
210000., 0.3
```

```
*Plastic, rate=0.
776.,0.
809., 0.01
829., 0.02
842., 0.03
866., 0.06
883., 0.1
895., 0.15
910., 0.25
922., 0.4
953.,2.
*Plastic, rate=0.001
791.,0.
824., 0.01
846., 0.02
863., 0.03
899., 0.06
931., 0.1
958., 0.15
995., 0.25
1030., 0.4
1170.,2.
*Plastic, rate=0.01
799.,0.
831., 0.01
855., 0.02
874., 0.03
916., 0.06
955., 0.1
989., 0.15
1040., 0.25
1090., 0.4
1280.,2.
*Plastic, rate=0.1
805.,0.
838., 0.01
863., 0.02
884., 0.03
933., 0.06
978., 0.1
1020., 0.15
1080., 0.25
1140., 0.4
1390.,2.
*Plastic, rate=1.
808.,0.
842., 0.01
869., 0.02
893., 0.03
946., 0.06
998., 0.1
1050., 0.15
1120., 0.25
1190., 0.4
1490.,2.
*Plastic, rate=10.
810.,0.
```

```
846., 0.01
876., 0.02
901., 0.03
960., 0.06
1020., 0.1
1070., 0.15
1150., 0.25
1240., 0.4
1600.,2.
*Plastic, rate=100.
812.,0.
850., 0.01
882., 0.02
909., 0.03
974., 0.06
1040., 0.1
1100., 0.15
1190., 0.25
1280., 0.4
1700.,2.
*Plastic, rate=1000.
815.,0.
855., 0.01
888., 0.02
917., 0.03
987., 0.06
1060., 0.1
1130., 0.15
1230., 0.25
1330., 0.4
1810.,2.
**
** INTERACTION PROPERTIES
**
*Surface Interaction, name=IntProp-1
*Friction
0.,
*Surface Behavior, pressure-overclosure=HARD
**
** BOUNDARY CONDITIONS
**
** Name: BC-1 Type: Symmetry/Antisymmetry/Encastre
*Boundary
_PickedSet11, YSYMM
** Name: BC-2 Type: Symmetry/Antisymmetry/Encastre
*Boundary
_PickedSet12, XSYMM
** Name: BC-3 Type: Symmetry/Antisymmetry/Encastre
*Boundary
_PickedSet13, PINNED
**
** PREDEFINED FIELDS
**
** Name: Predefined Field-1   Type: Velocity
*Initial Conditions, type=VELOCITY
_PickedSet14, 1, 0.
_PickedSet14, 2, 0.
```

```
_PickedSet14, 3, -800000.
**
** INTERACTIONS
**
** Interaction: Int-1
*Contact, op=NEW
*Contact Inclusions, ALL EXTERIOR
*Contact property assignment
 ,  , IntProp-1
*Contact, op=NEW
*Contact Inclusions
surf1,
*Contact controls assignment, nodal erosion=no
** ----------------------------------------------------------------
**
** STEP: Step-1
**
*Step, name=Step-1
*Dynamic, Explicit, element by element
, 0.0002
*Bulk Viscosity
0.06, 1.2
** Mass Scaling: Semi-Automatic
**               Whole Model
*Variable Mass Scaling, dt=2e-09, type=below min, frequency=1
**
** OUTPUT REQUESTS
**
*Restart, write, number interval=1, time marks=NO
**
** FIELD OUTPUT: F-Output-1
**
*Output, field, variable=PRESELECT
**
** HISTORY OUTPUT: H-Output-2
**
*Output, history
*Node Output, nset=Casing-mesh-1-1.casing
V3,
**
** HISTORY OUTPUT: H-Output-3
**
*Node Output, nset=Core-mesh-1-1.core
V3,
**
** HISTORY OUTPUT: H-Output-1
*DIAGNOSTICS, CUTOFF RATIO=6.0
**
*Output, history, variable=PRESELECT
*End Step
```

VITA

Advait Bhat

Candidate for the Degree of

Master of Science

Thesis: FINITE ELEMENT MODELING AND DYNAMIC IMPACT RESPONSE EVALUATION FOR BALLISTIC APPLICATIONS

Major Field: Mechanical and Aerospace Engineering

Biographical:

Education:

Completed the requirements for the Master of Science in Mechanical and Aerospace Engineering at Oklahoma State University, Stillwater, Oklahoma in December, 2009.

Completed the requirements for the Bachelor of Science in Mechanical Engineering at Mumbai University, Mumbai, India in July, 2007.

Experience:

- Teaching Assistant for Materials Science and Mechanical Metallurgy courses at the Mechanical and Aerospace Engineering Department, Oklahoma State University.

- Research Assistant for Dr. Jay Hanan at the Mechanical and Aerospace Engineering Department, Oklahoma State University.

Name: Advait Bhat Date of Degree: December, 2009

Institution: Oklahoma State University Location: Stillwater, Oklahoma

Title of Study: FINITE ELEMENT MODELING AND DYNAMIC IMPACT RESPONSE EVALUATION FOR BALLISTIC APPLICATIONS

Pages in Study: 117 Candidate for the Degree of Master of Science

Major Field: Mechanical and Aerospace Engineering

A Hybrid-Composite-Armor insert for a level III NIJ 0101.06 ballistic vest standard was designed and successfully tested. A novel sandwich design concept of incorporating collapsible Metallic Glass Teardrop celled honeycomb structure between Dyneema HB50 laminates was used for this insert. Manufactured prototypes were ballistic tested and NDT using CT scanning. Results from these tests showed significant improvement in ballistic performance as compared to Dyneema HB50 baseline. The test method used was standardized for repeatability and accuracy by experimenting on heat treated 4130 steel plates. Methods for evaluating quasi-static and dynamic properties of the Teardrop celled honeycomb were envisioned and standards were set. An FEA modeling procedure for dynamic impact in ABAQUS 6.8.2 was investigated and methodology of conducting simulations was refined. The experiment setup conditions from steel plate testing served as a guideline for this FEA modeling procedure. The current study was thus successful in demonstrating a design methodology wherein mechanical testing and software based FEA analysis could be used in conjunction to evaluate performance of armor design concepts.

ADVISER'S APPROVAL: Dr. Jay C. Hanan